

Model-Based Robust Deep Learning

Alexander Robey, Hamed Hassani, and George J. Pappas

Department of Electrical and Systems Engineering
University of Pennsylvania

Abstract

While deep learning has resulted in major breakthroughs in many application domains, the frameworks commonly used in deep learning remain fragile to artificially-crafted and imperceptible changes in the data. In response to this fragility, adversarial training has emerged as a principled approach for enhancing the robustness of deep learning with respect to norm-bounded perturbations. However, there are other sources of fragility for deep learning that are arguably more common and less thoroughly studied. Indeed, natural variation such as lighting or weather conditions can significantly degrade the accuracy of trained neural networks, proving that such natural variation presents a significant challenge for deep learning.

In this paper, we propose a paradigm shift from perturbation-based adversarial robustness toward *model-based robust deep learning*. Our objective is to provide general training algorithms that can be used to train deep neural networks to be robust against natural variation in data. Critical to our paradigm is first obtaining a *model of natural variation* which can be used to vary data over a range of natural conditions. Such models may be either known a priori or else learned from data. In the latter case, we show that deep generative models can be used to learn models of natural variation that are consistent with realistic conditions. We then exploit such models in three novel model-based robust training algorithms in order to enhance the robustness of deep learning with respect to the given model.

Our extensive experiments show that across a variety of naturally-occurring conditions and across various datasets including MNIST, SVHN, GTSRB, and CURE-TSR, deep neural networks trained with our model-based algorithms significantly outperform both standard deep learning algorithms as well as norm-bounded robust deep learning algorithms. Our approach can result in accuracy improvements as large as 20-30 percentage points compared to state-of-the-art classifiers on tasks involving challenging natural conditions. Furthermore, our model-based framework is reusable in the sense that models of natural variation can be used to facilitate robust training across different datasets. Such models can also be composed to provide robustness against multiple forms of natural variation. Lastly, we performed out-of-distribution experiments on the challenging CURE-TSR dataset in which classifiers were trained on images with low levels of natural variation and tested on images with high levels of the same form of variation. We found that classifiers trained using our model-based algorithms improve by as much as 15 percentage points over state-of-the-art classifiers.

Our results suggest that exploiting models of natural variation can result in significant improvements in the robustness of deep learning when deployed in natural environments. This paves the way for a plethora of interesting future research directions, both algorithmic and theoretical, as well as numerous applications in which enhancing the robustness of deep learning will enable its wider adoption with increased trust and safety.

Contents

1	Introduction	7
2	Perturbation-based robust deep learning	9
3	Model-based robust deep learning	10
3.1	Adversarial examples versus natural variation	10
3.2	Model-based robust training formulation	12
3.3	Geometry of model-based robust training	13
4	Models of Natural Variation	15
4.1	Known models $G(x, \delta)$ of natural variation	15
4.2	Learning unknown models of natural variation $G(x, \delta)$ from data	17
4.3	Using deep generative models to learn models of natural variation for images	18
5	Model-based robust training algorithms	19
5.1	Model-based Robust Training (MRT)	21
5.2	Model-based Adversarial Training (MAT)	22
5.3	Model-based Data Augmentation (MDA)	23
6	Experiments	24
6.1	Experiments with one dataset	26
6.1.1	MNIST: robustness to background color	26
6.1.2	SVHN: robustness to contrast	27
6.1.3	GTSRB: robustness to brightness	28
6.1.4	Robustness with respect to other nuisances	29
6.1.5	Robustness to more challenging test data	31
6.2	Leveraging models across datasets	32
6.2.1	Leveraging one background color model across MNIST variants	32
6.2.2	Leveraging one brightness model across GTSRB and CURE-TSR	33
6.2.3	Composing models of natural variation	34
6.3	Out-of-distribution experiments	36
6.3.1	CURE-TSR: robustness with respect to snow	37
6.3.2	Robustness with respect to increasingly challenging nuisances	37
7	Discussion	39
7.1	Nuisance spaces of models of natural variation	39
7.2	Impact of model quality	39
7.3	Sampling versus adversarial algorithms	41
7.4	Hyperparameters and architectures for model-based training	43
8	Related works	45
8.1	Perturbation-based adversarial robustness	45
8.2	A broader view of robustness in deep learning	45
8.3	Generative models in the context of robustness	46
8.4	Equivariance and invariance to nuisances in computer vision	46

9 Conclusion and future directions	47
References	49
A Appendix A: Experiments on one domain	57
A.1 MNIST	57
A.1.1 Background color: gray to RGB	57
A.1.2 Background color: blue to red	58
A.1.3 Background color: half red, half blue	59
A.1.4 Background color: one red, nine blue	61
A.2 SVHN	63
A.2.1 Robustness to contrast	64
A.2.2 Robustness to brightness (low to high)	65
A.2.3 Robustness to brightness (medium to all)	66
A.2.4 Robustness to erasing with a known model	67
A.2.5 Robustness to erasing with a learned model	69
A.2.6 Robustness to colorization	71
A.2.7 Robustness to decolorization	72
A.2.8 Hue and background color	73
A.3 GTSRB	74
A.3.1 Robustness to contrast	74
A.3.2 Robustness to brightness	75
B Appendix B: Experiments across domains	77
B.1 MNIST variants	77
B.2 MNIST-m and SVHN	81
B.3 GTSRB and CURE-TSR	82
C Appendix C: Out-of-distribution experiments	84
C.1 Decolorization	84
C.2 Haze	84
C.3 Shadow	84
C.4 Rain	88
D Appendix D: Details concerning datasets and domains	90
D.1 Datasets used in this paper	90
D.2 Curating dataset domains	92
D.2.1 MNIST dataset colorization	92
D.2.2 SVHN and GTSRB thresholding	92
D.2.3 Artificial transformations	98
D.2.4 CURE-TSR: labeled challenges	98
E Appendix E: Training details and architectures	99
E.1 MUNIT framework	99
E.2 Hyperparameters and implementation of MUNIT	100

List of Figures

1	A new notion of robustness	11
2	Models of natural variation	12
3	Model-based robustness paradigm	13
4	Geometry of adversarial and model-based robustness	14
5	Known models of natural variation	15
6	Learning unknown models of natural variation	18
7	Robustness to background colors on MNIST	27
8	Robustness to contrast on SVHN	28
9	Robustness to brightness on GTSRB	29
10	Robustness to darkening on CURE-TSR with a model learned on GTSRB	35
11	Using a composition of models on SVHN	36
12	CURE-TSR snow challenge levels	37
13	Out-of-distribution robustness to snow on CURE-TSR	38
14	Nuisance spaces of learned models	41
15	A better models implies more robustness	42
16	Classifier architecture selection	44
17	Robustness to red backgrounds on MNIST	58
18	Robustness to background colors on MNIST: half blue, half red	59
19	MNIST: half red, half blue analysis	60
20	Robustness to background colors on MNIST: one red, nine blue	61
21	MNIST: half red, half blue analysis	62
22	Gridding a model of contrast for SVHN	64
23	Robustness to brightness on SVHN	65
24	Gridding a model of brightness on SVHN	66
25	Robustness to all levels of brightness of SVHN	67
26	Robustness to erasing on SVHN with a known model	68
27	Robustness to erasing on SVHN with a learned model	70
28	Gridding a model of erasing on SVHN	70
29	Robustness to colorization on SVHN	71
30	Robustness to decolorization on SVHN	72
31	Gridding a model of decolorization on SVHN	73
32	Robustness to hue on SVHN	74
33	Gridding a model of hue on SVHN	75
34	Robustness to contrast on GTSRB	76
35	Gridding a model of contrast on GTSRB	76
36	Gridding a model of brightness on GTSRB	77
37	Reusing a learned model on MNIST variants with mixed label colors	79
38	Reusing a learned model of background colors on MNIST variants	80
39	Robustness to color on SVHN with a model learned on MNIST-m	81
40	Robustness to exposure on CURE-TSR using a model learned on GTSRB	83
41	Out-of-distribution robustness to decolorization on CURE-TSR	85
42	Out-of-distribution robustness to haze on CURE-TSR	86
43	Out-of-distribution robustness to shadow on CURE-TSR	87

44	Out-of-distribution robustness to rain on CURE-TSR	89
45	Samples from the datasets used in this paper	91
46	Creating the colorized MNIST dataset.	92
47	SVHN brightness thresholding overview	94
48	SVHN contrast thresholding overview	95
49	GTSRB brightness thresholding overview	96
50	SVHN contrast thresholding overview	97
51	Decolorized samples from MNIST-m	98

List of Tables

1	Models of natural variation	20
2	Model-based training on one dataset	30
3	Model-based training with a more challenging test set	31
4	Passing samples from other datasets through a model learned on MNIST	33
5	Reusing learned models on new datasets	34
6	Out-of-distribution results on CURE-TSR	40
7	Varying the architecture of the classifier used for model-based training	44
8	Applying a model learned on MNIST-m to SVHN	82
9	Applying a model learned on GTSRB to CURE-TSR	83
10	Dataset descriptions	90
11	Thresholds for SVHN and GTSRB	93
12	MUNIT hyperparameters	100

1 Introduction

Over the last decade, we have witnessed unprecedented breakthroughs in deep learning [1]. Rapidly growing bodies of work continue to improve the state-of-the-art in generative modeling [2, 3, 4], computer vision [5, 6, 7], and natural language processing [8, 9]. Indeed, the progress in these fields has prompted large-scale integration of deep learning into a myriad of domains; these include autonomous vehicles, medical diagnostics, and robotics [10, 11]. Importantly, many of these domains are *safety-critical*, meaning that the detections, recommendations, or decisions made by deep learning systems can directly impact the well-being of humans [12]. To this end, it is essential that the deep learning systems used in safety-critical applications are robust and trustworthy [13].

It is now well-known that many deep learning frameworks including neural networks are fragile to seemingly innocuous and imperceptible changes to their input data [14]. Well-documented examples of such fragility to carefully-designed noise can be found in the context of image detection [15], video analysis [16, 17], traffic sign misclassification [18], machine translation [19], clinical trials [20], and robotics [21]. In addition to this vulnerability to artificial noise, deep learning is also fragile to changes in the environment, such as changes in background scenes or lighting. In all deep learning applications and in particular in safety-critical domains, it is of fundamental importance to improve the robustness of deep learning.

In response to this vulnerability to imperceptible changes, a vastly growing body of work has focused on improving the robustness of deep learning. In particular, the literature concerning *adversarial robustness* has sought to improve robustness to small, imperceptible perturbations of data, which have been shown to cause misclassification [14]. By and large, works in this vein assume that adversarial data can only be generated by applying a small, norm-bounded perturbation. To this end, the adversarial robustness literature has developed novel robust training algorithms [22, 23, 24, 25, 26, 27, 28] as well as certifiable defenses to norm-bounded data perturbations [29, 30]. Robust training approaches, i.e. the method of adversarial training [31], typically incorporate norm-bounded, adversarial data perturbations in a robust optimization formulation [22, 23].

Adversarial training has provided a rigorous framework for understanding, analyzing, and improving the robustness of deep learning. However, the adversarial framework used in these approaches is limited in that it cannot capture a wide range of natural phenomena. More specifically, while schemes that aim to provide robustness to norm-bounded perturbations can resolve security threats arising from artificial tampering of the data, these schemes do not provide similar levels of robustness to changes that may arise due to more natural variations [15]. Such changes include unseen distributional shifts including variation in image lighting, background color, blurring, contrast, or other weather conditions [32, 33]. In image classification, such variation can arise from changes in the physical environment, such as varying weather conditions, or from imperfections in the camera, such as decolorization or blurring.

It is therefore of great importance to expand the family of robustness models studied in deep learning beyond imperceptible norm-bounded perturbations to include natural and possibly unbounded forms of variation that occur due to natural conditions such as lighting, weather, or camera defects. To capture these phenomena, it is necessary to obtain an accurate model that describes how data can be varied. Such a model may be known a priori, as is the case for geometric transformations such as rotation or scaling. On the other hand, in some settings a model of natural variation may not be known beforehand and therefore must be learned from data. For example,

there are not known models of how to change the weather conditions in images. Once such a model has been obtained, it should then be exploited in rethinking the robustness of deep learning against naturally varying conditions.

In this paper, we propose a paradigm shift from perturbation-based adversarial robustness to *model-based robust deep learning*. Our objective is to provide general algorithms that can be used to train neural networks to be robust against natural variation in data. To do so, we introduce a robust optimization framework that exploits novel models that describe how data naturally varies to train neural networks to be robust against challenging or worst-case natural conditions. Notably, our approach is model-agnostic and adaptable, meaning that it can be used with models that describe arbitrary forms of variation, regardless of whether such models are known a priori or learned from data. We view this approach as a key contribution to the literature surrounding robust deep learning, especially because robustness to these forms of natural variation has not yet been thoroughly studied in the adversarial robustness community. Our experiments show that across a variety of naturally-occurring and challenging conditions, such as changes in lighting, background color, haze, decolorization, snow, or contrast, and across various datasets, including MNIST, SVHN, GTSRB, and CURE-TSR, neural networks trained with our model-based algorithms significantly outperform both standard baseline deep learning algorithms as well as norm-bounded robust deep learning algorithms.

The contributions of our paper can be summarized as follows:

- **(Model-based robust deep learning.)** We propose a paradigm shift from norm-bounded adversarial robustness to model-based robust deep learning, wherein models of natural variation express changes due to challenging natural conditions.
- **(Robust optimization formulation.)** We formulate the novel problem of model-based robust training by constructing a general robust optimization procedure that searches for challenging model-based variation of data.
- **(Learned models of natural variation.)** For many different forms of natural variation commonly encountered in safety-critical applications, we show that deep generative models can be used to learn models of natural variation that are consistent with realistic conditions.
- **(Model-based robust training algorithms.)** We propose a family of novel robust training algorithms that exploit models of natural variation in order to improve the robustness of deep learning against worst-case natural variation.
- **(Broad applicability and robustness improvements)** We show empirically that models of natural variation can be used in our formulation to provide significant improvements in the robustness of neural networks for several datasets commonly used in deep learning. We report improvements as large as 20-30 percentage points in test accuracy compared to state-of-the-art adversarially robust classifiers on tasks involving challenging natural conditions such as contrast and brightness.
- **(Reusability and modularity of models of natural variation)** We show that models of natural variation can be reused on multiple new and different datasets without retraining to provide high levels of robustness against naturally varying conditions. Further, we show that models of natural variation can be easily composed to provide robustness against multiple forms of natural variation.

- **(Out-of-distribution robustness)** We show that our model-based paradigm can be used to provide robustness to unseen and out-of-distribution data that has been subjected to higher levels of natural variation than the data that is seen during training. In particular, on the CURE-TSR dataset [34], we show that classifiers trained using our paradigm on images with low levels of naturally varying weather conditions such as snow improve by as much as 15 percentage points over state-of-the-art classifiers (including adversarially robust classifiers) when tested on more challenging weather conditions.

While the experiments in this paper focus on image classification tasks subject to challenging natural conditions, our model-based robust deep learning paradigm is much broader and can, in principle, be applied to many other deep learning domains as long as one can obtain accurate models of how the data can vary in a natural and useful manner. In that sense, we believe that this approach will open up numerous directions for future research.

2 Perturbation-based robust deep learning

Improving the robustness of deep learning has promoted the development of *adversarial training* algorithms that defend neural networks against small, norm-bounded perturbations [31]. To make this concrete, we consider a standard classification task in which the data is distributed according to a joint distribution $(x, y) \sim \mathcal{D}$ over instances $x \in \mathbb{R}^d$ and corresponding labels $y \in [k] := \{0, 1, \dots, k\}$. We assume that we are given a suitable loss function $\ell(x, y; w)$; common examples include the cross-entropy or quadratic losses. In this notation, we let $w \in \mathbb{R}^p$ denote the weights of a neural network. The goal of the learning task is to find the weights w that minimize the risk over \mathcal{D} with respect to the loss function ℓ . That is, we wish to solve

$$\min_w \mathbb{E}_{(x, y) \sim \mathcal{D}} [\ell(x, y; w)]. \quad (2.1)$$

As observed in previous work [22, 23], solving the optimization problem stated in (2.1) does not result in robust neural networks. More specifically, neural networks trained by solving (2.1) are known to be susceptible to *adversarial attacks*. This means that given a datum x with a corresponding label y , one can find another datum x^{adv} such that (1) x is close to x^{adv} with respect to a given Euclidean norm and (2) x^{adv} is predicted by the learned classifier as belonging to a different class $c \neq y$. If such a datum x^{adv} exists, it is called an *adversarial example*.

The dominant paradigm toward training neural networks to be robust against adversarial examples relies on a robust optimization [35] perspective. In particular, the approach used in [22, 23] to provide robustness to adversarial examples works by considering a distinct yet related optimization problem to (2.1). In particular, the idea is to train neural networks to be robust against a *worst-case* perturbation of each instance x . This worst-case perspective can be formulated in the following way:

$$\min_w \mathbb{E}_{(x, y) \sim \mathcal{D}} \left[\max_{\delta \in \Delta} \ell(x + \delta, y; w) \right] \quad (2.2)$$

We can think of (2.2) as comprising two coupled optimization problems: an inner maximization problem and an outer minimization problem. First, in the inner maximization problem $\max_{\delta \in \Delta} \ell(x + \delta, y; w)$, we seek a perturbation $\delta \in \Delta$ that results in large loss values when we perturb x by the

amount δ . The set of allowable perturbations Δ is typically of the form $\Delta := \{\delta \in \mathbb{R}^d : \|\delta\|_p \leq \epsilon\}$, meaning that data can be perturbed in a norm-bounded manner for a suitably-chosen Euclidean p -norm. In this sense, any solution δ^* to the inner maximization problem of (2.2) is a worst-case, norm-bounded perturbation in so much as the datum $x + \delta^*$ is most likely to be classified as any label c other than the true label y . If indeed the trained classifier predicts any class c other than y for the datum $x^{\text{adv}} := x + \delta^*$, then x^{adv} is a bona fide adversarial example.

After solving the inner maximization problem of (2.2), we can rewrite the outer minimization problem as

$$\min_w \mathbb{E}_{(x,y) \sim \mathcal{D}} [\ell(x + \delta^*, y; w)]. \quad (2.3)$$

From this point of view, the goal of the outer minimization problem is to find the weights w that ensure that the worst-case datum $x + \delta^*$ is classified by our model as having label y . To connect robust training to the standard training paradigm for deep networks given in (2.1), note that if $\delta^* = 0$ or if $\Delta = \{0\}$ is trivial, then the outer minimization problem (2.3) reduces to (2.1).

Limitations of perturbation-based robustness. While there has been significant progress toward making deep learning algorithms robust against norm-bounded perturbations [22, 23, 24], there are a number of limitations to this approach. Notably, there are many forms of *natural variation* that are known to cause misclassification. In the context of image classification, such natural variation includes changes in lighting, weather, or background color [18, 36, 37], spatial transformations such as rotation or scaling [38, 39], and sensor-based attacks [27]. These realistic forms of variation of data, which in the computer vision community are known as *nuisances*, cannot be modeled by the norm-bounded perturbations $x \mapsto x + \delta$ used in the standard adversarial training paradigm of (2.2) [40]. Therefore, an important open question is how deep learning algorithms can be made robust against realistic and natural forms of variation that are often inherent in safety-critical applications.

In this paper, we present a new training paradigm for deep neural networks that provides robustness against a broader class of natural transformations and variation. Rather than perturbing data in a norm-bounded manner, our robust training approach exploits *models of natural variation* that describe how data changes with respect to particular nuisances. However, we emphasize that our approach is *model-agnostic* in the sense that it provides a robust learning paradigm that is applicable across broad classes of naturally-occurring data variation. Indeed, in this paper we will show that even if a model of natural variation is not explicitly known a priori, it is still possible to train neural networks to be robust against natural variation by learning a model this variation in an offline and data-driven fashion. More broadly, we claim that the framework described in this paper represents a new paradigm for robust deep learning as it provides a methodology for improving the robustness of deep learning to arbitrary sources of natural variation.

3 Model-based robust deep learning

3.1 Adversarial examples versus natural variation

The norm-bounded, perturbation-based robust training formulation of (2.2) provides a principled mathematical foundation for robust deep learning. Indeed, as we showed in the previous section, the problem of defending neural networks against adversaries that can perturb data by a small



(a) **Perturbation-based adversarial example.** In a perturbation-based robustness setting, an input datum such as the image of the panda on the left is perceptually indistinguishable from the adversary example shown on the right.

(b) **Natural variation.** In this work, we study robustness scenarios in which data is subjected to natural variation. In this example, the image of the street in snowy weather on the right compared to the image on the left illustrates this form of natural variation.

Figure 1: **A new notion of robustness.** The adversarial robustness community has predominantly focused on *norm-bounded* adversaries. Such adversaries add artificial noise to an input image to produce an *adversarial example* that looks perceptually similar to the input, but fools a deep neural network. In this paper, we predominantly focus on adversaries which change an input datum by subjecting it to *natural variation*. Such variation often does not obey norm-bounded constraints and often renders transformed data perceptually quite different from the original image.

amount δ in some Euclidean p -norm can be formulated as the robust optimization problem described in (2.2). In this way, solving this optimization problem engenders neural networks that are robust to small but imperceptible noise $\delta \in \Delta$. This notion of robustness is illustrated in the canonical example shown in Figure 1a. In this example, the adversary can arbitrarily change any pixel values in the left-hand-side image to create a new image as long as the perturbation is bounded, meaning that $\delta \in \Delta := \{\delta \in \mathbb{R}^d : \|\delta\|_\infty \leq \epsilon\}$. When $\epsilon > 0$ is small, the two panda bears in Figure 1a are identical to the eye and yet the small perturbation δ can lead to different classifications, resulting in very fragile deep learning.

While adversarial training provides robustness against the imperceptible perturbations described in Figure 1a, in natural environments data varies in ways that cannot be captured by norm-bounded perturbations. For example, consider the two traffic signs shown in Figure 1b. Note that the images on the left and on the right show the same traffic sign; however, the image on the left shows the sign on a sunny day, whereas the image on the right shows the sign in the middle of a snow storm. This example prompts several relevant questions. How do we ensure that neural networks are robust to such natural variation? How can we rethink adversarial training algorithms to provide robustness against natural-varying and challenging data?

In this paper we advocate for a new notion of robustness in deep learning with respect to such natural variation or nuisances in the data. Critical to our approach is the existence of a *model of natural variation*, $G(x, \delta)$. Concretely, a model of natural variation G is a mapping that describes how an input datum x can be naturally varied by nuisance parameter δ resulting in image x' . Conceptually, an illustrative example of such a model is shown in Figure 2, where the input image x on the left (in this case, in sunny weather) can be naturally varied by δ and consequently transformed into the image on the right $x' := G(x, \delta)$ (in snowy weather).

For the time being, we assume the existence of such a model of natural variation $G(x, \delta)$; later, in Section 4, we will detail our approach for obtaining models of natural variation that correspond to a wide variety of nuisances. In this way, given a model of natural variation G , our goal is to exploit this model toward developing novel *model-based robust training algorithms* that ensure that

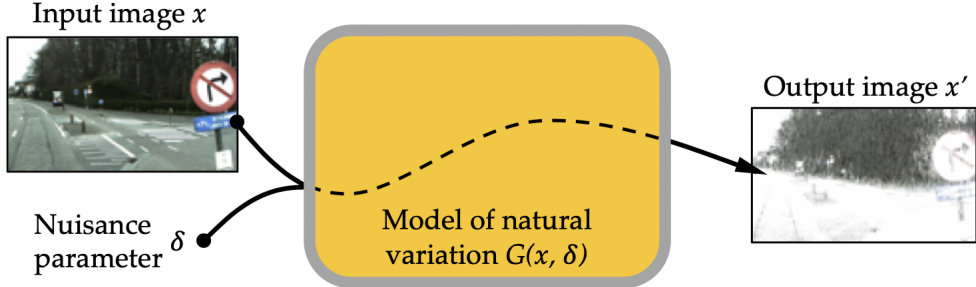


Figure 2: **Models of natural variation.** Throughout this paper, we will use *models of natural variation* to describe a wide variety of natural transformations that data are often subjected to. In our formulation, models of natural variation take the form $G(x, \delta)$, where x is an input datum such as an image and δ is a *nuisance parameter* that characterizes the extent to which the output datum $x' := G(x, \delta)$ is varied.

trained neural networks are robust to the natural variation captured by the model. For instance, if G models variation in the lighting conditions in an image, our model-based training algorithm will provide robustness to lighting discrepancies. On the other hand, if G models changes in the weather such as in Figure 1b, then our model-based formulation will improve the robustness of trained neural networks to varying weather conditions. More generally, our model-based robust training formulation is agnostic to the source of natural variation, meaning that our novel robust training paradigm is broadly applicable to any source of natural variation that G can capture.

3.2 Model-based robust training formulation

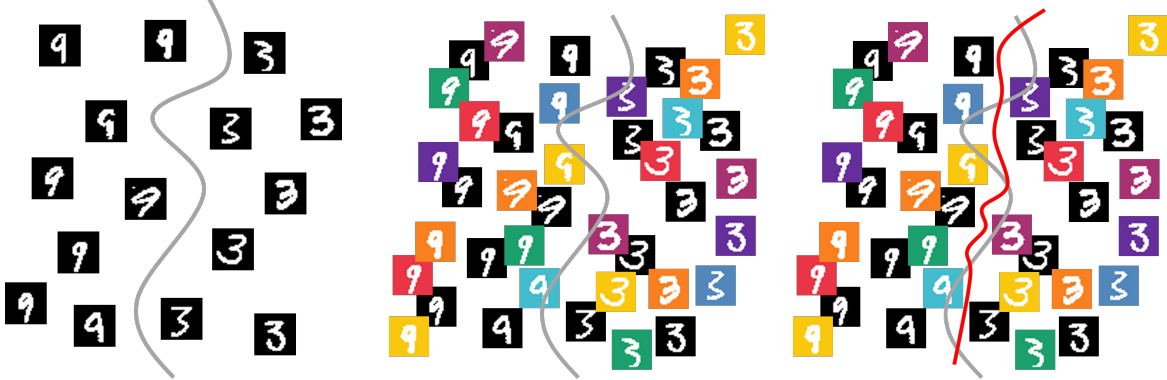
In what follows, we provide a mathematical formulation for the model-based robust training paradigm. This formulation will retain the basic elements of adversarial training described in Section 2. In this sense, we again consider a classification task in which the goal is to train a neural network with weights w to correctly predict the label y of a corresponding input instance x , where $(x, y) \sim \mathcal{D}$. This setting is identical to the setting described in the preamble to equation (2.1).

Our point of departure from the classical adversarial training formulation of (2.2) is in the choice of the so-called adversarial perturbation. In this paper, we assume that the adversary has access to a model of natural variation $G(x, \delta)$, which allows it to transform x into a distinct yet related instance $x' := G(x, \delta)$ by choosing different values of δ from a given *nuisance space* Δ . The goal of our model-based robust training problem is to learn a classifier that achieves high accuracy both on a test set drawn i.i.d. from \mathcal{D} and on *more-challenging* test data that has been subjected to the source of natural variation that G models. In this sense, we are proposing a new training paradigm for deep learning that provides robustness against models of natural variation $G(x, \delta)$.

In order to defend a neural network against such an adversary, we propose the following model-based robust training formulation:

$$\min_w \mathbb{E}_{(x, y) \sim \mathcal{D}} \left[\max_{\delta \in \Delta} \ell(G(x, \delta), y; w) \right]. \quad (3.1)$$

The intuition for this formulation is conceptually similar to that of (2.2). In solving the inner maximization problem, given an instance-label pair (x, y) , the adversary seeks a vector $\delta^* \in$



(a) **MNIST classification.** We begin by showing a classification boundary separating digits with the labels '9' and '3' from the MNIST dataset.

(b) **Natural variation.** Next, we introduce a source of natural variation by changing the background colors of the MNIST digits.

(c) **Robust boundaries.** Given this natural variation, we reclassify the data so that the boundary is robust to changes in background color.

Figure 3: **Model-based robustness paradigm.** We illustrate the essence of the model-based paradigm in the above panels. As shown in (b), the classification boundary used in (a) to separate the MNIST digits is not robust to difference background colors. The objective of model-based training is to learn a boundary that is robust against nuisances like background color, such as the boundary in (c).

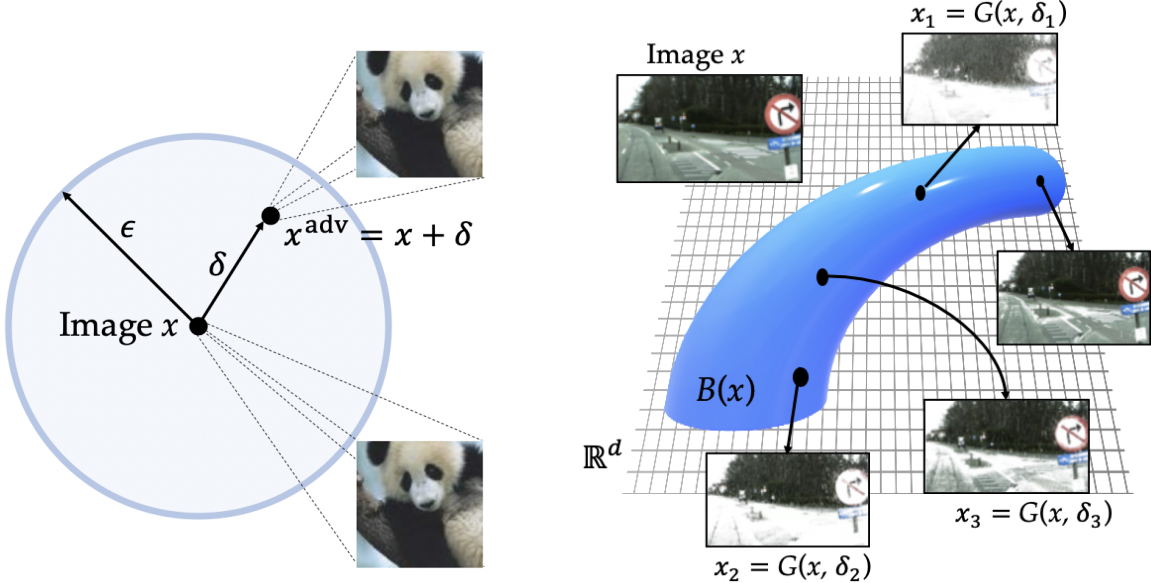
Δ that produces a corresponding instance $x' := G(x, \delta^*)$ which gives rise to high loss values $\ell(G(x, \delta^*), y; w)$ under the current weight w . One can think of this vector δ^* as characterizing the *worst-case* nuisance that can be generated by the model $G(x, \delta^*)$ for the original instance x . After solving this inner maximization problem, we solve the outer minimization problem in which we seek weights w that minimize the risk against the challenging instance $G(x, \delta^*)$. By training the network to correctly classify this worst-case datum, the intuition behind the model-based paradigm is that the neural network should become invariant to the model $G(x, \delta)$ for any $\delta \in \Delta$ and consequently to the original source of natural variation.

The optimization problem posed in (3.1) will be the central object of study in this paper. In particular, we will refer to this problem as the *model-based robust training paradigm*. In Section 4, we describe how to obtain models of natural variation. Then in Section 5 we will show how models of natural variation can be used toward developing robust training algorithms for solving (3.1).

3.3 Geometry of model-based robust training

To provide geometric intuition for the model-based robust training formulation, consider Figure 4. The geometry of the classical perturbation-based adversarial training is captured in Figure 4a, wherein each datum x can be perturbed to any other datum x^{adv} contained in a small ϵ -neighborhood around x . That is, the data can be additively perturbed via $x \mapsto x^{\text{adv}} := x + \delta$ where δ is constrained to lie in a set $\Delta := \{\delta \in \mathbb{R}^d : \|\delta\|_p \leq \epsilon\}$.

Figure 4b shows the geometry of the model-based robust training paradigm. Let us consider a task in which our goal is to correctly classify images of street signs in varying weather conditions. In our model-based paradigm, we are equipped with a model $G(x, \delta)$ of natural variation that can



(a) **Perturbation-based robustness.** In perturbation-based adversarial robustness, an adversary can perturb a datum x into a perceptually similar datum $x^{adv} := x + \delta$. When δ is constrained to lie in a set $\Delta := \{\delta \in \mathbb{R}^d : \|\delta\|_p \leq \epsilon\}$, the underlying geometry of the problem can be used to find worst-case additive perturbations.

(b) **Model-based robustness.** When data can vary with respect to a nonlinear nuisance transformation such as the weather conditions in an image, defenses cannot easily exploit the linearity or geometry of the underlying problem. Indeed, there may be no analytic form for the transformation $G(x, \delta)$ for the transformation from sunny to snowy weather.

Figure 4: **Geometry of adversarial and model-based robustness.** Oftentimes, when a form of natural variation in data can be described by a simple analytic expression, it is possible to take advantage of this form to derive adversarial training algorithms. However, when data can vary according to nonlinear natural or physical phenomena, one must devise different schemes for providing robustness.

naturally vary an image x by changing the nuisance parameter $\delta \in \Delta$. For example, if our data contains images x in sunny weather, the model $G(x, \delta)$ may be designed to continuously vary the weather conditions in the image without changing the scene or the street sign.

More generally, such model-based variations around x have a manifold-like structure and belong to $B(x) := \{x' \in \mathbb{R}^d : x' = G(x, \delta) \text{ for some } \delta \in \Delta\}$. Note that in many models of natural variation, the dimension of model parameter $\delta \in \Delta$, and therefore the dimension of manifold $B(x)$, will be significantly lower than the dimension of data $x \in \mathbb{R}^d$. In other words, $B(x)$ will be comprised of submanifolds around x in the data space \mathbb{R}^d .

One subtle underlying assumption in the classical adversarial robustness formulation for classification tasks is that the additive perturbation $x + \delta$ must preserve the label y of the original datum x . For instance, in Figure 4, it is essential that the mapping $x \mapsto x + \delta$ where $\|\delta\|_p \leq \epsilon$ produces an example $x^{adv} = x + \delta$ which has the same label as x . Similarly, in this paper we restrict our attention to models $G(x, \delta)$ that preserve the semantic label of the input datum x for any $\delta \in \Delta$. In other words, we focus on models $G(x, \delta)$ that can naturally vary data x using nuisance parameter

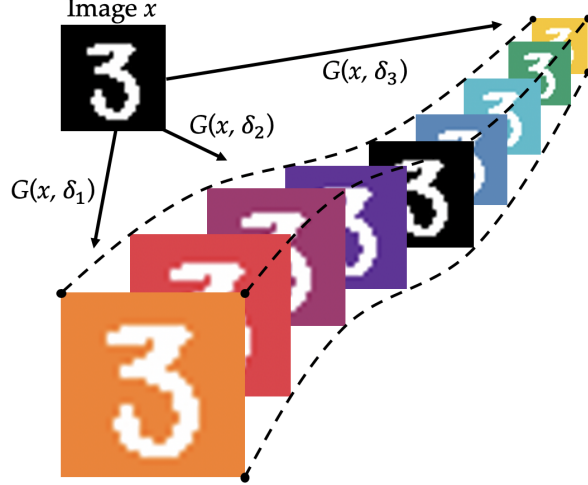


Figure 5: **Known models of natural variation.** In a variety of cases, a model of how data varies in a robustness problem is known a priori. In these cases, the model can immediately be exploited in our model-based training paradigm. As we will show in Section 6, a known model of how background colors change for the MNIST digits can be leveraged for model-based training.

δ (e.g. weather conditions, contrast, background color) while leaving the label of the original datum unchanged. In Figure 4b, this corresponds to all points $x' \in B(x)$ with varying snowy weather having the same label y as the original input datum x .

4 Models of Natural Variation

Our model-based robustness paradigm of (3.1) critically relies on the existence of a model $x \mapsto G(x, \delta) := x'$ that describes how a datum x can be perturbed to x' by the choice of a *nuisance parameter* $\delta \in \Delta$. In this section, we consider cases in which (1) the model G is known a priori, and (2) the model G is unknown and therefore must be learned offline. In this second case in which models of natural variation must be learned from data, we propose a formulation for obtaining these models.

4.1 Known models $G(x, \delta)$ of natural variation

In many problems, the model $G(x, \delta)$ is known a priori and can immediately be exploited in our robust training formulation. One direct example in which a model of natural variation $G(x, \delta)$ is known is the classical adversarial training paradigm described by equation (2.2). Indeed, by inspecting equations (2.2) and (3.1), we can immediately extract the well-known norm-bounded adversarial model

$$G(x, \delta) = x + \delta \quad \text{for } \delta \in \Delta := \{\delta \in \mathbb{R}^d : \|\delta\|_p \leq \epsilon\}. \quad (4.1)$$

The above example of a known model shows that in some sense the perturbation-based adversarial training paradigm of equation (2.2) is a special case of the model-based robust training formulation

(3.1) when $G(x, \delta) = x + \delta$. Of course, for this choice of adversarial perturbations there is a plethora of robust training algorithms [22, 23, 24, 25, 26, 27, 28].

Another example of a known model of natural variation is shown in Figure 5. Consider a scenario where we would like to be robust to background color changes in the MNIST dataset. This would require having a model $G(x, \delta)$ that takes an MNIST digit x as input and reproduces the same digit but with various colorized RGB backgrounds which correspond to different values of $\delta \in \Delta$. This model is relatively simple to describe and can be found in Appendix A.1.1. In Section 6, we will use this known model of natural variation to train deep networks to be robust to changes in background color.

Moreover, there are many problems in which naturally-occurring variation in the data has structure that is known a priori. For example, in image classification tasks there are usually intrinsic geometric structures that identify how data can be rotated, translated, or scaled. Geometric models for rotating an image along a particular axis can be characterized by a one-dimensional angular parameter δ . In this case, a known model of natural variation for rotation can be described by

$$G(x, \delta) = R(\delta)x \quad \text{for } \delta \in \Delta := [0, 2\pi). \quad (4.2)$$

where $R(\delta)$ is a rotation matrix. Such geometric models can facilitate adversarial distortions of images using a low dimensional parameter δ . In prior work, this idea has been exploited to train neural networks to be robust to rotations of the data around a given axis [41, 42, 43].

More generally, geometric and spatial transformations have been explored in the field of computer vision in the development of *equivariant* neural network architectures. In many of these studies, one considers a transformation $T : \mathbb{R}^d \times \Delta \rightarrow \mathbb{R}^d$ where Δ has a group structure. By definition, we say that a function f is equivariant with respect to T if $f(T(x, \delta)) = T(f(x), \delta)$ for all $\delta \in \Delta$. That is, applying T to an input x and then applying f to the result is equivalent to applying T to $f(x)$. In contrast to the equivariance literature in computer vision, much of the adversarial robustness community has focused on what is often called *invariance*. A function f is said to be invariant to T if $f(T(x, \delta)) = f(x)$ for any $\delta \in \Delta$, meaning that transforming an input x by T has no impact on the output. This has prompted significant research toward designing neural networks that are equivariant to such transformations of data [6, 7, 44, 45, 46]. Recently, this has been extended to leveraging group convolutions, which can be used to provide equivariance with respect to certain symmetric groups [47] and to permutations of data [48].

In our context, these structured transformations of data $T : \mathbb{R}^d \times \Delta \rightarrow \mathbb{R}^d$ can be viewed as models of natural variation by directly setting $G(x, \delta) = T(x, \delta)$ where Δ may have additional group structure. While previous approaches exploit such transformations for designing deep network architectures that respect this structure, our goal is to exploit such known structures toward developing robust training algorithms.

Altogether, these examples show that for a variety of problems, *known models* can be used to analytically describe how data changes. Such models typically take a simple form according to underlying geometric or physical laws. In such cases, a known model can be exploited for robust training as has been done in the past literature. In the context of known models, our model-based approach offers a more general framework that is *model-agnostic* in the sense that it is applicable to all such models of how data varies. As shown above, in some cases, our model-based formulation also recovers several well-known adversarial robustness formulations. More importantly, the generality of our approach enables us to pursue model-based robust training even when a model $G(x, \delta)$ is *not known a priori*. This is indeed the case in the context of natural variation in images due

to nuisances such as lighting, snow, rain, decolorization, haze, and many others. For such problems, in the next section we will show how to learn models of natural variation $G(x, \delta)$ from data.

4.2 Learning unknown models of natural variation $G(x, \delta)$ from data

While geometry and physics may provide known analytical models that can be exploited toward robust training of neural networks, in many situations such models are not known or are too costly to obtain. For example, consider Figure 4b in which a model of natural variation $G(x, \delta)$ describes the impact of adding snowy weather to an image x . In this case, the transformation $G(x, \delta)$ takes an image x of a street sign in sunny weather and maps it to an image $x' := G(x, \delta)$ in snowy weather. Even though there is a relationship between the snowy and the sunny images, obtaining a model G relating the two images is extremely challenging if we resort to physics or geometric structure. For such problems with unknown models we advocate for *learning* the model $G(x, \delta)$ from data *prior to* model-based robust training. That is, we propose first learning a model of natural variation $G(x, \delta)$ offline using some previously collected data; following this process, we will use the learned model to perform robust training on a new and possibly different data set.

In order to learn¹ an unknown model $G(x, \delta)$, we assume that we have access to two unpaired image domains A and B that are drawn from a common dataset or distribution. In our setting, domain A contains the original data, such as the image of the traffic sign in sunny weather in Figure 2, and domain B contains data transformed by the underlying natural phenomena. For instance, the data in domain B may contain images of street signs in snowy weather. We emphasize that the domains A and B are unpaired, meaning that it may not be possible to select an image of a traffic sign in sunny weather from domain A and find a corresponding image of that same street sign in the same scene with snowy weather in domain B . Our approach toward formalizing the idea of learning $G(x, \delta)$ from data is to view G as a mechanism that transforms the distribution of data in domain A so that it resembles the distribution of data in domain B . More formally, let \mathbb{P}_A and \mathbb{P}_B be the data distributions corresponding to domains A and B respectively. Our objective is to find a mapping G that takes as input a datum $x \sim \mathbb{P}_A$ and a nuisance parameter $\delta \in \Delta$ and then produces a new datum $x' \sim \mathbb{P}_B$. Statistically speaking, the nuisance parameter δ represents the extra randomness or variation required to generate x' from x . For example, when considering images with varying weather conditions, the randomness in the nuisance might control whether an image of a sunny scene is mapped to a corresponding image with a dusting of snow or to an image in an all-out blizzard. In this way, we without loss of generality we assume that the nuisance parameter is independently generated from a simple distribution \mathbb{P}_Δ (e.g. uniform or Gaussian) to represent the extra randomness required to generate x' from x .² Using this formalism, we can view $G(\cdot, \cdot)$ as a mapping that transforms the distribution $\mathbb{P}_A \times \mathbb{P}_\Delta$ into the distribution \mathbb{P}_B . More specifically, G pushes forward the measure $\mathbb{P}_A \times \mathbb{P}_\Delta$, which is defined over $A \times \Delta$, to \mathbb{P}_B , which is defined over B . That is, $\mathbb{P}_B = G \# (\mathbb{P}_A \times \mathbb{P}_\Delta)$, where $\#$ denote the push-forward measure.

Now in order to learn a model of natural variation G , we consider a parametric family of models $\mathcal{G} := \{G_\theta : \theta \in \Theta\}$ defined over a parameter space $\Theta \subset \mathbb{R}^m$. We can express the problem of learning a model of natural variation G_{θ^*} parameterized by $\theta^* \in \Theta$ that best fits the above formalism in the

¹In this section we describe one specific approach to learn G . Indeed, exploring other approaches is an important future direction—see Section 9.

²The role of the nuisance parameter is similar to the role of the noise variable in generative adversarial networks [49].

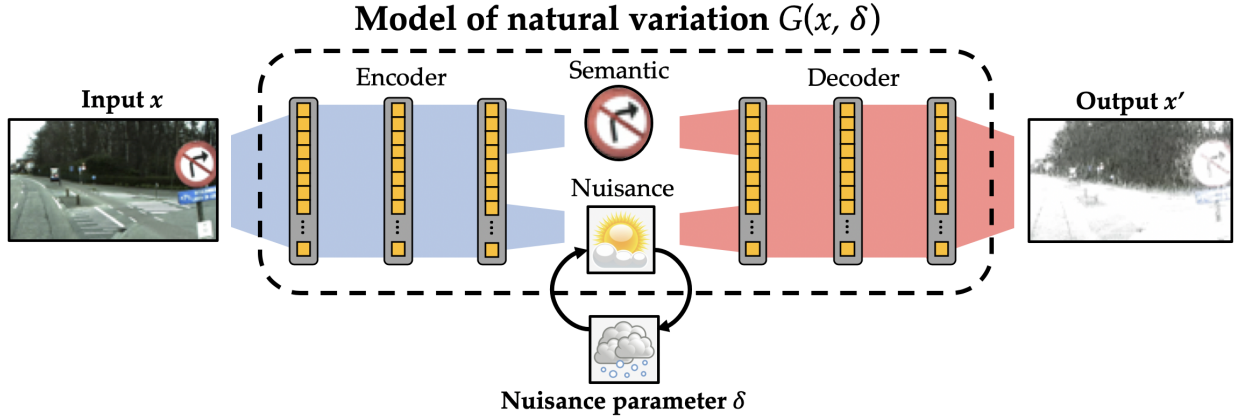


Figure 6: **Learning unknown models of natural variation.** In the case when a model of natural variation is not explicitly known, it is still possible to learn a suitable model from data. For image data, we choose to exploit breakthroughs in style-transfer and generative modeling as a framework for learning $G(x, \delta)$ from data. Many such architectures use an encoder-decoder network structure, in which an encoding network learns to separate *semantic* from *nuisance* content in two latent spaces, and the decoder learns to reconstruct an image from the representations in these latent spaces [4, 52].

following way:

$$\theta^* = \arg \min_{\theta \in \Theta} d(\mathbb{P}_B, G_\theta \# (\mathbb{P}_A \times \mathbb{P}_\Delta)). \quad (4.3)$$

Here $d(\cdot, \cdot)$ is an appropriately-chosen distance metric that measures the distance between two probability distributions (e.g. the KL-divergence, total variation, Wasserstein distances, etc.). This formulation has received broad interest in the machine learning community thanks to the recent advances in generative modeling. In particular, in the fields of image-to-image translation and style-transfer, learning mappings between unpaired image domains is a well-studied problem [4, 50, 51]. In the next subsection, we will show how the breakthroughs in these fields can be used to learn a model of natural variation G that approximates underlying natural phenomena.

4.3 Using deep generative models to learn models of natural variation for images

Recall that in order to learn a model of natural variation from data, we aim to solve (4.3) and consequently discover a model G_{θ^*} that transforms $x \sim \mathbb{P}_A$ into corresponding samples $x' \sim \mathbb{P}_B$. Importantly, a number of methods have been designed toward achieving this goal. In the fields of image-to-image translation, such methods include CycleGAN [2], DualGAN [51], Augmented CycleGAN [53], BicycleGAN [50], CVAE [52], UNIT [54], and MUNIT [4]. Among these methods, CVAE, BicycleGAN, Augmented CycleGAN, and MUNIT seek to learn *multimodal* mappings that disentangle the *semantic content* of a datum (i.e. its label or the characterizing component on the image) from the *nuisance content* (e.g. background color, weather conditions, etc.) by solving the statistical problem of (4.3). We highlight these methods because learning a multimodal mapping is a concomitant property toward learning models that can produce images with *varying* nuisance content. To this end, in this paper we will predominantly use MUNIT, which stands for

Unsupervised Multimodal Image-to-Image Translation, to learn models of natural variation. For completeness, we provide a complete characterization of the MUNIT model and the hyperparameters we used for MUNIT in Appendix E.

At its core, MUNIT combines two autoencoding networks and two generative adversarial networks (GANs) to learn two mappings: one that maps images from domain A to corresponding images in B and one that maps in the other direction from B to A . For the purposes of this paper, we will only exploit the mapping from A to B , although one direction for future work is to incorporate both mappings. For the remainder of this section, we will let G denote this mapping from A to B . In essence, the map $G : A \times \Delta \rightarrow B$ learned in the MUNIT framework can be thought of as taking as input an image $x \in A$ and a nuisance parameter $\delta \in \Delta$ and outputting an image $x' \in B$ that has the same semantic content as the input image x but that has different nuisances.

In Table 1, we show images from several datasets and corresponding images generated by models of natural variation learned using the MUNIT framework. Each of these learned models of natural variation corresponds to a different source of natural variation. In each of these models, we used a two dimensional latent space $\Delta \subset \mathbb{R}^2$ and generated the output images by sampling different values from Δ . Throughout the paper, we will let \mathbb{P}_Δ be a standard normal Gaussian distribution $\mathcal{N}(0, I)$.

In the next section, we will begin by assuming that a model of natural variation $G(x, \delta)$ is given – whether G is a known model or G has been learned from data – and then show how G can be leveraged toward formulating model-based robust training algorithms.

5 Model-based robust training algorithms

In the previous section, we described a procedure that can be used to obtain a model of natural variation $G(x, \delta)$. In some cases, such models may be *known a priori* while in other cases such models may be *learned* offline from data. Regardless of their origin, we will now assume that we have access to a suitable model $G(x, \delta)$ and shift our attention toward exploiting G in the development of novel robust training algorithms for neural networks.

To begin, recall the optimization-based formulation of (3.1). Given a model G , (3.1) is a nonconvex-nonconcave min-max problem, and is therefore difficult to solve exactly. We will therefore resort to approximate methods for solving this challenging optimization problem. To elucidate our approach for solving (3.1), we first characterize the problem in the finite-sample setting. That is, rather than assuming access to the full joint distribution $(x, y) \sim \mathcal{D}$, we assume that we are given a finite number of samples $\mathcal{D}_n := \{(x^{(j)}, y^{(j)})\}_{j=1}^n$ distributed i.i.d. according to the true data distribution \mathcal{D} . The empirical version of (3.1) in the finite-sample setting can be expressed in the following way:

$$\min_w \frac{1}{n} \sum_{j=1}^n \left[\max_{\delta \in \Delta} \ell \left(G \left(x^{(j)}, \delta \right), y^{(j)}; w \right) \right]. \quad (5.1)$$

Concretely, we search for the parameter w that induces the smallest empirical error while each sample $(x^{(j)}, y^{(j)})$ is varied according to $G(x^{(j)}, \delta)$. In particular, while subjecting each datum $(x^{(j)}, y^{(j)})$ to the source of natural variation modeled by G , we search for nuisance parameters $\delta \in \Delta$ so as to train the classifier on the most challenging natural conditions.

When the learnable weights w parameterize a neural network f_w , the outer minimization problem and the inner maximization problem are inherently nonconvex and nonconcave respectively.

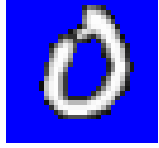
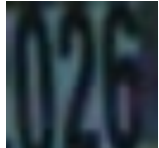
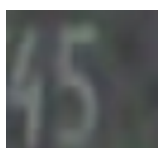
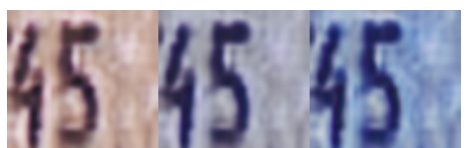
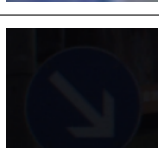
Dataset	Natural Variation	Images		
		Original	Generated	
MNIST	Background color			
SVHN	Brightness			
	Contrast			
	Hue			
GTSRB	Contrast			

Table 1: **Models of natural variation.** For a range of datasets, we show images generated by passing data through learned models of natural variation. Each of these datasets – MNIST [55], SVHN [56], and GTSRB [57] – are well-known image-classification benchmarks.

Therefore, we will rely on zeroth- and first-order optimization techniques for solving this problem to a locally optimal solution. We will propose three algorithmic variants: (1) *Model-based Robust Training* (MRT), (2) *Model-based Adversarial Training* (MAT), and (3) *Model-based Data Augmentation* (MDA). At a high level, each of these methods involves augmenting the original training set \mathcal{D}_n with new data generated by the model of natural variation G . Past approaches have used similar adversarial [22] and statistical [58] augmentation techniques. However, the main differences between the past work and our algorithms concern how our algorithms exploit models of natural variation G to generate new data. In particular, MRT randomly queries G to generate several new data points and then selects those generated data that induce the highest loss in the inner-maximization problem. On the other hand, MAT employs a gradient-based search in the nuisance space Δ to find loss-maximizing generated data. Finally, MDA augments the training set with generated data by sampling randomly in Δ . We now describe each algorithm in detail.

Algorithm 1 Model-based Robust Training (MRT)

Input: data sample $\mathcal{D}_n = \left\{ \left(x^{(j)}, y^{(j)} \right) \right\}_{j=1}^n$, model G , weight initialization w , parameter $\lambda \in [0, 1]$, number of steps k , batch size $m \leq n$
Output: learned weight w

```

1: repeat
2:   for minibatch  $B_m := \left\{ \left( x^{(1)}, y^{(1)} \right), \left( x^{(2)}, y^{(2)} \right), \dots, \left( x^{(m)}, y^{(m)} \right) \right\} \subset \mathcal{D}_n$  do
3:
4:   Initialize  $max\_loss \leftarrow 0$ 
5:   Initialize  $\delta_{\text{adv}} := (\delta_{\text{adv}}^{(1)}, \delta_{\text{adv}}^{(2)}, \dots, \delta_{\text{adv}}^{(m)}) \leftarrow (0_q, 0_q, \dots, 0_q)$ 
6:   for  $k$  steps do
7:     Sample  $\delta^{(j)}$  randomly from  $\Delta$  for  $j = 1, \dots, m$ 
8:      $current\_loss \leftarrow \sum_{j=1}^m \ell \left( G \left( x^{(j)}, \delta^{(j)} \right), y^{(j)}; w \right)$ 
9:     if  $current\_loss > max\_loss$  then
10:       $max\_loss \leftarrow current\_loss$ 
11:       $\delta_{\text{adv}}^{(j)} \leftarrow \delta^{(j)}$  for  $j = 1, \dots, m$ 
12:    end if
13:   end for
14:
15:    $g \leftarrow \nabla_w \sum_{j=1}^m \left[ \ell \left( G \left( x^{(j)}, \delta_{\text{adv}}^{(j)} \right), y^{(j)}; w \right) + \lambda \cdot \ell \left( x^{(j)}, y^{(j)}; w \right) \right]$ 
16:    $w \leftarrow \text{Update}(g, w)$ 
17: end for
18: until convergence

```

5.1 Model-based Robust Training (MRT)

In general, solving the inner maximization problem in (5.1) is difficult and motivates the need for methods that yield approximate solutions. In this vein, one simple scheme is to sample different values of the nuisance parameter $\delta \in \Delta$ for each instance-label pair $(x^{(j)}, y^{(j)})$ and among those sampled values, find the nuisance parameter δ^{adv} that gives the highest empirical loss under G . Indeed, this approach is not designed to find an exact solution to the inner maximization problem; rather it aims to find a difficult example by sampling in the nuisance space of the model.

Once we obtain this difficult example via sampling in Δ , the next objective is to solve the outer minimization problem. The procedure we propose in this paper for solving this problem amounts to using the worst-case nuisance parameter δ^{adv} obtained via the inner maximization problem to perform data-augmentation. That is, for each instance-label pair $(x^{(j)}, y^{(j)})$, we treat $(G(x^{(j)}, \delta_{\text{adv}}^{(j)}), y^{(j)})$ as a new instance-label pair that can be used to supplement the original dataset \mathcal{D}_n . These training data can be used together with first-order optimization methods to solve the outer minimization problem to a locally optimal solution w^* .

Algorithm 1 contains the pseudocode for this model-based robust training approach. In particular, in lines 4-13, we search for a difficult example by sampling in Δ and picking the parameter

Algorithm 2 Model-based Adversarial Training (MAT)

Input: data sample $\mathcal{D}_n = \left\{ \left(x^{(j)}, y^{(j)} \right) \right\}_{j=1}^n$, model G , weight initialization w ,
 parameter $\lambda \in [0, 1]$, number of steps k , batch size $m \leq n$
Output: learned weight w

```

1: repeat
2:   for minibatch  $B_m := \left\{ \left( x^{(1)}, y^{(1)} \right), \left( x^{(2)}, y^{(2)} \right), \dots, \left( x^{(m)}, y^{(m)} \right) \right\} \subset \mathcal{D}_n$  do
3:   Initialize  $\delta_{\text{adv}} := (\delta_{\text{adv}}^{(1)}, \delta_{\text{adv}}^{(2)}, \dots, \delta_{\text{adv}}^{(m)}) \leftarrow (0_q, 0_q, \dots, 0_q)$ 
4:   for  $k$  steps do
5:      $g \leftarrow \nabla_{\delta_{\text{adv}}} \sum_{j=1}^m \ell \left( G \left( x^{(j)}, \delta_{\text{adv}}^{(j)} \right), y^{(j)}; w \right)$ 
6:      $\delta_{\text{adv}} \leftarrow \Pi_{\Delta} \left[ \delta_{\text{adv}} + \alpha g \right]$ 
7:   end for
8:
9:    $g \leftarrow \nabla_w \sum_{j=1}^m \left[ \ell \left( G \left( x^{(j)}, \delta_{\text{adv}}^{(j)} \right), y^{(j)}; w \right) + \lambda \cdot \ell \left( x^{(j)}, y^{(j)}; w \right) \right]$ 
10:   $w \leftarrow \text{Update}(g, w)$ 
11: end for
12: until convergence

```

$\delta^{\text{adv}} \in \Delta$ that induces the highest empirical loss. Then in lines 15-16, we calculate a stochastic gradient of the loss with respect to the model parameter; we then use this gradient to update the model parameter using a first-order method. There a number of potential algorithms for this Update function in line 16, including stochastic gradient descent (SGD), Adam [59], and Adadelta [60].

Throughout the experiments in the forthcoming sections, we will train classifiers via MRT with different values of k . In this algorithm, k controls the number of data points we consider when searching for a loss-maximizing datum. To make clear the role of k in this algorithm, we will refer to Algorithm 1 as MRT- k when appropriate.

5.2 Model-based Adversarial Training (MAT)

At first look, the sampling-based approach used by MRT may not seem as powerful as a first-order (i.e. gradient-based) adversary that has been shown to be effective at improving the robustness of trained classifiers [61] against norm-bounded, perturbation-based attacks. Indeed, it is natural to extend the ideas encapsulated in this previous work that advocate for first-order adversaries to this model-based setting. That is, under the assumption that our model of natural variation $G(x, \delta)$ is differentiable, in principle we can use projected gradient ascent (PGA) in the nuisance space $\Delta \subset \mathbb{R}^q$ of a given model to solve the inner maximization problem. This idea motivates the formulation of our second algorithm, which we call Model-based Adversarial Training (MAT).

In Algorithm 2, we present pseudocode for MAT. Notably, by ascending the stochastic gradient with respect to δ_{adv} in lines 4-8, we seek a nuisance parameter δ_{adv}^* that maximizes the empirical

Algorithm 3 Model-Based Data Augmentation (MDA)

Input: data sample $\mathcal{D}_n = \left\{ \left(x^{(j)}, y^{(j)} \right) \right\}_{j=1}^n$, model G , weight initialization w ,
 parameter $\lambda \in [0, 1]$, number of steps k , batch size $m \leq n$
Output: learned weight w

```

1: repeat
2:   for minibatch  $B_m := \left\{ \left( x^{(1)}, y^{(1)} \right), \left( x^{(2)}, y^{(2)} \right), \dots, \left( x^{(m)}, y^{(m)} \right) \right\} \subset \mathcal{D}_n$  do
3:
4:   Initialize  $x_i^{(j)} \leftarrow 0_d$  for  $i = 1, \dots, k$  and for  $j = 1, \dots, m$ 
5:   for  $k$  steps do
6:     Sample  $\delta^{(j)}$  randomly from  $\Delta$  for  $j = 1, \dots, m$ 
7:      $x_i^{(j)} \leftarrow G(x^{(j)}, \delta^{(j)})$  for  $j = 1, \dots, m$ 
8:   end for
9:
10:   $g \leftarrow \nabla_w \sum_{j=1}^m \left[ \sum_{i=1}^k \ell \left( x_i^{(j)}, y^{(j)}; w \right) + \lambda \cdot \ell \left( x^{(j)}, y^{(j)}; w \right) \right]$ 
11:   $w \leftarrow \text{Update}(g, w)$ 
12: end for
13: until convergence

```

loss. In particular, in line 7 we perform the update step of PGA to obtain δ_{adv} ; in this notation, Π_Δ denotes the projection onto the set Δ . However, performing PGA until convergence at each iteration leads to a very high computational complexity. Thus, at each training step, we perform k steps of projected gradient ascent. Following this procedure, we use this loss-maximization nuisance parameter δ_{adv}^* to augment \mathcal{D}_n with data subject to worst-case nuisance variability. The update step is then carried out by computing the stochastic gradient of the loss over the augmented training sample with respect to the learnable weights w in line 10. Finally, we update w in line 11 in a similar fashion as was done in the description of the MRT algorithm.

An empirical analysis of the performance of MAT will be given in Section 6. To emphasize the role of the number of gradient steps k used to find a loss maximizing nuisance parameter $\delta_{\text{adv}}^* \in \Delta$, we will often refer to Algorithm 2 as MAT- k .

5.3 Model-based Data Augmentation (MDA)

Both MRT and MAT adhere to the common philosophy of selecting loss-maximizing, model-generated data to augment the original training dataset \mathcal{D}_n . That is, in keeping with the min-max formulation of (3.1), both of these methods search *adversarially* over Δ to find challenging natural variation. More specifically, for each data point $(x^{(j)}, y^{(j)})$, these algorithms select $\delta \in \Delta$ such that $G(x^{(j)}, \delta) =: x_{\text{adv}}^{(j)}$ maximizes the loss term $\ell(x_{\text{adv}}^{(j)}, y^{(j)}; w)$. The guiding principle behind these methods is that by showing the neural network these challenging, model-generated data during training, the trained neural network will be able to robustly classify data over a wide spectrum of natural variations.

Another interpretation of (3.1) is as follows. Rather than taking an adversarial point of view in

which we expose neural networks to the most challenging model-generated examples, an intriguing alternative is to expose these networks to a *diversity* of model-generated data during training. In this approach, by augmenting \mathcal{D}_n with model-generated data corresponding to a wide range of natural variations $\delta \in \Delta$, one might hope to achieve higher levels of robustness with respect to a given model of natural variation $G(x, \delta)$.

This idea motivates the third and final algorithm, which we call Model-based Data Augmentation (MDA). The pseudocode for this algorithm is given in Algorithm 3. Notably, rather than searching adversarially over Δ to find model-generated data subject to worst-case (i.e. loss-maximizing) natural variation, in lines 4-8 of MDA we randomly sample in Δ to obtain a diverse array of nuisance parameters. For each such nuisance parameter, we augment \mathcal{D}_n with a new datum and calculate the stochastic gradient with respect to the weights w in line 10 using both the original dataset \mathcal{D}_n and these diverse augmented data.

In MDA, the parameter k controls the number of model-based data points per data point in \mathcal{D}_n that we append to the training set. To make this explicit, we will frequently refer to Algorithm 3 as MDA- k .

6 Experiments

In this section, we demonstrate the broad applicability of our model-based robust deep learning framework by presenting experiments over a range of datasets. The experiments reveal that our framework is not only applicable across many datasets but also improves robustness with respect to many models of natural variation. However before proceeding to these results, we first present our deep network architectures, data sets, and baseline approaches that will be used throughout the experiments.

Neural network architectures and hyperparameters. For each of the experiments we present, a model of natural variation G will either be known a priori or we will learn G from data before training f . When we learn G from data, we use the MUNIT architecture which we described in Section 4. We note that other architectural choices for learning G are possible and will be explored in future work. Once the model of natural variation G has been obtained, it will be treated as if it is known. Accordingly, we will use this model to perform model-based robust training using the three algorithms we introduced in Section 5: MRT, MAT, and MDA.

Throughout these experiments, we fix the architecture of the convolutional neural network (CNN) used for the classifier. In particular, we use a network with two convolutional layers and two fully-connected layers with max-pooling [62], dropout [63], and ReLU activations [64]. In Section 7, we explore the impact of varying the architecture of the classifier used for model-based training. All classifiers used in these experiments were trained with the Adadelta optimizer [60] with an initial learning rate of 1.0 and a mini-batch size of 64. We also used a trade-off parameter of $\lambda = 1$ for each of the model-based algorithms. More information about hyperparameter and architecture selection are given in Appendix E.

Datasets and domains. Throughout this section, we consider a wide range of datasets, including MNIST [55], SVHN [56], GTSRB [57], CURE-TSR [34], MNIST-m [65], Fashion-MNIST [66], EMNIST [67], KMNIST [68], QMNIST [69], and USPS [70]. For many of these datasets, we extract subsets corresponding to different factors of natural variation; henceforth, we will call these subsets *domains*.

Details concerning how we curated these domains can be found in Appendix D.

Note that each domain we use in this paper contains a training set and a test set. While both the training and test set come from the same distribution, neither the models of natural variation nor the classifiers have access to the test data from any domain during the training phase. More explicitly, we emphasize that when learning models of natural variation G and training classifiers f , we used data from the *training set* of the relevant domains. Conversely, when testing the classifiers, we used data from the *test set* of the relevant domains.

Baseline algorithms. In order to benchmark the robustness and accuracy of our model-based approach, we compare our model-based training algorithms of Section 5 against two training paradigms: standard training of deep networks without any robustness considerations and adversarial training using the norm-based model of data perturbation. In the first approach, we train classifiers using batched first-order optimization techniques; we refer to these classifiers as *Vanilla* classifiers. In the second approach, we adversarially train classifiers using PGD [22], which is known to be one of the strongest defenses in the perturbation-based adversarial robustness setting. In particular, we used a perturbation budget of $\epsilon = 0.3$, a step size of 0.01, and we performed twenty steps of gradient ascent per batch. We refer to these classifiers in the figures as PGD.

It should be noted that these baseline algorithms were not designed from the outset to address the notion of robustness against models of natural variation considered in this paper. Therefore such comparisons need to be appropriately contextualized as these algorithms provide defenses in different contexts. That said, such algorithms are widely used as the main robust training paradigm across numerous datasets and challenges. In other words, in comparing against these baselines our goal is to show the robustness of our model-based training paradigm across many novel forms of natural variation that are not explicitly considered by these baseline paradigms. As such, we aim to show the broad effectiveness of our model-based paradigm in a model-agnostic manner against other training paradigms that focus on a different notion of robustness.

Experimental overview. The experiments presented in this section are broadly divided into three categories. In what follows, we give a short summary of each of the three kinds of experiments.

In Section 6.1, we show that for a range of datasets and various nuisances, we can effectively exploit both known and learned models of natural variation in order to provide significant robustness improvements against challenging sources of natural variation. These experiments offer a convincing demonstration that classifiers trained using our model-based paradigm provide meaningful robustness across datasets and across models of natural variation.

In Section 6.2, we demonstrate the reusability and modularity of models of natural variation with respect to performing model-based robust training on multiple datasets. In particular, we show how a model of natural variation learned from one dataset \mathcal{D} can be reused for model-based robust training of classifiers on a new dataset \mathcal{D}' . These experiments demonstrate that once an efficacious model of natural variation has been learned, that model can be reused on similar datasets, resulting in robust classifiers for different datasets. Furthermore, we demonstrate that models of natural variation are composable, meaning that models of natural variation can be combined in a modular fashion to provide robustness against multiple nuisances.

Finally, in Section 6.3, we consider a challenging scenario in which we train classifiers using our model-based framework on datasets containing low levels of natural variation and test them on datasets with higher levels of natural variation. Across various challenging nuisances, these experiments demonstrate that it is possible to provide robustness against challenging nuisances

that neither the model nor the classifier has seen during training.

In the remainder of this section, each subsection will present representative results corresponding to the experiments described above. We also provide tables containing of all of the results obtained in this work and invite the reader to see the Appendices for a complete characterization of these results.

6.1 Experiments with one dataset

As described in Section 4, models of natural variation can be obtained in two ways. If an explicit model is known *a priori*, such as in the perturbation-based adversarial robustness setting, it can be directly exploited in our model-based framework. On the other hand, if one does not have access to a model G corresponding to a given nuisance, one can leverage the methods described in Section 4 to learn a suitable model G . In either case, once a model has been obtained, the next step in the model-based paradigm is to leverage this model using the model-based algorithms we presented in Section 5.

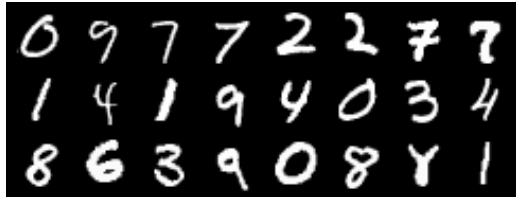
Consider a setting in which we have access to a single dataset \mathcal{D} of instance-label pairs which is divided into two subsets, called *domains*, A and B . These subsets are curated to encode a particular form of natural variation. For example, for a dataset of images of traffic signs, domain A may contain images of signs taken during the day and B may contain images of signs taken at night. In the case of a known model G , we directly train each classifier with data from domain A ; the model-based classifiers also train on data that has been passed through the known model G . We then test each classifier on data from the test set of domain B . In the case of an unknown model, we first learn a model $G : A \times \Delta \rightarrow B$ that maps samples from domain A into domain B . Then, after obtaining this model, we train all classifiers on samples from domain A . By leveraging such models of natural variation that can translate images from domain A into domain B , we seek to show that our model-based paradigm results in improved performance with respect to the source of natural variation modeled by G .

6.1.1 MNIST: robustness to background color

To begin, we consider a known model of natural variation on the well-known MNIST dataset [55], which is a standard benchmark for machine learning algorithms. Notably, it has been observed that classifiers trained on RGB-image datasets often overfit to various nuisances such as background color [36]; indeed several works seek to remove biases induced by such nuisances by resampling methods [71]. As a first step in demonstrating the efficacy of the approach outlined in this paper, we use a known model G to change the background color of the original (grayscale) MNIST dataset. Pseudocode for this known model is given in Appendix A.1.1.

To this end, we let domain A contain the original MNIST dataset. Next, we change the background colors of the MNIST digits to form domain B using the known model G . Samples from domains A and B are shown in Figures 7a and 7b respectively. In this case, we let $\Delta := [0, 1]^3 \subset \mathbb{R}^3$.

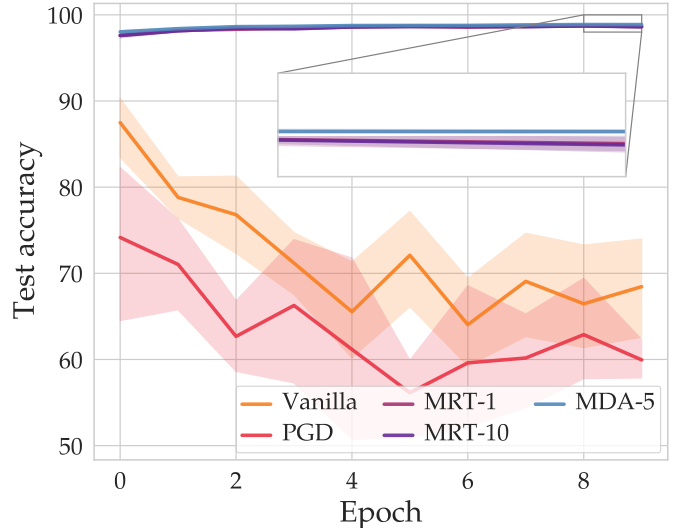
Figure 7c shows that the test accuracy of the baseline classifiers falls as they are trained. This indicates that these classifiers overfit to the background color, as they are unable to effectively recognize the same digits with different background colors. On the other hand, the classifiers that leverage the known model G achieve greater than 99% test accuracy on the samples with varying background colors. In this way, classifiers trained using the model-based paradigm retain high levels of robustness to the entire RGB spectrum of background colors. Note that as this known



(a) **Training data.** Domain A contained samples from the original (grayscale) MNIST dataset.



(b) **Test data.** Domain B consisted of the MNIST digits with randomly selected background colors.



(c) **Results.** Classifiers trained with the model-based algorithms achieved greater than 99% test accuracy on samples from domain B , whereas the baseline classifiers both dropped below 70% test accuracy.

Figure 7: Robustness to background colors on MNIST. On the well-known MNIST dataset, we examine the impact of the background color on classification accuracy. In particular, by leveraging a known model of background colors, we show that our model-based algorithms yield significant improvements over the baseline classifiers. In this case, all model-based approaches have nearly identical test accuracies.

model is non-differentiable, we did not include test accuracies corresponding to classifiers trained with MAT in Figure 7c.

6.1.2 SVHN: robustness to contrast

Next, we consider a slightly more difficult classification problem on the Street View House Numbers (SVHN) dataset [56]. Three-channel RGB datasets like SVHN contain a wide range of diversity with respect to several important sources of natural variation. Among these challenges, contrast is one of the most apparent. In Figure 8a and 8b, we show the contrast discrepancy in the SVHN dataset. Details concerning how we curated these data subsets are left to Appendix D. In particular, in Figure 48 we show the full distribution of contrast for SVHN.

To explore the impact that changes in contrast have on the performance of trained classifiers, we took domain A to be images from SVHN with low contrast and domain B to be images with high contrast. To this end, we first use the approach in Section 4 to learn a model $G : A \times \Delta \rightarrow B$ that changes the contrast of the images from A to resemble those in B . The learned model G is then used in our model-based robust training algorithms to engender classifiers that are robust to contrast variation.

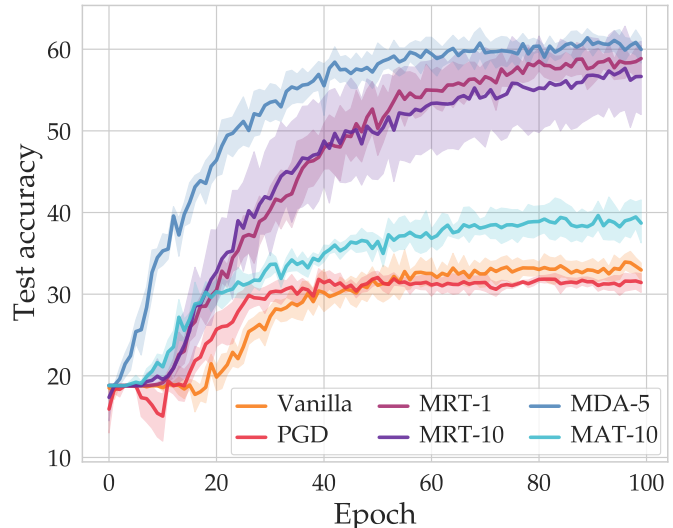
The results for this experiment are shown in Figure 8c. In this task, the baseline classifiers trained on domain A achieve test accuracies of around 30% when tested on high-contrast samples



(a) **Training data.** Domain A consisted of low-contrast images collected from SVHN.



(b) **Test data.** Domain B consisted of high-contrast images collected from SVHN.



(c) **Results.** The baseline classifiers lack robustness to this shift in contrast from A to B ; both achieve slightly greater than 30% test accuracy, whereas the model-based classifiers approach 60% test accuracy on domain B .

Figure 8: **Robustness to contrast on SVHN.** The variation in contrast in the SVHN dataset poses a significant challenge from a robustness perspective. We show that trained model-based classifiers can be made robust against variations in contrast by learning a model that compensates for this discrepancy.

from domain B . On the other hand, classifiers trained using our MRT and MDA algorithms achieve 60% test accuracy, which is a 30% improvement over the baseline classifiers. This increase in performance can be attributed to the model’s capability to generate realistic images that are similar to the high-contrast samples from domain B .

In Figure 8c we see that despite the fact that MAT is more robust to the shift in contrast than either of the baselines, it still lags nearly 20% behind the other model-based classifiers. This highlights an essential difference between training with MAT and training with either MRT or MDA. Fundamentally, MAT searches *locally* around each training image in domain A to find data that approximately solve the inner maximization problem in (5.1). In the applications we consider in this paper, local search may not be able to find challenging training examples; rather, finding diverse samples is more effectively done by sampling *globally* in Δ . Both MRT and MDA employ this global search in Δ , and we find that empirically this results in a significant gap between the test accuracy on domain B for classifiers trained with MRT and MDA versus classifiers trained with MAT.

6.1.3 GTSRB: robustness to brightness

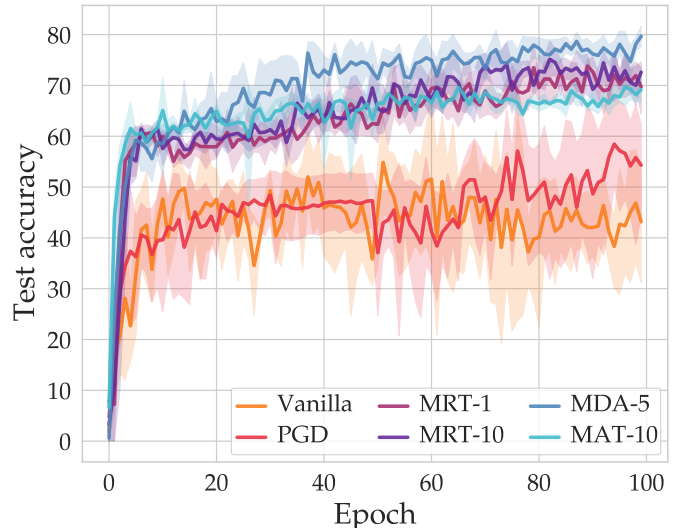
In the safety-critical application of autonomous vehicles, deep learning must be able to robustly recognize landmarks, signage, and pedestrians. Unfortunately, it has been shown that perception systems can be fooled by weather or lighting conditions [32]. In order to demonstrate the utility



(a) **Training data.** Domain A consisted of low-brightness samples from GTSRB.



(b) **Test data.** Domain B consisted of high-brightness samples from GTSRB.



(c) **Results.** By leveraging a learned model of brightness, the model-based classifiers achieved between 10 and 20% improvements over the baseline classifiers.

Figure 9: **Robustness to brightness on GTSRB.** Like SVHN, the GTSRB dataset has significant variation in brightness. To test the robustness of trained models against shifts in the distribution of brightness, we learned a model of brightness and compared the performance of the baseline classifiers trained to that of the model-based classifiers.

of our approach in such a realistic application, we focus on a traffic signs recognition task with data from the German Traffic Signs Recognition Benchmark (GTSRB) [57] dataset. In particular, we consider classification tasks in which the goal is to correctly classify signs from the ten largest classes on GTSRB subject to changes in brightness.

We first extracted two image subsets from GTSRB: domain A contained images with low brightness (i.e. taken at night) whereas domain B contained images with high brightness (i.e. taken during the day). Samples from domains A and B are shown in Figure 9a and 9b respectively. Using these domains, we learned a model of natural variation mapping low-brightness samples to high-brightness samples. In Figure 9c, we see that the baseline classifiers achieve around 50% test accuracy. On the other hand, the model-based classifiers achieve between 10 and 20% improvement over these methods. Once more, this is because our brightness model is able to generate realistic images of signs in daylight from low-brightness samples, resulting in robustness to physically meaningful brightness variation.

6.1.4 Robustness with respect to other nuisances

Our model-based robust training paradigm clearly shows significant improvements in robustness to different nuisances across various datasets. As we have shown, incorporating a known model of background variation dramatically improved the robustness of the classification task on MNIST with respect to changes in background color. Similarly, we showed that using a learned model of contrast (resp. brightness) variation significantly improved the classification accuracy on SVHN

Dataset	Challenge	Domains		Test accuracy across five trials					
		A	B	Vanilla	PGD	MRT-1	MRT-10	MDA-5	MAT-10
MNIST	Background color	Blue	Red	84.4	82.4	97.2	97.3	97.3	91.8
		Gray	RGB*	87.8	75.9	98.8	98.8	98.9	–
SVHN	Contrast	Low	High	35.2	32.9	60.2	58.1	62.1	40.7
	Brightness	Day	Night	33.3	30.6	68.2	66.5	63.2	19.3
		Medium	All	61.7	62.6	73.9	73.0	68.7	51.3
	Hue	RGB	HSV	67.8	68.6	72.0	72.0	64.2	51.6
	Erasing	No erasing	Erasing	57.0	54.1	62.0	61.8	59.4	42.0
		No erasing	Erasing*	50.3	51.9	65.3	64.0	63.6	–
	Decolorization	RGB	Gray	74.5	74.5	75.0	74.2	69.2	51.8
GTSRB	Colorization	Gray	RGB	69.8	69.4	72.1	72.4	65.5	57.5
	Contrast	Low	High	67.0	69.5	73.6	73.9	78.4	78.8
	Brightness	Night	Day	65.0	67.6	78.5	79.1	82.0	74.8

Table 2: **Model-based training on one dataset.** For a range of datasets and nuisances, we show the test accuracy of baseline and model-based classifiers tested on data from the test distribution of domain *B*. Here the * denotes that we used a known model, and results with MAT are omitted for these challenges as the known models we used were non-differentiable.

(resp. GTSRB) under challenging natural conditions.

We now show that the robustness improvements of our model-based paradigm adhere to a similar trend across many forms of natural variation in these three datasets. Table 2 summarizes the test accuracies for numerous experiments we performed across MNIST, SVHN, and GTSRB. For each of these datasets, we considered robustness with respect to a variety of nuisances, including background color, contrast, brightness, hue, erasing, and decolorization. For each nuisance, by leveraging a suitable model of natural variation, our model-based robust classifiers consistently outperformed their baseline counterparts. For some challenging sources of natural variation such as erasing on SVHN or contrast on GTSRB, our algorithms achieved as much as 15 or 20% improvements in test accuracy. On the other hand, some challenges such as hue on SVHN do not pose a significant robustness challenge, and so our model-based methods improve only marginally over the baseline classifiers. The complete description of all these experiments can be found in Appendix A.

Dataset	Challenge	Domains			Test accuracy across five trials				
		A	B	Test	Vanilla	PGD	MRT-1	MRT-10	MDA-5
MNIST	Background color	Blue 0-4, red 5-9	Blue 0-4, red 5-9	Red	50.7	50.6	96.2	96.4	97.7
		Red 0, blue 1-9	Red 0, blue 1-9	Red	9.8	9.8	97.5	97.4	97.4
SVHN	Brightness	Medium	All	Night	55.8	56.1	77.5	77.4	72.9
	Contrast	Medium	All	High	50.0	56.5	58.4	58.3	44.0
		Medium	All	Low	63.5	65.8	70.6	68.1	71.9

Table 3: **Model-based training with a more challenging test set.** For these experiments, we train a model to map from domain A to B . We then construct a more challenging test set than the images in either A or B , and test all of the classifiers on this set.

6.1.5 Robustness to more challenging test data

In the experiments presented so far, we have trained classifiers using data from domain A and then tested these classifiers on test data from domain B . In some of these experiments, the intersection of the domains A and B was nonempty, meaning there were images in domain A that were also in domain B . For instance, in one experiment recorded in Table 2, domain A is chosen to contain medium-brightness samples from SVHN, whereas domain B is chosen to be all of SVHN. Although the model-based classifiers outperform baseline classifiers in this experiment, we now focus on the more challenging problem of testing on test data from $A^c \cap B$. In order words we now test on data from domain B that we have not seen in domain A . This setup in which we train on domain A and test on domain $A^c \cap B$ represents a more significant robustness challenge as none of the classifiers have access to $A^c \cap B$ at training time.

In Table 3, we record the test accuracy on $A^c \cap B$ for several challenging scenarios. In these experiments, the performance improvements are more pronounced than those observed in Table 2. For instance, for the brightness challenge described in Table 2 for SVHN, when testing on all of domain B we achieve an approximate 11% improvement over baselines. However, when we restrict the test domain to only contain SVHN images with low brightness, the margin further increases to nearly 22% in favor of model-based classifiers.

Further, in Table 3, we consider several challenging tasks on MNIST in which domains A and B both contain the same data. In these tasks, we choose the test distributions to contain images with nuisances that do not appear in the test set. For example, in the first row of Table 3, we let A and B contain the following MNIST training data: for digits with labels 0-4, we set the background color to be blue, and for digits with labels 5-9, we set the background color to be red. We then test on digits from the MNIST test set with red backgrounds. Note that although none of the classifiers saw the digits 0-4 with red backgrounds, the model-based classifiers achieve upwards of 96% classification accuracy. This is because the learned model that maps from A to B learns to generate images of the MNIST digits with both red and blue backgrounds. More details on these experiments and on the models learned for this task are available in Appendix A.1.

6.2 Leveraging models across datasets

The experiments presented in the previous section clearly show that by leveraging models of natural variation, one can improve the robustness of deep learning with respect to a variety of nuisances. However, nuisances such as brightness are physical variations across all natural images and are not dataset-dependent. In other words, brightness affects images across different datasets in similar ways. This raises the important question of whether the same model of natural variation can be exploited across different datasets. This would allow us, for example, to learn a model of natural variation on one dataset and then subsequently leverage it for model-based training on new and entirely different datasets.

To this end, we are seeking a powerful model of natural variation that can be *universally* applied across different datasets to describe a specific nuisance such as brightness. This would mean that for a given nuisance, we can simply learn a model of natural variation on one dataset and then reuse it across similar datasets, broadening the applicability of our model-based framework. Once such a model of natural variation is obtained on one dataset – regardless of whether it is known a priori or else learned from data – it can be directly exploited as a *known* model in our model-based robust training training procedure on many other datasets.

In what follows, we show that leveraging models of variation across datasets is indeed possible. To do so, we first obtain a model of natural variation on a given dataset \mathcal{D} . To obtain such a model, in each of the experiments we assume that two subsets A and B can be extracted from \mathcal{D} , where A and B encode some factor of natural variation. We then learn a model $G : A \times \Delta \rightarrow B$ using the framework described in Section 4. Next, we use this learned model G to perform model-based training on a different dataset \mathcal{D}' . In particular, we separate \mathcal{D}' into two domains A' and B' that encode the same kind of natural variation as do the subsets A and B . For instance, datasets \mathcal{D} and \mathcal{D}' may contain images of street signs in different languages or from different countries; in this spirit, domains A and A' may contain images during the day whereas B and B' may contain images taken at night. We train baseline and model-based classifiers on training data from domain A' ; in addition, all of the model-based classifiers have access to the model G that was trained on dataset \mathcal{D} . We then test all classifiers on test data from domain B' .

6.2.1 Leveraging one background color model across MNIST variants

We begin by considering the problem of changing the background colors in images from blue to red across different datasets. In this way, we first create two new variants of MNIST: MNIST-Red and MNIST-Blue. As these names suggest, MNIST-Red contains images of the MNIST digits with red backgrounds, whereas MNIST-Blue contains the same MNIST digits with blue backgrounds. Together, domains A and B comprise the dataset \mathcal{D} . We then learn a model of natural variation for background color that maps images from MNIST-Red into MNIST-Blue. That is, if we let domain A consist of MNIST-Red and domain B consist of MNIST-Blue, we first learn a model of natural variation $G : A \times \Delta \rightarrow B$.

Now given this learned model of natural variation, we show that it can be used to effectively perform model-based training on a family of related datasets which share similar characteristics to MNIST. In particular, we consider the following datasets: Fashion-MNIST [66], EMNIST [67], KMNIST [68], QMNIST [69], and USPS [70]. Just as in the original MNIST dataset, each of these datasets contains images of exactly one object on top of a monochromatic background. For example, Fashion-MNIST contains images of items of clothing and EMNIST contains images of handwritten

		Dataset \mathcal{D}'				
		QMNIST	EMNIST	KMNIST	Fashion-MNIST	USPS
Images from \mathcal{D}'						
Model-based images						

Table 4: **Passing samples from other datasets through a model learned on MNIST.** The first row of images in this table are samples taken from colorized versions of Q-MNIST, E-MNIST, K-MNIST, Fashion-MNIST, and USPS. The second row of images shows samples passed through a model trained on the original MNIST dataset to change the background color from blue to red.

letters from the Latin alphabet. For each of these datasets, we create separate variants with red and with blue backgrounds.

As an illustrative example, let Fashion-MNIST be the dataset \mathcal{D}' . We let domain A' be Fashion-MNIST-Blue, which comprises Fashion-MNIST images with blue backgrounds, and we let domain B' be Fashion-MNIST-Red, which comprises Fashion-MNIST images with red backgrounds. We train all classifiers on this domain A' . Our model-based algorithms have access to the model $G : A \times \Delta \rightarrow B$ which was learned on MNIST, which contains images of handwritten digits rather than items of clothing. Ideally, the model learned on MNIST should be able to effectively change the background colors of the articles of clothing in Fashion-MNIST even though the model of natural variation has not been trained specifically on these images.

A summary of the results for this experiment for the five datasets mentioned above is given in Table 5. Notably, for each dataset \mathcal{D}' , the classifiers trained with the background color model learned on MNIST result in between 5% and 40% accuracy improvements against the change in background color. As expected, this increase in robustness to background colors is due to the broad applicability of the model for background color across all datasets. To show the quality of the images that the same model generates across numerous datasets, we took representative samples from each of the five datasets and display them in Table 4. The first row of images show samples from each dataset with blue backgrounds while the second row of images shows images generated by applying the model of natural variation learned on MNIST to each sample in the row above. These input-output pairs for each dataset \mathcal{D}' are shown in Table 4. While some detail is lost and artifacts appear for the images from Fashion-MNIST and EMNIST, the content of the reconstructions strongly resemble that of the input images.

6.2.2 Leveraging one brightness model across GTSRB and CURE-TSR

In the same spirit as the experiments we just presented on MNIST and the related datasets, we now consider the more realistic and challenging setting where a model of natural variation for

Model dataset \mathcal{D}	Train/Test dataset \mathcal{D}'	Challenge	Test accuracy across five trials					
			Vanilla	PGD	MRT-1	MRT-10	MDA-5	MAT-10
MNIST	Fashion-MNIST	Background color	69.3	67.7	81.4	80.1	79.1	76.1
			87.0	79.9	98.0	98.0	97.9	98.0
			63.5	49.3	86.1	85.9	85.6	84.1
			47.9	47.7	89.1	89.3	88.2	86.8
			89.8	87.4	93.3	93.4	93.3	91.9
MNIST-m	SVHN	Decolorization	76.1	75.3	77.1	76.7	74.7	64.3
		Colorization	70.3	69.2	72.2	72.2	70.0	67.2
GTSRB	CURE-TSR darkening	Brightness	47.6	43.6	73.0	71.4	72.4	67.8
	CURE-TSR exposure		66.0	64.7	65.9	66.6	66.4	72.8

Table 5: **Reusing learned models on new datasets.** By reusing models trained on one dataset \mathcal{D} to perform model-based robust training on another dataset \mathcal{D}' , we can achieve significant improvements in robustness. A more thorough analysis of the results presented in this table are provided in Appendix B.

brightness learned on the GTSRB dataset will be used for model-based training on the CURE-TSR dataset. The CURE-TSR dataset [34], which we will revisit later in Section 6.3, contains images of street signs with varying natural nuisances such as haze, rain, and snow. To this end, we reuse the model of natural variation for brightness that we learned in Section 6.1.3 on GTSRB. We then train baseline and model-based classifiers on samples from CURE-TSR of street signs in plain daylight, and we test each classifier on images of street signs taken at night. Figure 10 shows that while baseline classifiers achieve around 40% test accuracy on the data of images taken at night from CURE-TSR, by leveraging the model learned on GTSRB the model-based classifiers achieve between 60 and 70% test accuracy. Thus although the model we used was trained on GTSRB, we were able to leverage it in our model-based framework to provided significant robustness for the CURE-TSR darkening dataset.

In Appendix B, we explore experiments of the same stripe for further datasets and nuisances. In particular, we show that models trained on MNIST-m, which is an RGB dataset containing the MNIST digits with various images in the background, can be used for model-based training on SVHN.

6.2.3 Composing models of natural variation

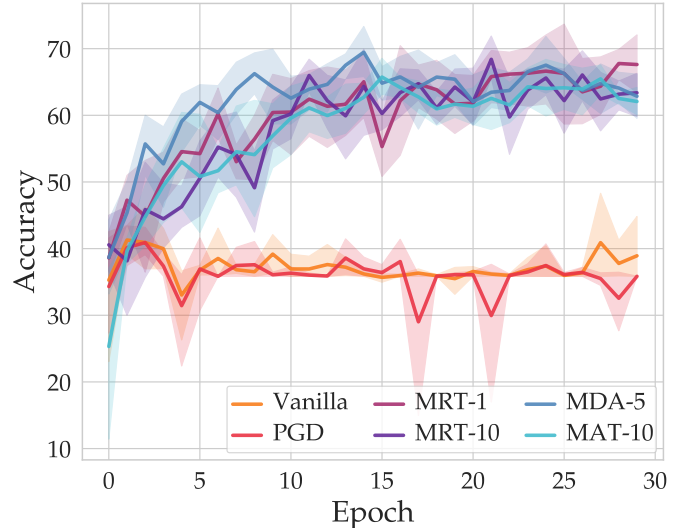
In harsh environments it is natural to encounter not just one but a combination of challenging conditions. For example, perception tasks may be complicated simultaneously by changes in



(a) **Training data.** The training data consisted of samples from CURE-TSR taken in daylight.



(b) **Test data.** The test data consisted of samples from CURE-TSR taken at night.



(c) **Results.** The model-based classifiers all reach around 60% test accuracy, whereas the baselines can only reach around 40%.

Figure 10: **Robustness to darkening on CURE-TSR with a model learned on GTSRB.** By first learning a model of darkening on GTSRB, we were able to perform model-based training on CURE-TSR. Our results show that despite the fact that the model was learned on a different dataset, we can still improve significantly over baseline algorithms.

natural conditions, such as inclement weather, in addition to variation in sensor quality, such as the contrast of a camera lens. From a robustness perspective, such combinations of nuisances poses a significant challenge given that it may be difficult to even obtain data subject to multiple factors of natural variation.

Our model-based approach is naturally suited for providing robustness with respect to simultaneous nuisances due to the composable nature of models of natural variation. In other words, if the model $G_1(x, \delta)$ maps images of street signs during the day to images of street signs at night and model $G_2(x, \delta)$ maps images with low contrast to images with high contrast, G_1 and G_2 can be composed to form a new model $G(x, \delta) := G_1(G_2(x, \delta), \delta)$. Therefore by composing simpler models of natural variation, we can create new, more complex models that can be used to provide robustness against multiple simultaneous nuisances.

To demonstrate the utility of this approach, we consider a scenario in which domain A consists of samples that have low brightness and low contrast on SVHN. Further, we let domain B contain samples with high brightness and high contrast. Thus, two simultaneous sources of natural variation complicate the classification task: brightness and contrast. Figures 11a and 11b show images from domains A and B respectively.

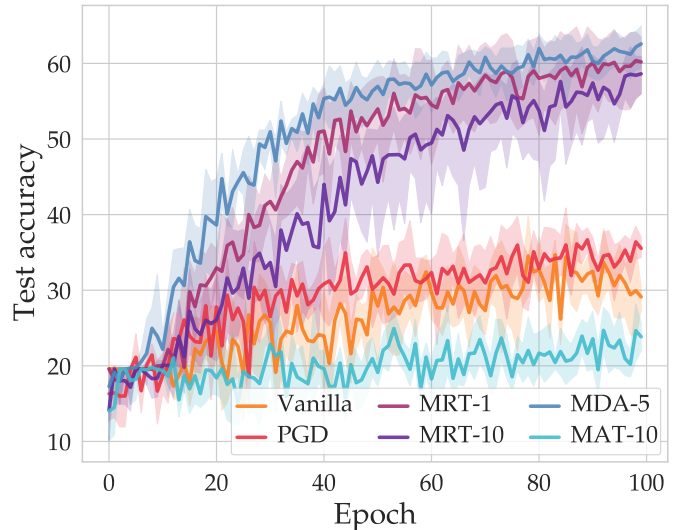
Our goal is to obtain a model of natural variation $G : A \times \Delta \rightarrow B$ where Δ captures both contrast and brightness. In this case, both the contrast model $G_c(x, \delta)$ and the brightness model $G_b(x, \delta)$ were trained separately on samples with low- and high-contrast and on samples with low- and high-brightness separately respectively. The model used for contrast was discussed in Section 6.1.2, whereas the model used for brightness is discussed in Appendix A.2.2. By composing these models,



(a) **Domain A.** Domain A consisted of low-brightness and low-contrast samples from SVHN.



(b) **Domain B.** Domain B consisted of high-contrast and high-brightness images from SVHN.



(c) **Results.** The model-based classifiers achieve a nearly 25% improvement over baseline classifiers.

Figure 11: **Using a composition of models on SVHN.** We consider the task of providing robustness against multiple sources of natural variation. To do so, we compose two separately trained models of natural variation; one corresponds to contrast while the other corresponds to brightness.

we created a new model $G(x, \delta) := G_c(G_b(x, \delta), \delta)$. In Figure 11c, we show the results of using this composite model $G(x, \delta)$ to perform model-based training. In particular, note that the model-based classifiers achieve a nearly 25% improvement in robustness over baseline algorithms.

6.3 Out-of-distribution experiments

A challenging application of our model-based training paradigm is in learning to correctly classify out-of-distribution data. In this section we investigate whether a classifier trained with data from one domain can generalize to classify more challenging test data from an unseen domain. More specifically, we assume access to a dataset \mathcal{D} with domains (i.e. subsets) A , B , and C . These domains will be chosen to be of increasing difficulty with respect to classification. In other words, C is the most challenging domain, B is slightly less challenging than C , and A is the least challenging subset of the three. For example, domain A might contain images of street signs on a sunny day at noon, domain B might contain images of street signs on the same day in the late afternoon, and domain C might contain images in the late evening or at night.

To carry out experiments of this stripe, we employ the recently curated CURE-TSR dataset [34]. This dataset contains images of common street signs with labeled forms of natural variation, including decolorization, snow, rain, and haze. More importantly, for each source of variation, CURE-TSR contains a subset of images which are labelled with the numbers 0-5 according to the severity of the challenge, where challenge-level 0 means that there is no natural variation, and challenge-level 5 means that there are very high levels of natural variation. Figure 12 shows different challenge levels with respect to snow.

In each experiment and for each nuisance, we first learn a model G on the CURE-TSR dataset



Figure 12: **CURE-TSR snow challenge levels.** From left to right we show the same image with different levels of snow natural variation. Challenge-level 0 corresponds to no natural variation, whereas challenge-level 5 corresponds to the highest level of natural variation.

that maps from challenge-level 0 images to challenge-level 1 images. Next, we train baseline and model-based classifiers the same challenge-level 0 and 1 images that were used to train the model of natural variation G . Finally, we test the trained classifiers on the more challenging data from subsets with challenge-levels 2, 3, 4, and 5. In doing so, we aim to show two properties of classifiers trained using the model-based algorithms. Firstly, we show that model-based classifiers provide high levels of robustness against the given nuisance for each test subset. Secondly, we show that when tested on more challenging test data, the gap between the test accuracy of the model-based and baseline classifiers increases. This demonstrates that the model-based classifiers offer comparatively stronger performance against worst-case natural variation.

6.3.1 CURE-TSR: robustness with respect to snow

Varying weather conditions in images presents a significant challenge to perception-based classification algorithms [32]. Throughout this paper, we have illustrated this point with recurring images of the same street sign in sunny conditions and in conditions with heavy snow. To this end, we consider the out-of-distribution experiment described above on the images from the CURE-TSR dataset with varying levels of snow. Images illustrating the varying challenge levels of this dataset are shown in Figure 12³.

Figure 13 shows the results of this out-of-distribution experiment. We see that the performance of the baseline classifiers degrades significantly as the amount of snow in the image increases. This shows that sources of natural variation such as snowy weather conditions pose a significant threat to neural-network-based classifiers. On the other hand, despite the fact that the model-based classifiers have access to exactly the same data as the baseline classifiers, the model-based classifiers are able to find challenging examples and consequently achieve higher levels of robustness. Indeed, although all classifiers perform well when tested on challenge-level 2 test data, the model-based classifiers drop by between 20 and 25% when tested on challenge level 5; in contrast, the baseline classifiers suffer nearly 40% drops in test accuracy, which shows that the model-based classifiers are much more robust against the challenging conditions of the challenge-level 5 dataset.

6.3.2 Robustness with respect to increasingly challenging nuisances

To further explore the ability of the model-based paradigm to provide robustness against challenging sources of natural variation from the CURE-TSR dataset, we repeated the experiments of

³Note that these images are taken from the CURE-TSD dataset. The CURE-TSR consists solely of images from CURE-TSD that are cropped so that only the street sign is visible. We use the CURE-TSD versions here for clarity of exposition.

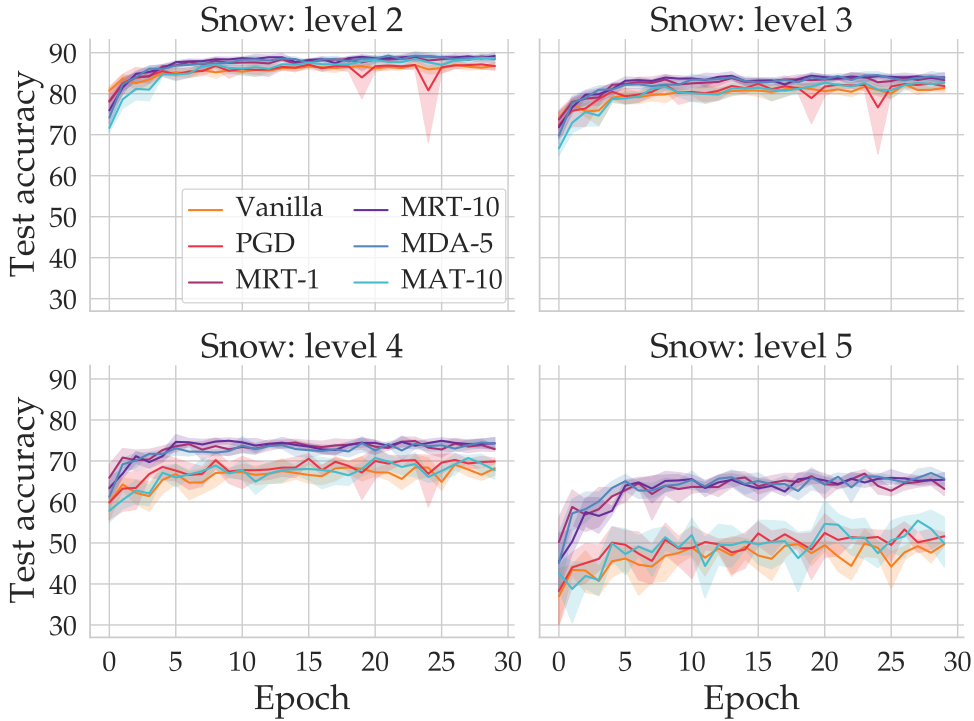


Figure 13: **Out-of-distribution robustness to snow on CURE-TSR.** In the upper left panel, we see that all classifiers achieve essentially the same performance when tested on challenge-level 2 data. However, as natural variation in the test data becomes more challenging, the gap between the test accuracies of the baseline and model-based classifiers becomes more pronounced. Indeed, on challenge-level 5, the gap between the baseline and model-based classifiers approaches 15% on average.

Figure 13 by focusing on four different natural conditions: decolorization, shadow, haze, and rain. The complete set of results from these experiments are summarized in Table 6, and we defer the reader to Appendix C for more details.

Table 6 generalizes the robustness benefits that were illustrated for snow in Figure 13 but for various nuisances and levels of difficulty. On the rain challenge, we achieve only modest improvements over the baseline classifiers, as the magnitude of natural variation in the images of street signs in rain is less pronounced as in other challenges. However, for most challenges, notably, for the decolorization, shadow, and haze subsets, our model-based classifiers achieve between 5% and 10% improvements in test accuracy over baseline classifiers when tested against the most challenging natural conditions. Once more, the more challenging the dataset, the larger the robustness gap between our model-based paradigm and the other training paradigms. This provides clear empirical evidence that our model-based training paradigm can be used to provide high levels of robustness against challenging out-of-distribution test data.

At this point, we find it prudent to acknowledge that in each of the tasks considered in this subsection, we have not provided the models or classifiers access to data corresponding to challenge-levels 2, 3, 4, or 5. Indeed, if we had provided either of these networks with this data, the test

accuracy of each of the classifiers would have undoubtedly improved. However, we find that removing access to this more challenging data is the most natural way to measure the *robustness* of trained classifiers. In future work, we plan to explore how classifiers trained using our model-based robust training algorithms compare to classifiers that are trained directly with more challenging test data.

7 Discussion

7.1 Nuisance spaces of models of natural variation

In various experiments in Section 6, we learned models G of natural variation from data that allowed us to provide robustness against numerous nuisance-based challenges. Indeed, we evaluated the performance of model-based classifiers over a range of datasets to show that our model-based strategy is widely applicable to myriad different scenarios.

To better visualize the data generated by using a learned model of natural variation, in Figure 14, we analyze the nuisance space Δ used in two different experiments in this paper. In particular, in Figure 14a, we show an image from domain A for the experiment described in Appendix A in which we learned a model that could change the background color of the MNIST digits from blue to red. Further, by gridding the nuisance space Δ for this learned model, in Figure 14b we show the range of output images induced by passing the image in Figure 14a through this model on all the grid points. Notably, this reveals that half of the generated images have red backgrounds and half have blue backgrounds; this reflects the fact that domains A and B had an equal number of images with red and blue backgrounds.

On the right side of Figure 14, we show similar images for an experiment described in Appendix A in which domain A consisted of medium brightness samples for SVHN and domain B consisted of the entirety of SVHN. For this experiment, a representative image from domain A is shown in Figure 14c. Further, for this image, we show the images generated by gridding Δ in a rectangle centered at the origin. This gridding shows that by selecting different $\delta \in \Delta$ and passing it through the model G , we can generate data with varying brightness. In particular, the images on the left side of the grid have low brightness, and the brightness of these images increases from left to right.

7.2 Impact of model quality

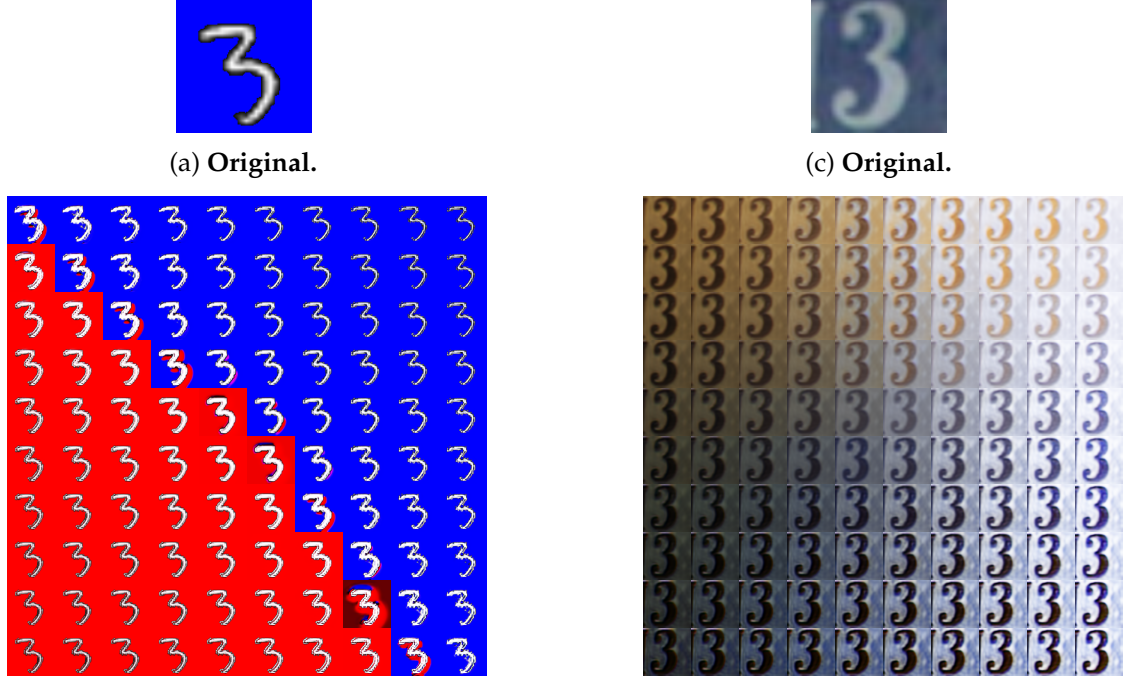
An essential yet so far undiscussed piece of the efficacy of the model-based paradigm is the impact of the model quality on the robustness we are ultimately able to provide. In scenarios where we don't have access to a known model, the ability to provide any sort of meaningful robustness relies on learned models that can accurately render realistic looking data with varying nuisances. To this end, it is reasonable to expect that models that can more effectively render realistic yet challenging data should result in classifiers that are more robust to shifts in natural variation.

To examine the impact of models in our paradigm, we consider the task of of Section 6.1.2, in which we learned a model that mapped low-contrast samples, which comprised domain A , to high-contrast samples, which comprised domain B . While learning this model, we saved snapshots of the model at various points during the training procedure. In particular, we collected a family of intermediate models

$$\mathcal{G} = \{G_{10}, G_{100}, G_{250}, G_{500}, G_{1000}, G_{2000}, G_{3000}, G_{4000}\}$$

Challenge	Training data	Test data	Test accuracy across five trials					
			Vanilla	PGD	MRT-1	MRT-10	MDA-5	MAT-10
Snow	0, 1	5	52.8	56.1	68.4	68.4	68.5	58.3
		4	72.0	73.3	76.0	76.8	75.8	72.6
		3	83.2	83.9	85.2	85.6	85.3	83.9
		2	88.0	88.4	89.6	90.2	90.2	89.4
Decolorization	0, 1	5	69.5	74.3	80.3	80.6	81.0	69.7
		4	80.3	80.8	81.9	82.3	83.4	73.3
		3	86.3	86.0	83.5	83.9	86.1	76.8
		2	88.4	88.1	85.0	85.0	87.7	78.2
Shadow	0, 1	5	76.4	73.6	81.0	79.5	80.6	76.0
		4	82.5	82.9	85.8	85.0	84.8	85.4
		3	87.9	88.4	87.8	87.6	86.9	89.0
		2	90.3	90.3	89.1	88.7	87.8	90.6
Haze	0, 1	5	51.2	51.1	58.8	60.4	62.5	47.0
		4	54.8	55.5	67.9	69.6	70.7	50.5
		3	78.8	80.7	84.1	84.4	83.3	65.0
		2	89.0	89.3	89.0	89.1	87.8	75.8
Rain	0, 1	5	80.4	81.3	81.3	81.6	79.8	63.3
		4	83.9	84.2	84.2	84.5	83.6	66.2
		3	84.9	85.6	85.7	85.9	84.9	69.5
		2	85.7	86.6	86.5	86.7	85.5	72.0

Table 6: **Out-of-distribution results on CURE-TSR.** For a variety of nuisances in the CURE-TSR dataset, we train models of natural variation on challenge-level 0 and 1 data. Then we train all classifiers, including the model-based classifiers, on challenge-level 0 and 1 data; we then test all classifiers on data corresponding to challenge-levels 2, 3, 4, and 5. These results indicate that as the test data gets more challenging, the model-based classifiers outperform the baselines by larger margins.



(b) **Gridding of Δ .** We grid Δ in $[-1, 1] \times [-1, 1]$ to visualize the kinds of images that can be obtained by querying this learned model on MNIST. The fact that there are an equal number of images with red and blue backgrounds in domain A for this experiment is reflected in the symmetry of Δ .

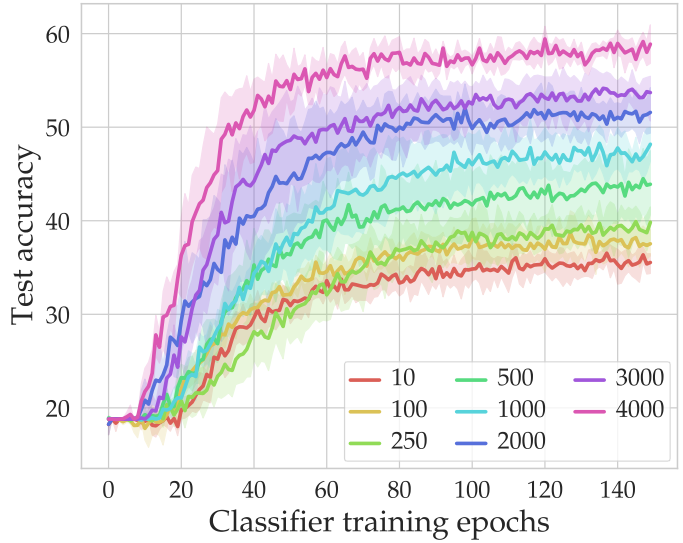
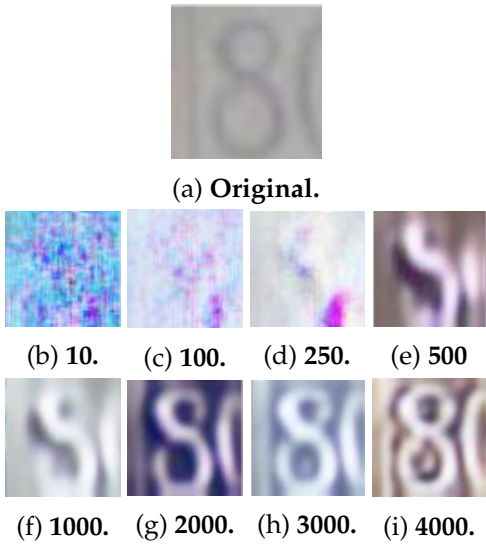
(d) **Gridding of Δ .** We grid Δ in $[-3, 3] \times [-3, 3]$ to visualize the kinds of images that can be obtained by querying this learned model on SVHN. In this experiment, domain B contained all of SVHN, which is reflected in the range of brightness that the model produces for the input image in (d).

Figure 14: **Nuisance spaces of learned models.** On the left, we show an MNIST digit with a blue background and its reconstruction after being passed through a learned model of background colors in (a) and (b) respectively. In (c), we show the images that result from gridding the 2-dimensional nuisance space Δ in a neighborhood of the origin and passing the image in (a) through the learned model with the grid points as nuisance parameters. The figures in the column on the right follow the same format and were obtained from a model learned for brightness on SVHN.

In Figure 15j, we show the result of training classifiers with MRT using each model $G \in \mathcal{G}$. Note that the models that are trained for more training steps engender classifiers that provide higher levels of robustness against the shift in nuisance variation. Indeed, as the model G_{10} produces random noise, the performance of this classifier performs at effectively the level as the baseline classifier discussed in Section 6.1.2. On the other hand, the model G_{4000} is able to accurately preserve the semantic content of the input data while varying the nuisance content, and is therefore able to provide high levels of robustness. In other words, better models provide improved test accuracy for classifiers using model-based robust training.

7.3 Sampling versus adversarial algorithms

From an optimization perspective, we can group our model-based algorithms into two categories: sampling (zeroth-order) methods and adversarial (first-order) methods. Sampling-based methods



Output images from models in \mathcal{G} . We show an example image from domain A in (a), and subsequently show the corresponding output images for each $G \in \mathcal{G}$ for a randomly chosen $\delta \in \Delta$ in (b)-(i).

(j) MRT using models from \mathcal{G} . For each model in \mathcal{G} , we run MRT for five trials and show the resulting test accuracy on samples from the test set from Domain B . Note that the robustness of the trained classifier increases as the number of training steps used to train the model increases.

Figure 15: **A better model implies more robustness.** By learning a family of models \mathcal{G} that are trained for different numbers of steps, we show empirically that models that can more accurately reconstruct input data subject to varying nuisances engender classifiers with higher levels of robustness.

refer to those that seek to solve the inner maximization term in (3.1) by querying the model. This is particularly important for models that are not differentiable. Both MRT and MDA are sampling (zeroth-order) methods in that we obtain new data by sampling different nuisance parameters $\delta \in \Delta$ for each batch in the training set. On the other hand, the technique used to obtain new data in the MAT algorithm is an adversarial (first-order) method, as we statistically approximate the gradient of the model $\nabla_\delta G(x, \delta)$ to perform the optimization—i.e. search for the worst-case nuisance parameter. If the model G is differentiable (which is not required in our framework), then one can directly compute the gradient of the model $\nabla_\delta G(x, \delta)$.

Throughout the experiments, in general we see that the sampling algorithms presented in this paper achieve higher levels of robustness against almost all sources of natural variation. This finding stands in stark contrast to field of perturbation-based robustness, in which adversarial methods have been shown to be the most effective in improving the robustness against small, norm-bounded perturbation [61]. Furthermore, as the next subsection discusses, MRT-1 generally outperforms MRT-10 suggesting that data diversity using a good model may be more important than adversarial data. Going forward, an interesting research direction is not only to consider new algorithms but also to understand whether sampling-based or adversarial techniques provide more robustness with respect to a given model.

7.4 Hyperparameters and architectures for model-based training

In the remainder of this section, we examine the impact of the parameter k in each of the model-based training algorithms, and we discuss the architectural choices made for the classifier.

The impact of k in MRT and MDA. To begin, consider the MRT- k algorithm described in Algorithm 1. In this algorithm, the hyperparameter k controls the number of selections we make for $\delta \in \Delta$ while seeking a loss-maximizing batch of data. Throughout the experiments and in particular in Tables 2 and 3, we see that in general, classifiers trained with MRT-1 generally outperform classifiers trained with MRT-10. That is, larger values of k marginally decrease the test accuracy of classifiers trained with MRT. In this way, it seems that oftentimes the “worst-case” perspective of MRT for high values of k is at time less efficacious than simply augmenting the training set with batches corresponding to randomly sampled nuisance vectors $\delta \in \Delta$.

In support of this conjecture, we see that when we augment the training set with more than one image corresponding to *randomly* selected vectors $\delta \in \Delta$ (e.g. by running MDA-5), we can at times achieve some improvements over MRT-1. Indeed, throughout Tables 2 and 3, MDA-5 outperforms MRT-1 for several different nuisances. From this we can conclude that rather than adopting an adversarial or “worst-case” perspective, when providing robustness against nuisance-based shifts in the data distribution, it is often more efficacious to augment the dataset with a diversity of examples rather than loss-maximizing data.

Classifier architecture selection. The problem of selecting an appropriate neural network architecture has been a fundamental part of incorporating prediction algorithms into application domains even before the current era of deep learning [72]. While we have used a standard CNN with a fixed architecture throughout the experiments section, we note that other architectural choices are possible. Figure 16 shows that regardless of the architecture of the classifier, model-based classifiers outperform baseline classifiers when tested on challenging data. In the experiments shown in Figure 16, we let domain A contain medium-brightness samples from SVHN and we let domain B consist of all of SVHN. By training every classifier on data from domain A and then testing each classifier on low-brightness samples from SVHN, we show that regardless of the classifier architecture, MRT and MDA outperform baseline classifiers on this low-brightness test set.

More specifically, throughout the experiments section, we used the following architecture:

```
c32-3, c64-3, p2, c128-3, p2, d0.25, flat, fc128, d0.5, fc10.
```

Here we use the following conventions for describing network architectures. `c32-3` refers to a 2D convolutional operator with 32 kernels, each of which has shape 3×3 . `p2` refers to a max-pooling layer with kernel size 2. `d0.25` refers to a dropout layer, which drops an activation with probability 0.25. `flat` refers to a flattening layer. `fc-128` refers to a fully-connected layer mapping into \mathbb{R}^{128} .

The peak test accuracies for four similar CNN architectures are given in Table 7. Note that across the four architectures in this table, the classifiers trained with MRT and MDA significantly outperform the baselines.

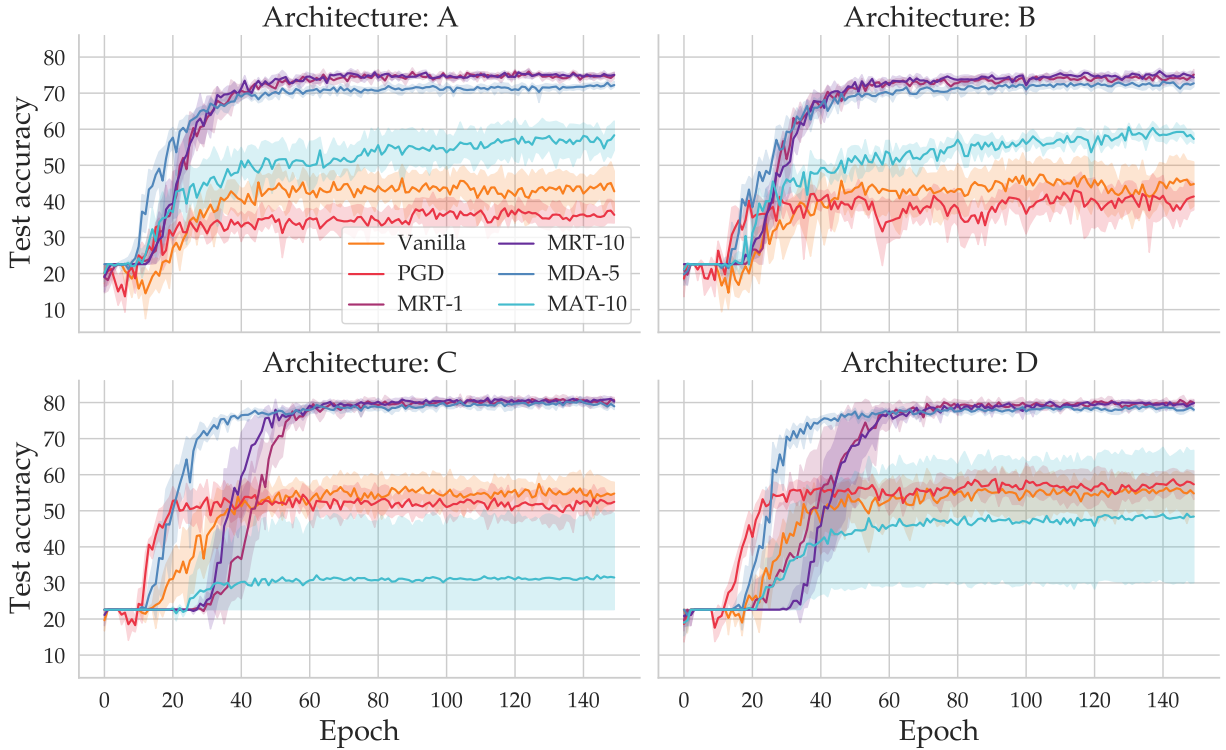


Figure 16: **Classifier architecture selection.** We show that for a range of architectures, classifiers trained with MDA and MRT outperform the baseline classifiers on a robustness challenge corresponding to different levels of contrast with data from SVHN.

Name	Architecture	Test accuracies across five trials					
		Vanilla	PGD	MRT-1	MRT-10	MDA-5	MAT-10
A	c32-3, c64-3, p2, d0.25, flat, fc128, d0.5, fc10	49.3	40.3	77.1	77.1	73.7	60.6
B	c32-3, c64-3, p2, d0.25, flat, fc256, d0.5, fc64, fc10	50.8	47.8	76.3	76.7	74.3	62.4
C	c32-3, c64-3, p2, c128-3, p2, d0.25, flat, fc128, d0.5, fc10	59.6	58.0	82.5	82.5	81.3	32.1
D	c32-3, c64-3, p2, c128-3, p2, d0.25, flat, fc256, d0.5, fc64, fc10	59.0	60.8	81.9	81.4	80.0	50.1

Table 7: **Varying the architecture of the classifier used for model-based training.** We report the average peak accuracy across five trials for four different classifier architectures. Notably, the classifiers trained with MRT and MDA significantly outperform the baselines.

8 Related works

8.1 Perturbation-based adversarial robustness

A rapidly growing body of work has addressed adversarial robustness of deep networks with respect to small norm-bounded perturbations. This problem has motivated an arms-race-like amalgamation of adversarial attacks and defenses within the scope of norm-bounded adversaries [73, 61]. And while some defenses have withstood a variety of strong adversaries [22], it remains an open question as to how best to defend against such attacks.

Several notable works that propose methods for defending against adversarial attacks formulate so-called adversarial training algorithms, the goal of which is to defend neural networks against worst-case perturbations [31, 28, 26]. Some of the most successful works take a robust optimization perspective, in which the goal is to find the worst-case adversarial perturbation of data by solving a min-max problem [22, 23]. In a different yet related line of work, optimization-based methods have been proposed to provide certifiable guarantees on the robustness of neural networks against small perturbations [74, 30, 29]. On the other hand, others have studied how adapting network architectures can be used to defend against adversarial examples [75, 76].

As adversarial training methods have become more sophisticated, a range of adaptive adversarial attacks, or attacks specifically targeting a particular defense, have been proposed [73]. Prominent among the attacks on robustly-trained classifiers have been algorithms that circumvent so-called obfuscated gradients [61, 77]. Such attacks generally focus on generating adversarial examples that are perceptually similar to a given input image [78, 79].

In summary, the commonality among all the approaches mentioned above is that they consider norm-bounded adversarial perturbations which are perceptually indistinguishable from the true examples. Contrary to these approaches, in this work we propose a paradigm shift from norm-bounded perturbation-based robust deep learning to model-based robust deep learning. Our objective is to provide training algorithms that are robust against model-based perturbations of the data. As such, model-based perturbations can encode perceptible changes in natural variation such as different lighting or weather conditions.

8.2 A broader view of robustness in deep learning

More recently, a different line of work has considered the robustness of neural networks against transformations that are more likely to be encountered in applications. Nuisances that have recently received attention from the adversarial robustness community include adversarial quilting [80], adversarial patches and clothing [81], geometric transformations [42, 82, 41, 43], distortions [83], deformations and occlusions [84], and nuisances encountered by unmanned aerial vehicles [85]. In response to these works and motivated by myriad safety-critical applications, first steps toward robust defenses against specific nuisances have recently been proposed. The resulting methodologies generally leverage properties specific to the transformation of interest.

While this progress has helped to motivate new notions of robustness, the approaches that propose defense against these nuisances are limited in the sense that they do not generalize to a learning paradigm that applies across different forms of natural variation. This contrasts with the motivation behind this paper, which is to provide general robust training algorithms that can improve the robustness of trained neural networks across a variety of scenarios and applications.

8.3 Generative models in the context of robustness

Another line of work that focuses on attack and defense strategies against adversarial examples use generative models in the loop of training. In [86], [87], and [88], the authors propose attack strategies that use the generator from a generative adversarial network (GAN) to generate additive perturbations that can be used to attack a classifier. On the other hand, a framework called DefenseGAN, which uses a Wasserstein GAN to “de-noise” adversarial examples [89], has been proposed to defend against perturbation-based attacks. This defense method was later broken by the Robust Manifold Defense [90], which searches over the parameterized manifold induced by a generative model to find worst-case perturbations of data. The min-max formulation used in this work is analogous to the projected gradient descent (PGD) defense [22].

Closer to the approach we describe in this paper are works that use generative models to generate adversarial inputs themselves, rather than generating small perturbations. The authors of [91] and [92] use the generator from a GAN to generate adversarial examples that obey norm-based constraints. Alternatively, [93] use GANs to construct adversarial patterns that can be used to transfer adversarial examples from one domain to another. Similarly, [94] and [95] generate unrestricted adversarial examples, or examples that are not subject to a norm-based constraint [96] via a generative model. Finally, [97, 98] use a GAN to perform data augmentation by generating perceptually realistic samples.

In this work, we use generative networks to learn and model the natural variability within data. This is indeed different than generating norm-based adversarial perturbations or perceptually realistic adversarial examples as considered in the literature. Our generative models aim at learning a natural factor of variability that is present in the data while the relevant literature has aimed at creating synthetic adversarial nuisances to fool neural networks.

8.4 Equivariance and invariance to nuisances in computer vision

Parallel to the progress made toward training neural networks to be robust against small, norm-bounded adversarially-chosen perturbations, a related line of work in the computer vision community has sought to design equivariant neural networks. In the context of adversarial robustness, if T is a function that perturbs an input by a small amount, neural networks are often trained to give the same prediction for $f(T(x))$ and $f(x)$ [99, 100]. Interestingly, it has been shown that rotationally equivariant neural networks are significantly less vulnerable to geometric invariance-based adversarial attacks [101].

More generally, several more recent works have sought to provide robustness or invariance against nuisance-based attacks; such works have included [102], which used an information theoretic approach to edit the nuisance content of images to create perceptually similar data that caused misclassification. Similarly, another line of work has sought to use differentiable renderers to produce “semantic adversarial examples” [103]. In this line of work, mechanisms are often used to edit nuisance factors such as rotation or scaling in images by creating perturbations in a given semantic latent space [104].

The progress toward equivariant and invariant neural networks in computer vision has largely focused on designing new network topologies to combat a given transformation or a set of related transformations. Our model-based robust training framework differs fundamentally from the above approaches in the following aspects. Rather than changing the topology of the neural network, we propose to change the robust training procedure according to the model of variation.

In the case where the model is known (e.g. the transformation T mentioned above) we can use it during training to provide worst-case examples to train the neural network. In more challenging and natural cases where the model is unknown (and hence cannot be used to alter the topology) we propose to learn the model in advance and then use it for training. Our model-based robust training paradigm could provide an intellectual bridge between robust deep learning and exploiting invariances in computer vision.

9 Conclusion and future directions

In this paper, we formulated a novel problem addressing the robustness of deep learning with respect to naturally occurring nuisances. Motivated by perceptible nuisances in computer vision, such as lighting changes, we propose a novel *model-based robust training paradigm* for deep learning that provides robustness with respect to natural variation. Our notion of robustness offers a departure from the notion of adversarial training with respect to norm-bounded data perturbations.

Our optimization-based formulation for model-based training results in a family of training algorithms that we refer to as *model-based robust training*. These algorithms exploit either known or previously learned models of natural variations using both robust and adversarial approaches. Given a model of natural variation G that models naturally occurring nuisances, the main idea across these algorithms is to use G to perform model-based data-augmentation or model-based adversarial training to produce samples with varying nuisances. In the case of unknown nuisances, by blending generative models G with adversarial training, we empirically find that our model-based paradigm provides significant robustness improvements for numerous physically meaningful nuisances across various datasets. Our model-based paradigm is naturally compositional, leverages models across datasets, and shows improved robustness as datasets become more challenging.

Our model-based robust training paradigm open numerous directions for future work. In what follows, we briefly highlight several of these broad directions.

Learning a library of nuisance models. First, the problem of how to best learn a model of natural variation to perform model-based training is an open and interesting problem. In this paper, we used the MUNIT framework [4], but other existing architectures may be better suited for specific nuisances or datasets. Indeed, a more rigorous statistical analysis of problem (4.3) may lead to the discovery of new architectures designed specifically for model-based training. To this end, recent work in learning equivariances in computer vision may provide insight into learning physically meaningful models. Beyond computer vision, learning such models in other domains (such as robot dynamics) would enable new applications.

Model-based algorithms and architectures. Another important direction involves the development of new algorithms for solving the min-max formulation of (3.1). In this paper, we presented three algorithms – MRT, MDA, and MAT – that can be used to approximately solve this problem, but other algorithms are possible and may result in higher levels of robustness. In particular, adapting first-order methods to search globally over the manifold induced by learned generative models in a latent space of variability may provide more efficient, scalable, or robust results. Do we need to decouple offline learning of a model of natural variation or it is possible to think of a new architecture in which the model and the classifier can be learned simultaneously? Another

interesting direction is to rethink deep network architectures in a model-based manner by taking inspiration from how equivariance is exploited in deep network architectures used in computer vision.

Applications beyond image classification. Throughout the paper, we have focused on empirical demonstrations of our approach in numerous image classification tasks. But our model-based paradigm could be broadly applied in numerous applications within computer vision as well as outside computer vision. Within computer vision, one can consider other tasks, such as segmentation, in the presence of challenging physical nuisances. Outside computer vision, one exciting area is to exploit physical models of robot dynamics with deep reinforcement learning for applications such as walking in unknown terrains. In any domain where one has access to good models, our approach allows domain experts to leverage these models in order to make deep learning far more robust.

Theoretical foundations. Finally, we believe that there are many exciting open questions with respect to the theoretical aspects of model-based robust training. What type of models provide significant robustness gain in our paradigm? How accurate does a model need to be to produce neural networks that are robust to natural variation? We would like to address such theoretical questions from a geometric, physical as well as a statistical perspective with an eye toward developing faster algorithms that are both more sample-efficient as well as more robust. Deeper theoretical understanding of our model-based deep learning paradigm could result in new approaches that blend model-based and data-based methods and algorithms.

Acknowledgements

This work has been partially supported by the Defense Advanced Research Projects Agency (DARPA) Assured Autonomy under Contract No. FA8750-18-C-0090, AFOSR under grant FA9550-19-1-0265 (Assured Autonomy in Contested Environments), NSF CPS 1837210, and ARL CRA DCIST W911NF-17-2-0181 program.

Authors

All authors are with the Department of Electrical and Systems Engineering, University of Pennsylvania, Philadelphia, PA 19104. The authors can be reached at the following email addresses:

{arobey1, hassani, pappasg}@seas.upenn.edu.

References

- [1] Yann LeCun, Yoshua Bengio, and Geoffrey Hinton. Deep learning. *Nature*, 521(7553):436–444, 2015.
- [2] Jun-Yan Zhu, Taesung Park, Phillip Isola, and Alexei A Efros. Unpaired image-to-image translation using cycle-consistent adversarial networks. In *Proceedings of the IEEE international conference on computer vision*, pages 2223–2232, 2017.
- [3] Andrew Brock, Jeff Donahue, and Karen Simonyan. Large scale gan training for high fidelity natural image synthesis. *arXiv preprint arXiv:1809.11096*, 2018.
- [4] Xun Huang, Ming-Yu Liu, Serge Belongie, and Jan Kautz. Multimodal unsupervised image-to-image translation. In *Proceedings of the European Conference on Computer Vision (ECCV)*, pages 172–189, 2018.
- [5] Sara Sabour, Nicholas Frosst, and Geoffrey E Hinton. Dynamic routing between capsules. In *Advances in neural information processing systems*, pages 3856–3866, 2017.
- [6] Max Jaderberg, Karen Simonyan, Andrew Zisserman, et al. Spatial transformer networks. In *Advances in neural information processing systems*, pages 2017–2025, 2015.
- [7] Carlos Esteves, Christine Allen-Blanchette, Xiaowei Zhou, and Kostas Daniilidis. Polar transformer networks. *arXiv preprint arXiv:1709.01889*, 2017.
- [8] Jacob Devlin, Ming-Wei Chang, Kenton Lee, and Kristina Toutanova. Bert: Pre-training of deep bidirectional transformers for language understanding. *arXiv preprint arXiv:1810.04805*, 2018.
- [9] Dzmitry Bahdanau, Kyunghyun Cho, and Yoshua Bengio. Neural machine translation by jointly learning to align and translate. *arXiv preprint arXiv:1409.0473*, 2014.
- [10] Marco Tulio Ribeiro, Sameer Singh, and Carlos Guestrin. "why should i trust you?" explaining the predictions of any classifier. In *Proceedings of the 22nd ACM SIGKDD international conference on knowledge discovery and data mining*, pages 1135–1144, 2016.
- [11] Andre Esteva, Alexandre Robicquet, Bharath Ramsundar, Volodymyr Kuleshov, Mark DePristo, Katherine Chou, Claire Cui, Greg Corrado, Sebastian Thrun, and Jeff Dean. A guide to deep learning in healthcare. *Nature medicine*, 25(1):24–29, 2019.
- [12] Luke Oakden-Rayner, Jared Dunnmon, Gustavo Carneiro, and Christopher Ré. Hidden stratification causes clinically meaningful failures in machine learning for medical imaging. In *Proceedings of the ACM Conference on Health, Inference, and Learning*, pages 151–159, 2020.
- [13] Tommaso Dreossi, Alexandre Donzé, and Sanjit A Seshia. Compositional falsification of cyber-physical systems with machine learning components. *Journal of Automated Reasoning*, 63(4):1031–1053, 2019.
- [14] Christian Szegedy, Wojciech Zaremba, Ilya Sutskever, Joan Bruna, Dumitru Erhan, Ian Goodfellow, and Rob Fergus. Intriguing properties of neural networks. *arXiv preprint arXiv:1312.6199*, 2013.

- [15] Dan Hendrycks and Thomas Dietterich. Benchmarking neural network robustness to common corruptions and perturbations. *arXiv preprint arXiv:1903.12261*, 2019.
- [16] Xingxing Wei, Jun Zhu, Sha Yuan, and Hang Su. Sparse adversarial perturbations for videos. In *Proceedings of the AAAI Conference on Artificial Intelligence*, volume 33, pages 8973–8980, 2019.
- [17] Vaishaal Shankar, Achal Dave, Rebecca Roelofs, Deva Ramanan, Benjamin Recht, and Ludwig Schmidt. A systematic framework for natural perturbations from videos. *arXiv preprint arXiv:1906.02168*, 2019.
- [18] Kevin Eykholt, Ivan Evtimov, Earlene Fernandes, Bo Li, Amir Rahmati, Chaowei Xiao, Atul Prakash, Tadayoshi Kohno, and Dawn Song. Robust physical-world attacks on deep learning visual classification. In *Proceedings of the IEEE Conference on Computer Vision and Pattern Recognition*, pages 1625–1634, 2018.
- [19] Eric Wallace, Mitchell Stern, and Dawn Song. Imitation attacks and defenses for black-box machine translation systems. *arXiv preprint arXiv:2004.15015*, 2020.
- [20] Konstantinos Papangelou, Konstantinos Sechidis, James Weatherall, and Gavin Brown. Toward an understanding of adversarial examples in clinical trials. In *Joint European Conference on Machine Learning and Knowledge Discovery in Databases*, pages 35–51. Springer, 2018.
- [21] Marco Melis, Ambra Demontis, Battista Biggio, Gavin Brown, Giorgio Fumera, and Fabio Roli. Is deep learning safe for robot vision? adversarial examples against the icub humanoid. In *Proceedings of the IEEE International Conference on Computer Vision Workshops*, pages 751–759, 2017.
- [22] Aleksander Madry, Aleksandar Makelov, Ludwig Schmidt, Dimitris Tsipras, and Adrian Vladu. Towards deep learning models resistant to adversarial attacks. *arXiv preprint arXiv:1706.06083*, 2017.
- [23] Eric Wong and J Zico Kolter. Provable Defenses Against Adversarial Examples Via the Convex Outer Adversarial Polytope. *arXiv preprint arXiv:1711.00851*, 2017.
- [24] Divyam Madaan and Sung Ju Hwang. Adversarial neural pruning. *arXiv preprint arXiv:1908.04355*, 2019.
- [25] Aaditya Prakash, Nick Moran, Solomon Garber, Antonella DiLillo, and James Storer. Deflecting adversarial attacks with pixel deflection. In *Proceedings of the IEEE conference on computer vision and pattern recognition*, pages 8571–8580, 2018.
- [26] Hongyang Zhang, Yaodong Yu, Jiantao Jiao, Eric P Xing, Laurent El Ghaoui, and Michael I Jordan. Theoretically principled trade-off between robustness and accuracy. *arXiv preprint arXiv:1901.08573*, 2019.
- [27] Alexey Kurakin, Ian Goodfellow, and Samy Bengio. Adversarial examples in the physical world. *arXiv preprint arXiv:1607.02533*, 2016.

- [28] Seyed-Mohsen Moosavi-Dezfooli, Alhussein Fawzi, and Pascal Frossard. Deepfool: a simple and accurate method to fool deep neural networks. In *Proceedings of the IEEE conference on computer vision and pattern recognition*, pages 2574–2582, 2016.
- [29] Aditi Raghunathan, Jacob Steinhardt, and Percy Liang. Certified defenses against adversarial examples. *arXiv preprint arXiv:1801.09344*, 2018.
- [30] Mahyar Fazlyab, Manfred Morari, and George J Pappas. Safety verification and robustness analysis of neural networks via quadratic constraints and semidefinite programming. *arXiv preprint arXiv:1903.01287*, 2019.
- [31] Ian J Goodfellow, Jonathon Shlens, and Christian Szegedy. Explaining and harnessing adversarial examples. *arXiv preprint arXiv:1412.6572*, 2014.
- [32] Kexin Pei, Yinzhi Cao, Junfeng Yang, and Suman Jana. Deepxplore: Automated whitebox testing of deep learning systems. In *proceedings of the 26th Symposium on Operating Systems Principles*, pages 1–18, 2017.
- [33] Alesia Chernikova, Alina Oprea, Cristina Nita-Rotaru, and BaekGyu Kim. Are self-driving cars secure? evasion attacks against deep neural networks for steering angle prediction. In *2019 IEEE Security and Privacy Workshops (SPW)*, pages 132–137. IEEE, 2019.
- [34] Dogancan Temel, Min-Hung Chen, and Ghassan AlRegib. Traffic sign detection under challenging conditions: A deeper look into performance variations and spectral characteristics. *IEEE Transactions on Intelligent Transportation Systems*, 2019.
- [35] Aharon Ben-Tal, Laurent El Ghaoui, and Arkadi Nemirovski. *Robust optimization*, volume 28. Princeton University Press, 2009.
- [36] Dan Hendrycks, Kevin Zhao, Steven Basart, Jacob Steinhardt, and Dawn Song. Natural adversarial examples. *arXiv preprint arXiv:1907.07174*, 2019.
- [37] Hossein Hosseini and Radha Poovendran. Semantic adversarial examples. In *Proceedings of the IEEE Conference on Computer Vision and Pattern Recognition Workshops*, pages 1614–1619, 2018.
- [38] Chaowei Xiao, Jun-Yan Zhu, Bo Li, Warren He, Mingyan Liu, and Dawn Song. Spatially transformed adversarial examples. *arXiv preprint arXiv:1801.02612*, 2018.
- [39] Nikolaos Karianakis, Jingming Dong, and Stefano Soatto. An empirical evaluation of current convolutional architectures’ ability to manage nuisance location and scale variability. In *Proceedings of the IEEE Conference on Computer Vision and Pattern Recognition*, pages 4442–4451, 2016.
- [40] Mahmood Sharif, Lujo Bauer, and Michael K Reiter. On the suitability of lp-norms for creating and preventing adversarial examples. In *Proceedings of the IEEE Conference on Computer Vision and Pattern Recognition Workshops*, pages 1605–1613, 2018.
- [41] Logan Engstrom, Brandon Tran, Dimitris Tsipras, Ludwig Schmidt, and Aleksander Madry. Exploring the landscape of spatial robustness. *arXiv preprint arXiv:1712.02779*, 2017.

[42] Mislav Balunovic, Maximilian Baader, Gagandeep Singh, Timon Gehr, and Martin Vechev. Certifying geometric robustness of neural networks. In *Advances in Neural Information Processing Systems*, pages 15287–15297, 2019.

[43] Sandesh Kamath, Amit Deshpande, and KV Subrahmanyam. Invariance vs. robustness of neural networks. *arXiv preprint arXiv:2002.11318*, 2020.

[44] Daniel E Worrall, Stephan J Garbin, Daniyar Turmukhambetov, and Gabriel J Brostow. Harmonic networks: Deep translation and rotation equivariance. In *Proceedings of the IEEE Conference on Computer Vision and Pattern Recognition*, pages 5028–5037, 2017.

[45] Carlos Esteves, Christine Allen-Blanchette, Ameesh Makadia, and Kostas Daniilidis. Learning so (3) equivariant representations with spherical cnns. In *Proceedings of the European Conference on Computer Vision (ECCV)*, pages 52–68, 2018.

[46] Taco S Cohen, Maurice Weiler, Berkay Kicanaoglu, and Max Welling. Gauge equivariant convolutional networks and the icosahedral cnn. *arXiv preprint arXiv:1902.04615*, 2019.

[47] Taco Cohen and Max Welling. Group equivariant convolutional networks. In *International conference on machine learning*, pages 2990–2999, 2016.

[48] Nicholas Guttenberg, Nathaniel Virgo, Olaf Witkowski, Hidetoshi Aoki, and Ryota Kanai. Permutation-equivariant neural networks applied to dynamics prediction. *arXiv preprint arXiv:1612.04530*, 2016.

[49] Ian Goodfellow, Jean Pouget-Abadie, Mehdi Mirza, Bing Xu, David Warde-Farley, Sherjil Ozair, Aaron Courville, and Yoshua Bengio. Generative adversarial nets. In *Advances in neural information processing systems*, pages 2672–2680, 2014.

[50] Jun-Yan Zhu, Richard Zhang, Deepak Pathak, Trevor Darrell, Alexei A Efros, Oliver Wang, and Eli Shechtman. Toward multimodal image-to-image translation. In *Advances in neural information processing systems*, pages 465–476, 2017.

[51] Zili Yi, Hao Zhang, Ping Tan, and Minglun Gong. Dualgan: Unsupervised dual learning for image-to-image translation. In *Proceedings of the IEEE international conference on computer vision*, pages 2849–2857, 2017.

[52] Jack Klys, Jake Snell, and Richard Zemel. Learning latent subspaces in variational autoencoders. In *Advances in Neural Information Processing Systems*, pages 6444–6454, 2018.

[53] Amjad Almahairi, Sai Rajeswar, Alessandro Sordoni, Philip Bachman, and Aaron Courville. Augmented cyclegan: Learning many-to-many mappings from unpaired data. *arXiv preprint arXiv:1802.10151*, 2018.

[54] Ming-Yu Liu, Thomas Breuel, and Jan Kautz. Unsupervised image-to-image translation networks. In *Advances in neural information processing systems*, pages 700–708, 2017.

[55] Yann LeCun, Corinna Cortes, and CJ Burges. Mnist handwritten digit database. *ATT Labs [Online]*. Available: <http://yann.lecun.com/exdb/mnist>, 2, 2010.

[56] Yuval Netzer, Tao Wang, Adam Coates, Alessandro Bissacco, Bo Wu, and Andrew Y Ng. Reading digits in natural images with unsupervised feature learning. *NIPS Workshop on Deep Learning and Unsupervised Feature Learning*, 2011.

[57] Johannes Stallkamp, Marc Schlipsing, Jan Salmen, and Christian Igel. The German Traffic Sign Recognition Benchmark: A multi-class classification competition. In *IEEE International Joint Conference on Neural Networks*, pages 1453–1460, 2011.

[58] Riccardo Volpi, Hongseok Namkoong, Ozan Sener, John C Duchi, Vittorio Murino, and Silvio Savarese. Generalizing to unseen domains via adversarial data augmentation. In *Advances in Neural Information Processing Systems*, pages 5334–5344, 2018.

[59] Diederik P Kingma and Jimmy Ba. Adam: A method for stochastic optimization. *arXiv preprint arXiv:1412.6980*, 2014.

[60] Matthew D Zeiler. Adadelta: an adaptive learning rate method. *arXiv preprint arXiv:1212.5701*, 2012.

[61] Anish Athalye, Nicholas Carlini, and David Wagner. Obfuscated gradients give a false sense of security: Circumventing defenses to adversarial examples. *arXiv preprint arXiv:1802.00420*, 2018.

[62] Alex Krizhevsky, Ilya Sutskever, and Geoffrey E Hinton. Imagenet classification with deep convolutional neural networks. In *Advances in neural information processing systems*, pages 1097–1105, 2012.

[63] Nitish Srivastava, Geoffrey Hinton, Alex Krizhevsky, Ilya Sutskever, and Ruslan Salakhutdinov. Dropout: a simple way to prevent neural networks from overfitting. *The journal of machine learning research*, 15(1):1929–1958, 2014.

[64] Xavier Glorot, Antoine Bordes, and Yoshua Bengio. Deep sparse rectifier neural networks. In *Proceedings of the fourteenth international conference on artificial intelligence and statistics*, pages 315–323, 2011.

[65] Yaroslav Ganin, Evgeniya Ustinova, Hana Ajakan, Pascal Germain, Hugo Larochelle, François Laviolette, Mario Marchand, and Victor Lempitsky. Domain-adversarial training of neural networks. *The Journal of Machine Learning Research*, 17(1):2096–2030, 2016.

[66] Han Xiao, Kashif Rasul, and Roland Vollgraf. Fashion-mnist: a novel image dataset for benchmarking machine learning algorithms. *arXiv preprint arXiv:1708.07747*, 2017.

[67] Gregory Cohen, Saeed Afshar, Jonathan Tapson, and Andre Van Schaik. Emnist: Extending mnist to handwritten letters. In *2017 International Joint Conference on Neural Networks (IJCNN)*, pages 2921–2926. IEEE, 2017.

[68] Tarin Clanuwat, Mikel Bober-Irizar, Asanobu Kitamoto, Alex Lamb, Kazuaki Yamamoto, and David Ha. Deep learning for classical japanese literature. *arXiv preprint arXiv:1812.01718*, 2018.

[69] Chhavi Yadav and Léon Bottou. Cold case: The lost mnist digits. In *Advances in Neural Information Processing Systems*, pages 13443–13452, 2019.

[70] Jonathan J. Hull. A database for handwritten text recognition research. *IEEE Transactions on pattern analysis and machine intelligence*, 16(5):550–554, 1994.

[71] Yi Li and Nuno Vasconcelos. Repair: Removing representation bias by dataset resampling. In *Proceedings of the IEEE Conference on Computer Vision and Pattern Recognition*, pages 9572–9581, 2019.

[72] John Moody and Joachim Utans. Architecture selection strategies for neural networks: Application to corporate bond rating prediction. In *Neural networks in the capital markets*, pages 277–300. Citeseer, 1994.

[73] Florian Tramer, Nicholas Carlini, Wieland Brendel, and Aleksander Madry. On adaptive attacks to adversarial example defenses. *arXiv preprint arXiv:2002.08347*, 2020.

[74] Mahyar Fazlyab, Alexander Robey, Hamed Hassani, Manfred Morari, and George Pappas. Efficient and accurate estimation of lipschitz constants for deep neural networks. In *Advances in Neural Information Processing Systems*, pages 11423–11434, 2019.

[75] Moustapha Cisse, Piotr Bojanowski, Edouard Grave, Yann Dauphin, and Nicolas Usunier. Parseval networks: Improving robustness to adversarial examples. In *Proceedings of the 34th International Conference on Machine Learning-Volume 70*, pages 854–863. JMLR. org, 2017.

[76] Dongyu Meng and Hao Chen. Magnet: a two-pronged defense against adversarial examples. In *Proceedings of the 2017 ACM SIGSAC Conference on Computer and Communications Security*, pages 135–147, 2017.

[77] Nicholas Carlini and David Wagner. Adversarial examples are not easily detected: Bypassing ten detection methods. In *Proceedings of the 10th ACM Workshop on Artificial Intelligence and Security*, pages 3–14, 2017.

[78] Jiawei Su, Danilo Vasconcellos Vargas, and Kouichi Sakurai. One pixel attack for fooling deep neural networks. *IEEE Transactions on Evolutionary Computation*, 23(5):828–841, 2019.

[79] Yinpeng Dong, Fangzhou Liao, Tianyu Pang, Hang Su, Jun Zhu, Xiaolin Hu, and Jianguo Li. Boosting adversarial attacks with momentum. In *Proceedings of the IEEE conference on computer vision and pattern recognition*, pages 9185–9193, 2018.

[80] Chuan Guo, Mayank Rana, Moustapha Cisse, and Laurens Van Der Maaten. Countering adversarial images using input transformations. *arXiv preprint arXiv:1711.00117*, 2017.

[81] Zuxuan Wu, Ser-Nam Lim, Larry Davis, and Tom Goldstein. Making an invisibility cloak: Real world adversarial attacks on object detectors. *arXiv preprint arXiv:1910.14667*, 2019.

[82] Can Kanbak, Seyed-Mohsen Moosavi-Dezfooli, and Pascal Frossard. Geometric robustness of deep networks: analysis and improvement. In *Proceedings of the IEEE Conference on Computer Vision and Pattern Recognition*, pages 4441–4449, 2018.

[83] Anish Athalye, Logan Engstrom, Andrew Ilyas, and Kevin Kwok. Synthesizing robust adversarial examples. *arXiv preprint arXiv:1707.07397*, 2017.

[84] Xiaolong Wang, Abhinav Shrivastava, and Abhinav Gupta. A-fast-rcnn: Hard positive generation via adversary for object detection. In *Proceedings of the IEEE Conference on Computer Vision and Pattern Recognition*, pages 2606–2615, 2017.

[85] Zhenyu Wu, Karthik Suresh, Priya Narayanan, Hongyu Xu, Heesung Kwon, and Zhangyang Wang. Delving into robust object detection from unmanned aerial vehicles: A deep nuisance disentanglement approach. In *Proceedings of the IEEE International Conference on Computer Vision*, pages 1201–1210, 2019.

[86] Chaowei Xiao, Bo Li, Jun-Yan Zhu, Warren He, Mingyan Liu, and Dawn Song. Generating adversarial examples with adversarial networks. *arXiv preprint arXiv:1801.02610*, 2018.

[87] Hyeungill Lee, Sungyeob Han, and Jungwoo Lee. Generative adversarial trainer: Defense to adversarial perturbations with gan. *arXiv preprint arXiv:1705.03387*, 2017.

[88] Huaxia Wang and Chun-Nam Yu. A direct approach to robust deep learning using adversarial networks. *arXiv preprint arXiv:1905.09591*, 2019.

[89] Pouya Samangouei, Maya Kabkab, and Rama Chellappa. Defense-gan: Protecting classifiers against adversarial attacks using generative models. *arXiv preprint arXiv:1805.06605*, 2018.

[90] Ajil Jalal, Andrew Ilyas, Constantinos Daskalakis, and Alexandros G Dimakis. The robust manifold defense: Adversarial training using generative models. *arXiv preprint arXiv:1712.09196*, 2017.

[91] Lukas Schott, Jonas Rauber, Matthias Bethge, and Wieland Brendel. Towards the first adversarially robust neural network model on mnist. *arXiv preprint arXiv:1805.09190*, 2018.

[92] Zhengli Zhao, Dheeru Dua, and Sameer Singh. Generating natural adversarial examples. *arXiv preprint arXiv:1710.11342*, 2017.

[93] Muhammad Muzammal Naseer, Salman H Khan, Muhammad Haris Khan, Fahad Shahbaz Khan, and Fatih Porikli. Cross-domain transferability of adversarial perturbations. In *Advances in Neural Information Processing Systems*, pages 12885–12895, 2019.

[94] Isaac Dunn, Tom Melham, and Daniel Kroening. Generating realistic unrestricted adversarial inputs using dual-objective gan training. *arXiv preprint arXiv:1905.02463*, 2019.

[95] Xiaosen Wang, Kun He, Chuan Guo, Kilian Q Weinberger, and John E Hopcroft. At-gan: A generative attack model for adversarial transferring on generative adversarial nets. *arXiv preprint arXiv:1904.07793*, 2019.

[96] Yang Song, Rui Shu, Nate Kushman, and Stefano Ermon. Constructing unrestricted adversarial examples with generative models. In *Advances in Neural Information Processing Systems*, pages 8312–8323, 2018.

[97] Simon Vandenhende, Bert De Brabandere, Davy Neven, and Luc Van Gool. A three-player gan: generating hard samples to improve classification networks. In *2019 16th International Conference on Machine Vision Applications (MVA)*, pages 1–6. IEEE, 2019.

- [98] Vinicius F Arruda, Thiago M Paixão, Rodrigo F Berriel, Alberto F De Souza, Claudine Badue, Nicu Sebe, and Thiago Oliveira-Santos. Cross-domain car detection using unsupervised image-to-image translation: From day to night. In *2019 International Joint Conference on Neural Networks (IJCNN)*, pages 1–8. IEEE, 2019.
- [99] Jeremy M Cohen, Elan Rosenfeld, and J Zico Kolter. Certified adversarial robustness via randomized smoothing. *arXiv preprint arXiv:1902.02918*, 2019.
- [100] Hadi Salman, Jerry Li, Ilya Razenshteyn, Pengchuan Zhang, Huan Zhang, Sébastien Bubeck, and Greg Yang. Provably robust deep learning via adversarially trained smoothed classifiers. In *Advances in Neural Information Processing Systems*, pages 11289–11300, 2019.
- [101] Beranger Dumont, Simona Maggio, and Pablo Montalvo. Robustness of rotation-equivariant networks to adversarial perturbations. *arXiv preprint arXiv:1802.06627*, 2018.
- [102] Jörn-Henrik Jacobsen, Jens Behrmann, Richard Zemel, and Matthias Bethge. Excessive invariance causes adversarial vulnerability. *arXiv preprint arXiv:1811.00401*, 2018.
- [103] Tommaso Dreossi, Somesh Jha, and Sanjit A Seshia. Semantic adversarial deep learning. In *International Conference on Computer Aided Verification*, pages 3–26. Springer, 2018.
- [104] Lakshya Jain, Wilson Wu, Steven Chen, Uyeong Jang, Varun Chandrasekaran, Sanjit Seshia, and Somesh Jha. Generating semantic adversarial examples with differentiable rendering. *arXiv preprint arXiv:1910.00727*, 2019.
- [105] Zhun Zhong, Liang Zheng, Guoliang Kang, Shaozi Li, and Yi Yang. Random erasing data augmentation. *arXiv preprint arXiv:1708.04896*, 2017.
- [106] Patrick J Grother. Nist special database 19 handprinted forms and characters database. *National Institute of Standards and Technology*, 1995.

Algorithm 4 Known model for background color

Inputs: image $x \in \mathbb{R}^{C \times H \times W}$, $\delta := (r, g, b) \in \Delta := [0, 255]^3$
Output: new image x

```
1:  $bgd\_image \leftarrow 0_{C \times H \times W}$ 
2:  $bgd\_image[0, :, :] \leftarrow r$ 
3:  $bgd\_image[1, :, :] \leftarrow g$ 
4:  $bgd\_image[2, :, :] \leftarrow b$ 
5:  $x \leftarrow \text{where}(x \leq 12, bgd\_image, x)$ 
```

A Appendix A: Experiments on one domain

A.1 MNIST

As discussed in the main text, the MNIST dataset is a well-known benchmark in machine learning. Despite this, as we have already seen, nuisances such as background color can degrade the performance of trained classifiers. In this section, we take a closer look at this fragility to background color and present experiments that support those provided in the main text.

A.1.1 Background color: gray to RGB

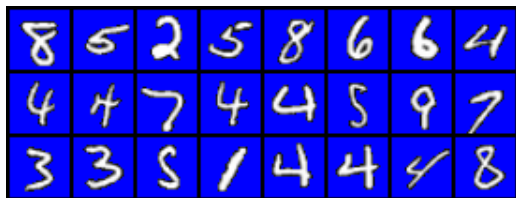
In Section 6.1.1, we showed that a known model can be used to provide robustness against changes in background color on the MNIST dataset. In each experiment that used this known model, we assumed that each image x was an element of $[C] \times [H] \times [W]$, where C is the number of channels, H is the width, and W is the width of the image. For all experiments on MNIST, we treated each handwritten digit as a three-channel ($C = 3$) image of size 28×28 ($H = 28$ and $W = 28$). In this case, the nuisance space $\Delta := [0, 255]^3$ is a compact subset of \mathbb{R}^3 , where each $\delta := (r, g, b) \in \Delta$ corresponds to a color in the RGB spectrum.

For clarity, we present pseudocode for this model in Algorithm 4. We begin in line 1 by initializing bgd_image to be a 3-tensor of all zeros with the same size as the input image. Next, we broadcast the red, green, and blue components of the inputted nuisance variable δ into the corresponding channels of bgd_image . Finally, in line 5 we replace those pixels in the original image x with value below an arbitrary threshold of 12 with the contents of bgd_image . For conciseness, we express this operation with the subroutine $\text{where}(\text{condition}, x, y)$, which takes three arguments. This function returns a tensor of elements gathered from x and y depending on the logical value of the condition, which is applied element-wise. More explicitly, for each index i in the input tensors, the corresponding output value z_i is defined as

$$z_i \leftarrow \begin{cases} x_i & \text{if the condition at the } i^{\text{th}} \text{ index is true} \\ y_i & \text{otherwise} \end{cases}$$

Such functionality is included in many standard computational libraries⁴.

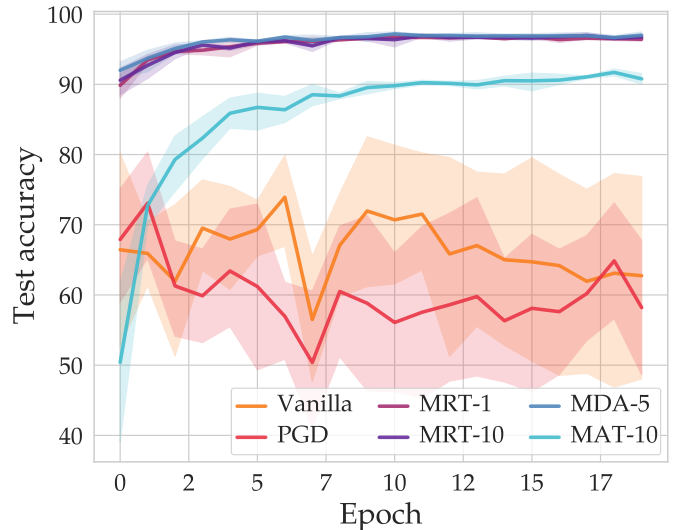
⁴<https://pytorch.org/docs/stable/torch.html#torch.where>



(a) **Domain A.** Domain A consisted of the MNIST digits with blue backgrounds.



(b) **Domain B.** Domain B consisted of the MNIST digits with red backgrounds.



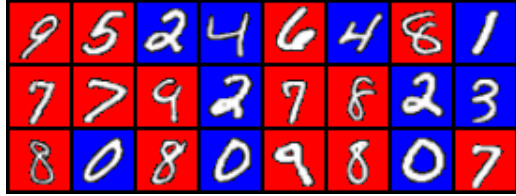
(c) **Results.** We show the test accuracies of baseline and model-based classifiers. After 20 epochs, the top-performing model-based classifiers outperform the baseline methods by as much as 35%.

Figure 17: **Robustness to red backgrounds on MNIST.** We show that by training on blue backgrounds and testing on red backgrounds, our model-based classifiers outperform baselines. In fact, the test accuracies of the baseline classifiers appear to decrease as they are trained for longer periods of time.

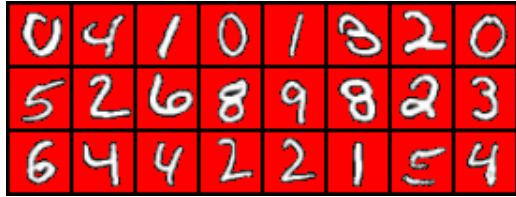
A.1.2 Background color: blue to red

With regard to the experiment described above in Appendix A.1.1, we wanted to narrow the scope of our experiments concerning robustness to background color on the MNIST dataset. In particular, we focused on robustness to changing from blue backgrounds to red backgrounds. In this way, we created two datasets – MNIST-blue and MNIST-red – which contain the MNIST digits with blue and red backgrounds respectively. In this experiment, we took domain A to be MNIST-blue and domain B to be MNIST-red. In Figures 17a and 7b, we show samples from these domains.

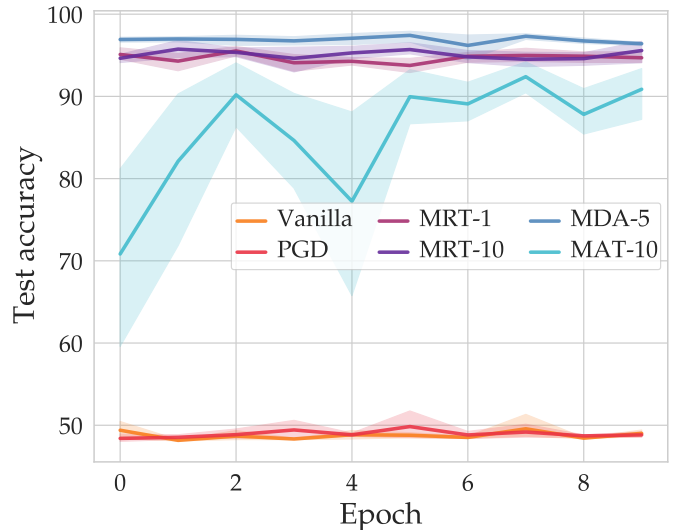
To perform model-based training, we first learned a model of background color changes using the MUNIT framework. This model was trained using data from the training sets for domains A and B . In Figure 17c, we show the test accuracies obtained by training on domain A and testing on the test set from domain B . Interestingly, both baseline methods drop in accuracy across twenty epochs in five independent trials. On the other hand, the classifiers trained with MDA and MRT both surpass 95% test accuracy on this task; MAT is not far behind and achieves upwards of 90% test accuracy after 20 epochs.



(a) **Domains A and B .** Both domains consist of the MNIST digits with different background colors. The digits with labels 0-4 were given blue backgrounds, whereas the digits with labels 5-9 were given red backgrounds.



(b) **Test data.** The test data consists of the MNIST digits with red backgrounds.



(c) **Results.** The baseline classifiers achieve a test accuracy of around 50% on the dataset of MNIST digits with red background, whereas the model-based classifiers achieve well over 95%.

Figure 18: **Robustness to background colors on MNIST: half blue, half red.** We consider an experiment in which domains A and B consist of the MNIST handwritten digits with differently colored backgrounds. In particular, we set the backgrounds of all digits with labels 0-4 to blue and we set the digits with labels 5-9 to red. We train the classifiers and a model of natural variation on this data, and then we tested the classifiers on a dataset consisting of all the MNIST digits with red backgrounds.

A.1.3 Background color: half red, half blue

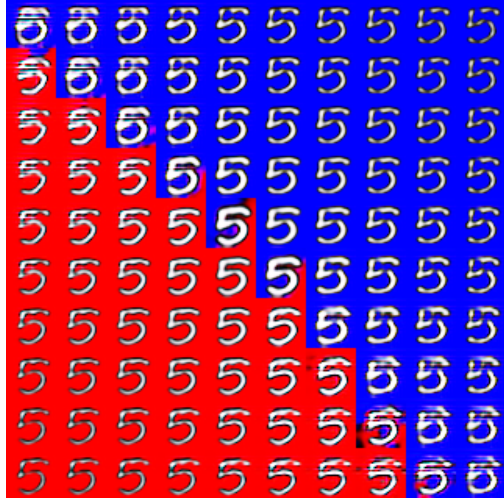
We let domains A and B contain instances from MNIST-Red that have labels 5-9 as well as images from MNIST-Blue with labels 0-4. Samples from domain A and B are shown in Figure 18a. Note that while training on domain A , all classifiers did not have access to images of digits with red backgrounds and the labels 0-4. We then test the classifiers on the entirety of MNIST-red to show that baseline classifiers overfit to the background colors of the training set. This test set is shown in Figure 18b.

The test accuracies for this experiment are shown in Figure 18c. Notably, the baseline classifiers achieve nearly 50% test accuracy on MNIST-Red, as they are not able to generalize beyond the unseen red backgrounds for digits with labels 0-4. On the other hand, the classifiers trained with our model-based methods generalize to correctly classify the digits in the test set of MNIST-Red with close to 98% accuracy.

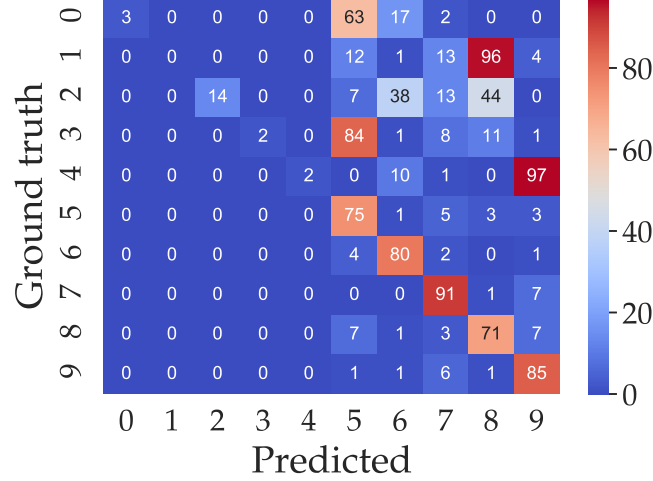
In Figure 19, we take a closer look at the model of background colors that was learned for this task. In particular, in Figure 19a, we show an image from domain A . Then in Figure 19b, we show the result of gridding the nuisance space Δ of the learned model. Note that in this neighborhood of the origin, the regions of the nuisance space that result in red and blue backgrounds are roughly the same size, which reflects the fact that half of the data in domains A and B have red backgrounds,



(a) Original image.



(b) **Nuisance space gridding.** Gridding the nuisance space in the rectangle $[-2, 2] \times [-2, 2]$ reveals that the approximately half of Δ will induce a red background, while the other half will induce a red background.

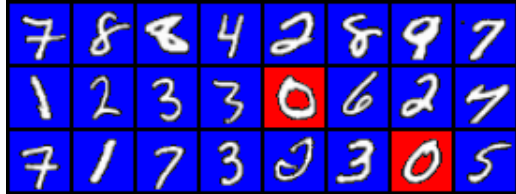


(c) **Prediction matrix for the baseline.** We compare the ground truth labels with the predictions for the baseline algorithm to evaluate its lack of robustness against the shift in background colors between the training and test distributions.

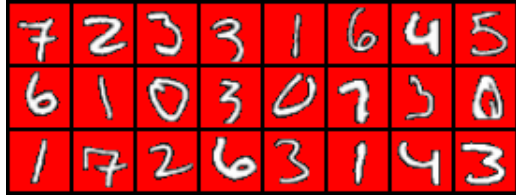
Figure 19: **MNIST: half red, half blue analysis.** In the left column, we show a gridding of the nuisance space for a representative sample from domain A . On the right, we show a matrix corresponding to the ground truth and predicted labels for this experiment.

whereas the other half have blue backgrounds.

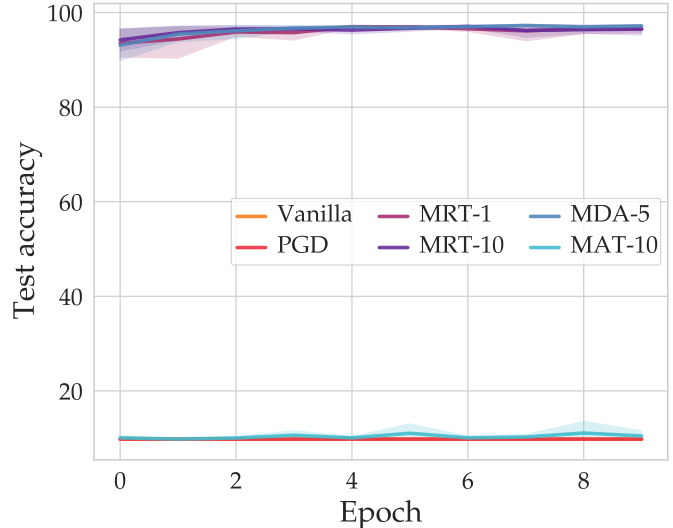
Finally, we also look at the prediction matrix for this experiment in Figure 19c. On the vertical axis, we show the ground truth labels and on the horizontal axis we show the predicted labels. Note that as the digits with labels 5-9 have red backgrounds in domain A , these images are generally classified correctly, while images with ground truth labels 0-4 are almost always misclassified.



(a) Domains A and B . Both domains consist of the MNIST digits with different background colors. The digits with label 0 were given red backgrounds, whereas the digits with labels 1-9 were given blue backgrounds.



(b) Test data. The test data consists of the MNIST digits with red backgrounds.



(c) Results. The baseline classifiers achieve a test accuracy of around 10% on the dataset of MNIST digits with red background, whereas the model-based classifiers achieve well over 95%.

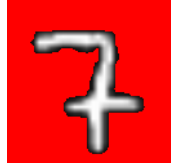
Figure 20: **Robustness to background colors on MNIST: one red, nine blue** We now look at a more challenging task corresponding to MNIST digits with different background colors. In particular, we set the backgrounds of all digits with labels 0 to red and we set the digits with labels 1-9 to blue. We train the classifiers and a model of natural variation on this data, and then we tested the classifiers on a dataset consisting of all the MNIST digits with red backgrounds.

A.1.4 Background color: one red, nine blue

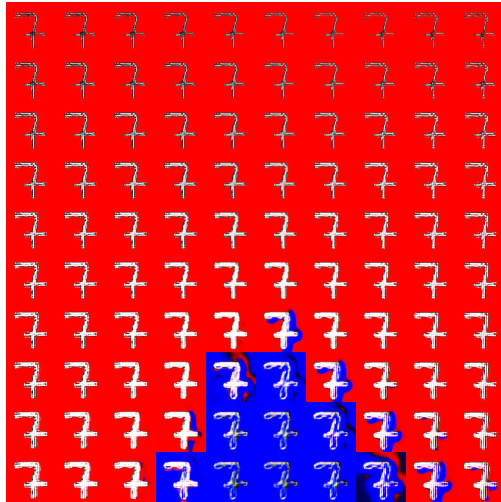
A slightly more illuminating variant of the above experiment involves changing how much exposure the baseline classifier gets to red backgrounds. To this end, we repeat the MNIST experiment described above, but we change the domains A and B . Namely, we take domains A and B to be the images from MNIST-Blue with labels 1-9 and images from MNIST-Red that have label 0. Again, the test distribution was taken to be the entirety of MNIST-Red. These datasets are shown in Figures 20a and 20b.

In Figure 20c, we show the test accuracies of each classifier. Notably, the classifiers trained with MRT and MDA achieve the same test accuracy as the upper bound of the ideal classifier. Furthermore, consider that for this ten-class prediction task, a classifier that predicts a random label for an input datum would achieve 10% accuracy. By this metric, it is clear that for this task the baseline classifiers do not outperform random classifiers for this task.

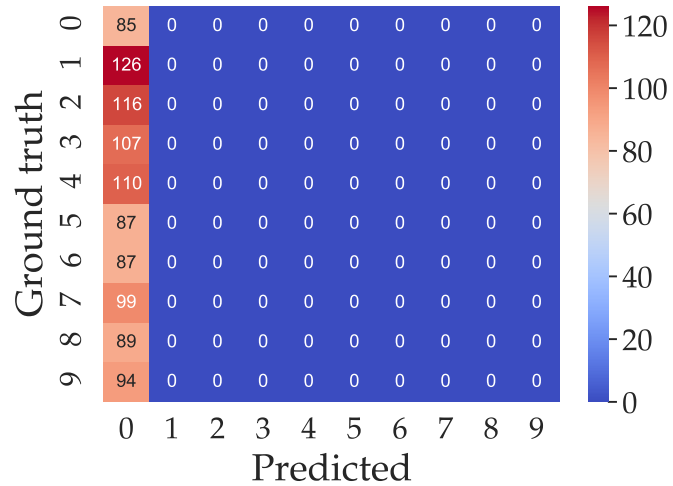
As in Section A.1.3, we examine the nuisance space and the prediction matrix for this experiment in Figure 21. In particular, Figure 21a shows an image from domain A . In 21b, we show a gridding of nuisance space Δ .



(a) Original image.



(b) **Nuisance space gridding.** Gridding the nuisance space in the rectangle $[-2, 2] \times [-2, 2]$ reveals that only a small region can generate images with blue backgrounds.



(c) **Prediction matrix for the baseline.** We compare the ground truth labels with the predictions for the baseline algorithm to evaluate its lack of robustness against the shift in background colors between the training and test distributions.

Figure 21: **MNIST: half red, half blue analysis.** In the left column, we show a gridding of the nuisance space for a representative sample from domain A . On the right, we show a matrix corresponding to the ground truth and predicted labels for this experiment.

A.2 SVHN

The SVHN is a richer and more diverse dataset than MNIST, and therefore there are a larger family of nuisances that present a significant challenge during classification from a robustness perspective. In particular, in this subsection we will consider the following nuisances: contrast, brightness, erasing, decolorization, colorization, and hue. As described in Appendix D, each of the domains for these experiments can be obtained via thresholding or by applying known transformations to data.



(a) **Original.** This is an example of a low-contrast image from SVHN.



(b) **Grid.** This figure shows a gridding of the nuisance space Δ in $[-2, 2] \times [-2, 2]$. Note that by gridding Δ , we can generate high-contrast images with the same semantic content as the image in (a).

Figure 22: **SVHN contrast gridding.** We show an image from domain A in (a) and a gridding of subset of the nuisance space Δ of the learned model of contrast in (b).

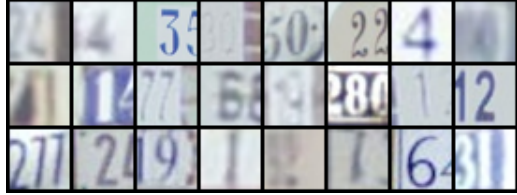
A.2.1 Robustness to contrast

In Section 6.1.2 of the main text, we showed that the model-based paradigm can provide high levels of robustness against changes in contrast between the training data and the test data. In particular, Figure 8c shows that the gap between the test accuracy of the baseline and model-based classifiers approached 30% after 100 epochs.

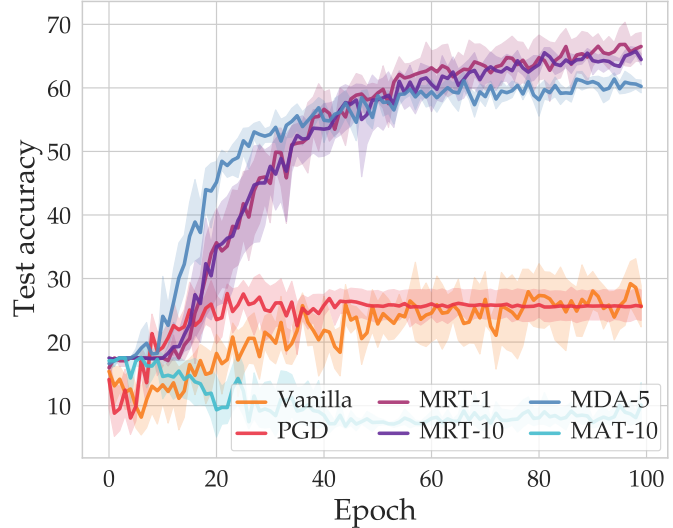
In Figure 22, we explore the nuisance space Δ for the model learned on domains A and B of the experiment described in Section 6.1.2 of the main text. In Figure 22a, we show an image from domain A . The model learned for this challenge is designed to transform low-contrast samples from domain A to resemble high-contrast samples from domain B . In Figure 22b, we see that by gridding Δ , the model effectively maps this low-contrast sample to samples with higher contrast. Moreover, this gridding reveals that rather than learning a one-to-one mapping between samples from A and corresponding samples in B , the model learns a multi-modal output distribution, which is evinced by the different background colors and hues seen in this grid.



(a) **Domain A.** Domain A consisted of low-brightness images from SVHN.



(b) **Domain B.** Domain B consisted of high-brightness images from SVHN.



(c) **Results.** Test accuracies of the trained classifiers.

Figure 23: **SVHN brightness.** Model based classifiers significantly outperform baseline classifiers when trained on low-brightness images and tested on high-brightness images. The gap between the baseline and model-based classifiers approaches 40 percentage points after 100 epochs.

A.2.2 Robustness to brightness (low to high)

In Section 6.1.3, we showed that differences in brightness on GTSRB can cause significant drops in test accuracy. Further, we showed that model-based training can help to provide robustness to this nuisance.

The story is similar on SVHN. In Figures 23a and 23b, we show images from domains A and B , which contain low- and high-brightness samples respectively. The goal of this experiment is to train on samples from domain A and then to test on samples from the test set of domain B . In Figure 23c, we see that baseline methods approach 30% test accuracy on the test set for domain B . Conversely, the MRT and MDA classifiers reach test accuracies of more than 60%. This represents a more than 30% improvement over the baselines.

Notably, the classifier trained with MAT does very poorly here. As discussed in Section 7, we find that in general zeroth order methods such as MRT and MDA are more natural algorithms for this task, as MAT cannot effectively leverage the geometry of the manifold at the output of the learned model.

In Figure 24, we show an image from domain A in (a). In Figure 24b. we show the images generated by gridding the 2-dimensional nuisance space Δ . This shows that by sampling $\delta \in \Delta$, we can generate a multimodal distribution of high-brightness images that correspond to low-brightness samples from domain A .



(a) **Original.** This is an example of a low-brightness image from SVHN.



(b) **Grid.** This figure shows a gridding of the nuisance space Δ in $[-2, 2] \times [-2, 2]$. Note that while each of these samples is brighter than the original image in (a), one can obtain a range of background colors and hues by sampling from Δ .

Figure 24: **Gridding a model of brightness on SVHN.** We show an image from domain A in (a) and a gridding of subset of the nuisance space Δ of the learned model of brightness in (b).

A.2.3 Robustness to brightness (medium to all)

In an experiment similar to that of the previous section, in this section we again consider the robustness of classifiers trained on subsets of SVHN that correspond to different brightness levels. In this case, we take domain A to be medium-brightness samples from SVHN and we take domain B to be all of SVHN. Samples from these domains are shown in Figures 25a and 25b.

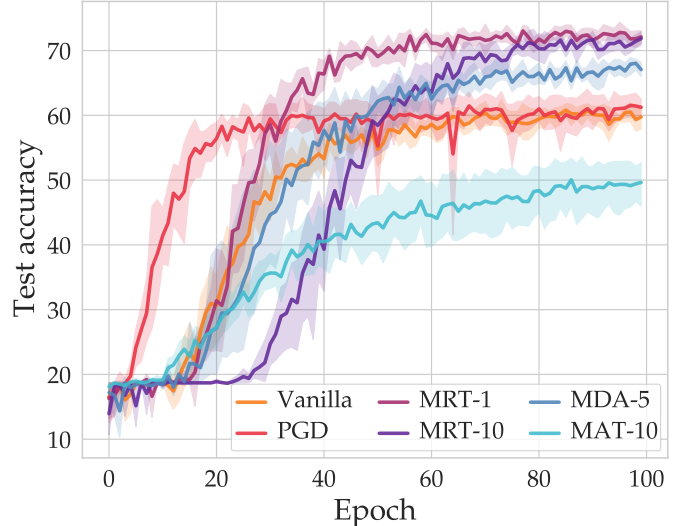
We train a model of natural variation to map samples from domain A to B and perform model-based training using this model. The test accuracies of the baseline and model-based classifiers are shown in Figure 25c. On this task, the classifiers trained with MRT and MDA outperform the baselines by as much as 10%. On the other hand, the classifier trained with MAT lags around 10% behind the baselines.



(a) **Domain A.** Domain A consisted of medium-brightness images from SVHN.



(b) **Domain B.** Domain B consisted of images of all different brightness levels in SVHN.



(c) **Results.** The MRT and MDA classifiers outperform the baselines by nearly 10% in this task.

Figure 25: **Robustness to all levels of brightness on SVHN.** We show that by training a model of natural variation to map from medium brightness samples from SVHN to all of SVHN, we can outperform baseline classifiers on test samples from all levels of brightness.

A.2.4 Robustness to erasing with a known model

In many cases, models of a source of natural variation are known and thus it is not necessary to learn these models from data. For example, one technique often used in the computer vision community to avoid overfitting is random erasing, or randomly removing parts of images and replacing them with black rectangles [105]. In the case of random erasure, an explicit model is readily available; a black rectangle can be artificially inserted into an image by randomly selecting a point in $\Delta \subset \mathbb{R}^4$ where the four dimensions represent the x - and y -component, width, and height of the rectangle. For clarity, we explicitly describe this transformation in Algorithm 5. Throughout, we use the notation $[k] := \{0, 1, \dots, k - 1\}$, and H, W are universal constants representing the height and width of the images in a given dataset.

Algorithm 5 Known model for erasure

Inputs: image $x \in \mathbb{R}^{C \times H \times W}$, $\delta := (x, y, h, w) \in \Delta := [W] \times [H] \times [W] \times [H]$
Outputs: new image $x \in \mathbb{R}^{C \times H \times W}$

```

1:  $max\_size \leftarrow \max\{H, W\}/2$ 
2:  $A := [0, \min(H - y, max\_size)]$ 
3:  $y\_h \leftarrow \Pi_A(h)$  # Get height of erased region
4:  $B := [0, \min(W - x, max\_size)]$ 
5:  $x\_w \leftarrow \Pi_B(w)$  # Get width of erasure region
6:  $x[:, y:y + y\_h, x:x + x\_w] = 0$  # Erase region in  $x$ 

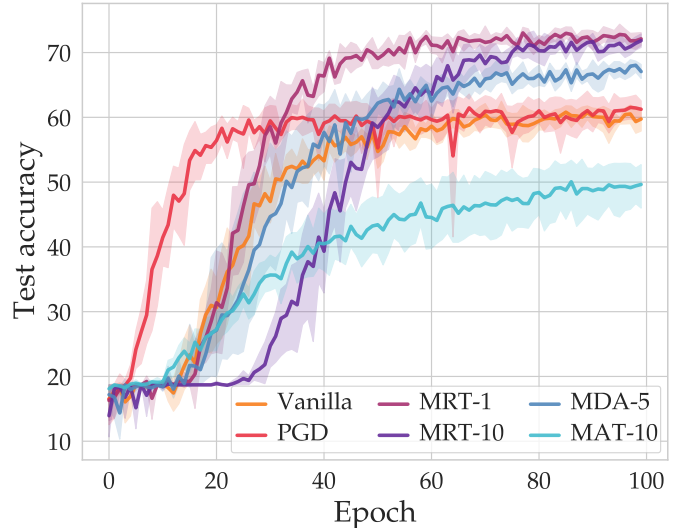
```



(a) **Domain A.** Domain A consisted of samples from SVHN.



(b) **Domain B.** Domain B consisted of samples from SVHN with random erasing.



(c) **Results.** By using the known model, the MRT and MDA classifiers achieved close to a 10% increase in test accuracy over the baselines.

Figure 26: **Robustness to erasing on SVHN with a known model.** We use a known model of erasing to test the robustness of model-based and baseline classifiers to random erasing.

To test the efficacy of a known model rather than a model learned from data, we let domain A comprise data from SVHN and domain B contain the same data with random erasure. These datasets are shown in Figures 26a and 26b respectively. In Figure 26c, we see that our model-based methods achieve more than 10% improvement over the baseline and PGD classifiers by leveraging the known model of random erasing. More specifically, since the model-based classifiers are exposed to images with random erasing during training time, they are consequently more robust to this transformation at test time.

A.2.5 Robustness to erasing with a learned model

We repeated the experiment of the previous section with a learned model. We also increased the probability of random erasing to 75% (as opposed to 50% in the previous experiment) so that the MUNIT model could be exposed to enough erased data. This made the task noticeably harder, and consequently the accuracy of the baseline classifiers dropped by 5-10% vis-a-vis the previous experiment. In this case, the improvements over the baselines are more modest than in the previous experiment. Indeed, by examining the impact of gridding the nuisance space Δ of this learned model in 28, we see that the model did not learn to erase patches in the image. The improvement in the test accuracy on the test set for domain B is therefore simply an artifact of the model’s ability to produce a diverse set of images with different hues and background colors.

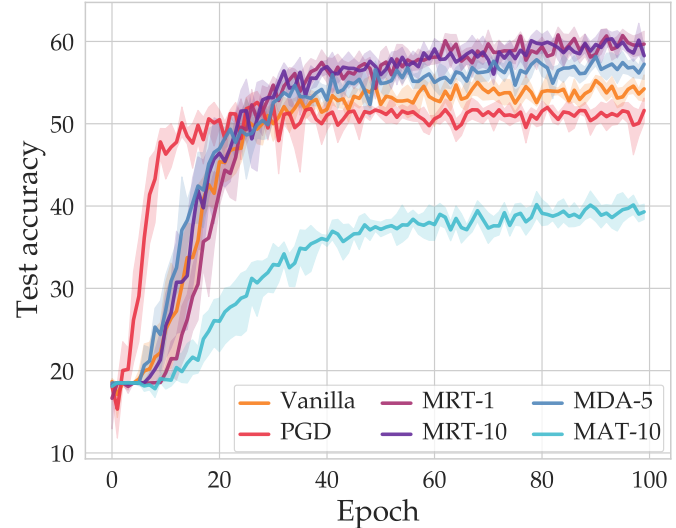
We can make a number of useful conclusions from this experiment. Firstly, if a known model is available, it is oftentimes effective to use it rather than train a model from data. Further, this experiment reinforces the notion that the utility of model-based training is limited by the quality of the underlying model. In Section 7.2, we look more closely at this conjecture. On the other hand, in this challenging task, we find that in spite of a model that doesn’t capture the essence of the desired factor of natural variation, the model-based classifiers still outperform the baselines. Thus even when models aren’t effectively learned, they can still introduce other factors of natural variation such as background color and hue into the training data. This exposure to a larger and more diverse set of data is a useful feature of model-based training, and one that we will explore in future work.



(a) **Domain A.** Domain A consisted of samples from SVHN.



(b) **Domain B.** Domain B consisted of samples from SVHN with random erasing.

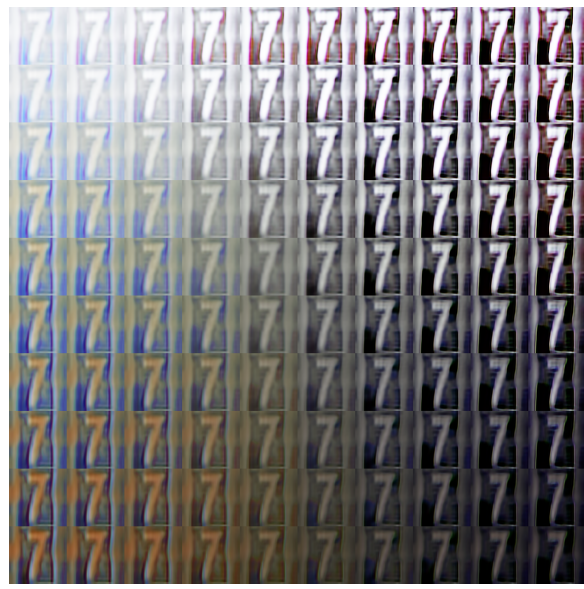


(c) **Results.** The gains made by the MRT and MDA classifiers over the baselines are less pronounced than in the previous experiment with the known model. These model-based classifiers achieve around a 5% improvement over the baselines.

Figure 27: **Robustness to erasing on SVHN with a learned model.** We repeat the experiment of the previous section with a learned model of erasing. We report more modest gains over the baseline classifiers for the MRT and MDA classifiers for this task than for the known model.



(a) **Original.** This is a representative image from SVHN.



(b) **Grid.** We gridded the nuisance space Δ of the learned model. In this case, it seems that the model did not learn a useful model for erasing.

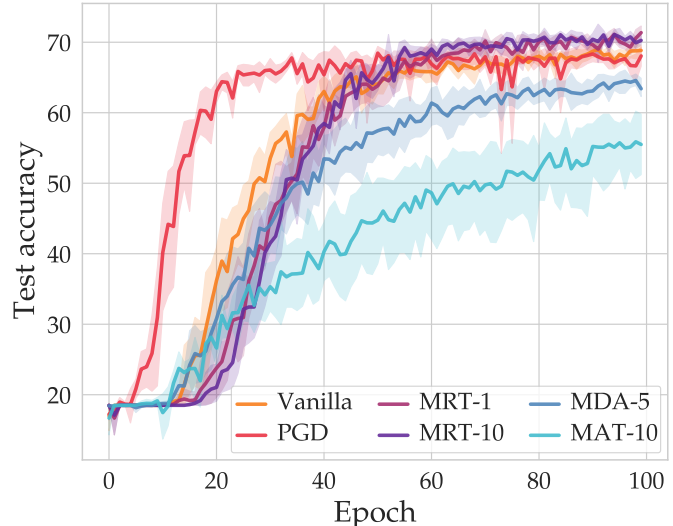
Figure 28: **Gridding a model of erasing on SVHN.** We show an image from domain A in (a) and a gridding of subset of the nuisance space Δ of the learned model of erasing in (b).



(a) **Domain A.** Domain A consisted of grayscale images from SVHN.



(b) **Domain B.** Domain A consisted of RGB images from SVHN.



(c) **Results.** We see modest improvements over the baselines in this task, which is largely due to the fact that the SVHN dataset already contains images that are close to grayscale.

Figure 29: **Robustness to colorization on SVHN.** By taking domains A and B to contain grayscale and RGB color images from SVHN respectively, we can achieve moderate levels of robustness against the shift from domain A to domain B .

A.2.6 Robustness to colorization

We next turn our attention to examining the robustness of SVHN with respect to colorization. That is, we take domain A to contain grayscale images from SVHN, and we take domain B to contain the corresponding RGB images. Images from both of these domains are shown in Figures 29a and 29b. We learned a model to map grayscale images in domain A to RGB images in domain B .

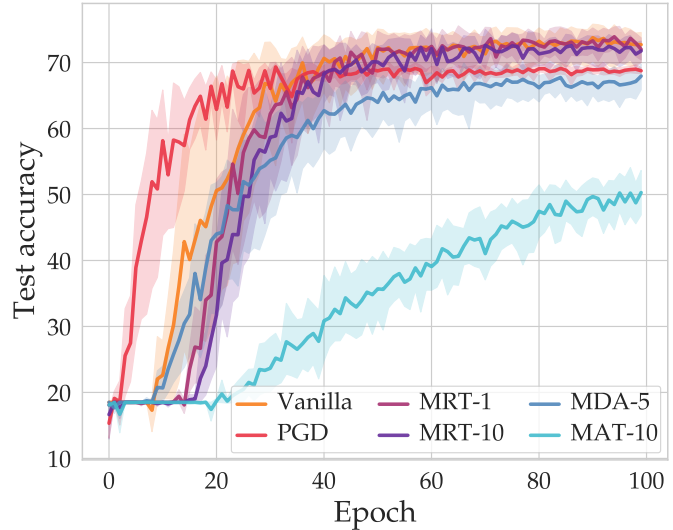
In Figure 29c, we show the test accuracies obtained by testing the baseline and model-based classifiers on test data from domain B . For this colorization task, we achieve a small improvement of close to 3% over the baseline classifiers.



(a) **Domain A.** Domain A consisted of RGB samples from SVHN.



(b) **Domain B.** Domain B consisted of grayscale images from SVHN.



(c) **Results.** On this task, we achieve approximately the same results as the baselines.

Figure 30: **Robustness to decolorization on SVHN.** We do not improve over the baselines in this task as there are already images in SVHN that are close to grayscale, and therefore the task does not present as significant a challenge as other presented in this section.

A.2.7 Robustness to decolorization

We also performed the inverse experiment to that of the previous section. That is, we let domain A contain RGB images from SVHN and we let domain B contain the corresponding grayscale images. As shown in Figure 30, this task is not as challenging as those reported previously, and consequently we achieve around the same performance as the baseline classifiers. A gridding of the nuisance space Δ of the learned model for this task is shown in Figure 31.

This experiment can be seen as the complement of the experiment for erasing on SVHN with a learned model presented in Section A.2.5. In this case, the model shown in Figure 31 creates realistic grayscale images that correspond closely to the original input image shown in Figure 31a. However, as this task is quite easy, the model is ineffective as the task is not challenging enough for the baselines.



(a) **Original.** This is a representative image from SVHN.



(b) **Grid.** We gridded the nuisance space Δ in $[-2, 2] \times [-2, 2]$ to show images that can be obtained by sampling from Δ .

Figure 31: **Gridding a model of decolorization on SVHN.** We show an image from domain A in (a) and a gridding of a subset of the nuisance space Δ of the learned model of decolorization in (b).

A.2.8 Hue and background color

Another notable challenge on SVHN is that of hue. In particular, we let domain A be RGB images from the SVHN dataset, and we took domain B to be the same images with an inverted HSV color spectrum. Example images from domains A and B are shown in Figures 32a and 32b. In contrast to other challenges, many datasets such as SVHN have a rich diversity in hue, and consequently this nuisance doesn't pose as significant a challenge as brightness or contrast.

In this experiment, the model that we learned reflected the fact that SVHN has a wide range of background colors and hues. In Figure 33a, we show an image from SVHN. Then in Figure 33b we show the output images generated by gridding the nuisance space Δ . This gridding reveals that by sampling different $\delta \in \Delta$, we can generate images with the same semantic content (i.e. the image contains the same "six" house sign number) but with different background colors and hues.

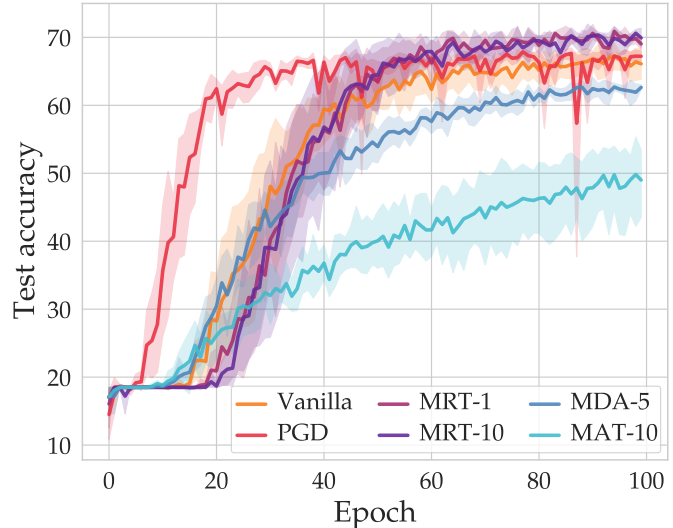
The results of this experiment are shown in Figure 32c. Indeed, as SVHN already contains a diversity of hues, the MDA classifiers perform below baseline methods as baseline methods can successfully generalize beyond background color. On the other hand, the MRT classifiers achieve higher test accuracies as they search *adversarially* for challenging images. In this way, it seems that searching for worst-case examples is more efficacious toward achieving high accuracy when datasets already contain a diversity of samples with respect to a particular challenge. That being said, in data-rich scenarios for factors of natural variation that are already present throughout the dataset, the utility of learning a model and doing model-based training is not as significant as for more challenging sources of variation.



(a) **Domain A.** Domain A consisted of (RGB) images from SVHN.



(b) **Domain B.** Domain B consisted of the same samples from A with an inverted HSV color spectrum.



(c) **Results.** The MRT classifiers improve marginally over the baselines in this experiment, while the MAT and MDA classifiers lag behind the baselines.

Figure 32: **Robustness to hue on SVHN.** We take domains A and B to be RGB and the corresponding HSV images from SVHN. We learned a model to map from domain A to domain B , which we used to perform model-based training.

A.3 GTSRB

In the final subsection of this appendix, we give additional details that correspond to the experiments in Section 6.1 that use the GTSRB dataset.

A.3.1 Robustness to contrast

We first consider the robustness of GTSRB to changes in contrast. More specifically, we let domain A contain low-contrast samples on GTSRB and we let domain B contain high-contrast samples from GTSRB. Images from these domains are shown in Figure 34a and 34b. As in previous experiments, we first train a model on training data from domains A and B . We then perform model-based training using this model with training data from domain A and we also train the baseline classifiers with the training data from domain A .

The results from this experiment are shown in Figure 34c. Interestingly, we see that the MAT classifier reaches the highest test accuracy on images from the test set of domain B . This stands in contrast to previous tasks in which the MAT classifiers lagged behind the baseline, MRT, and MDA classifiers. Notably, the MRT and MDA classifiers also outperform the baselines by around 5% on average.

In Figure 35, we grid the nuisance space Δ of the learned model to show that by sampling $\delta \in \Delta$, we can produce a range of images with the same semantic content but with varying contrast.



(a) **Original.** This image is a representative sample from SVHN.



(b) **Grid.** We gridded the nuisance space Δ in $[-2, 2] \times [-2, 2]$ of the learned model of hue to show that by sampling different $\delta \in \Delta$, we can generate images with different hues.

Figure 33: **Gridding a model of hue on SVHN.** By gridding the nuisance space of the model learned for hue on SVHN, we see that by varying $\delta \in \Delta$, we can achieve a diversity of background colors for the same image.

A.3.2 Robustness to brightness

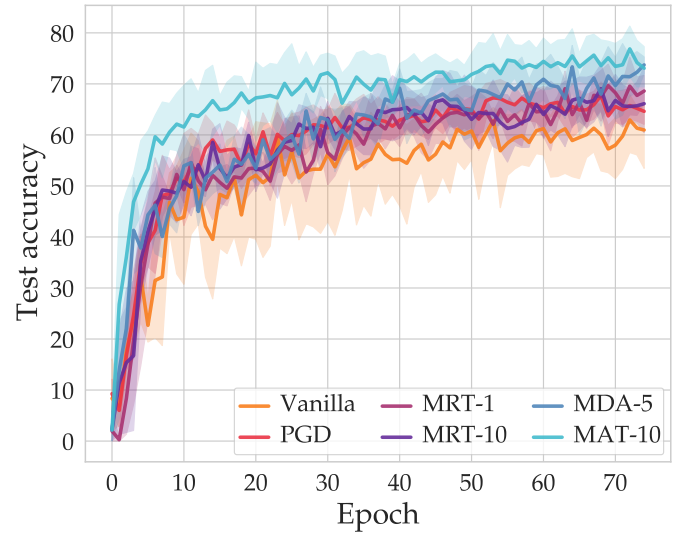
A gridding of the nuisance space in 36 for the learned model we used in Section 6.1.3 reveals that the model trained for this task was able to generate a range of images in daylight. Indeed, while this model retains artifacts such as the vertical lines in the background of the image in 36a, it learns to change the lighting conditions from dark to light.



(a) **Domain A.** Domain A consisted of low-brightness samples from GTSRB.



(b) **Domain B.** Domain B consisted of high-brightness sample from GTSRB.



(c) **Results.** The MAT and MDA classifiers improve over baselines by between 5 and 10% when tested on the test set from domain B .

Figure 34: **Robustness to contrast on GTSRB.** We consider a task in which domains A and B contain low- and high-brightness images respectively. When testing on domain B , we see that model-based classifiers outperform the baselines by between 5 and 10%.



(a) **Original.** This image is a representative low-contrast samples from GTSRB.



(b) **Grid.** We gridded the nuisance space Δ of the learned model of contrast to show the range of high-contrast images we obtain.

Figure 35: **Gridding a model of contrast on GTSRB.** We show an image from domain A in (a) and a gridding of subset of the nuisance space Δ of the learned model of contrast in (b).



(a) **Original.** This image is a representative low-brightness sample from GTSRB.



(b) **Grid.** We gridded the nuisance space Δ of the learned model of brightness to show the range of high-brightness images we obtain.

Figure 36: **Gridding a model of brightness on GTSRB.** We show an image from domain A in (a) and a gridding of subset of the nuisance space Δ of the learned model of brightness in (b).

B Appendix B: Experiments across domains

In this appendix, we present results that support those given in Section 6.2. In particular, we consider tasks in which we train a model of natural variation on one dataset and then use that model on another dataset.

B.1 MNIST variants

In Appendix A.1.2, we described an experiment in which we first trained a model to change the background colors in the MNIST digits from blue to red. Then by applying this model to other similar datasets with blue backgrounds, we performed model-based training and subsequently tested each trained classifier on images with red backgrounds.

In Figure 37, we show the test accuracy plots corresponding to Table 5 for this background color robustness task. Note that for each dataset, the model-based classifiers outperform the baseline classifiers despite the fact that the model of background color changes has been learned on MNIST. As shown in Table 4, the images produced by the model semantically resemble the corresponding inputs. This allows the model-based classifiers to perform well against the unseen red backgrounds on each of these datasets. On the other hand, the baseline classifiers are erratic. At times, such on the USPS dataset, the test accuracy approaches that of the model-based classifiers. In other cases, such as on E-MNIST and K-MNIST, the test accuracy is significantly below that of the model-based classifiers, signaling that these classifiers have overfit to blue backgrounds.

We also repeated the experiment described in Appendix A.1.4, wherein we colorized each MNIST digit according to its label. More specifically, we changed the background color for images

with the label 0 to red, and we change the background color for images with the labels 1-9 to blue. By letting these images comprise both domains A and B on MNIST, we learned a model that could generate images of all of the digits with red and blue backgrounds. See Appendix A.1.4 for details. After learning this model, we created similar domains for the MNIST variants mentioned in Section 6.2.1 and used the model learned on MNIST to perform model-based training.

The results of these experiments are shown in Figures 38. Notably, in each figure, despite the fact that the model G was trained on a separate dataset, classifiers trained with our model-based paradigm significantly outperformed the baseline methods.

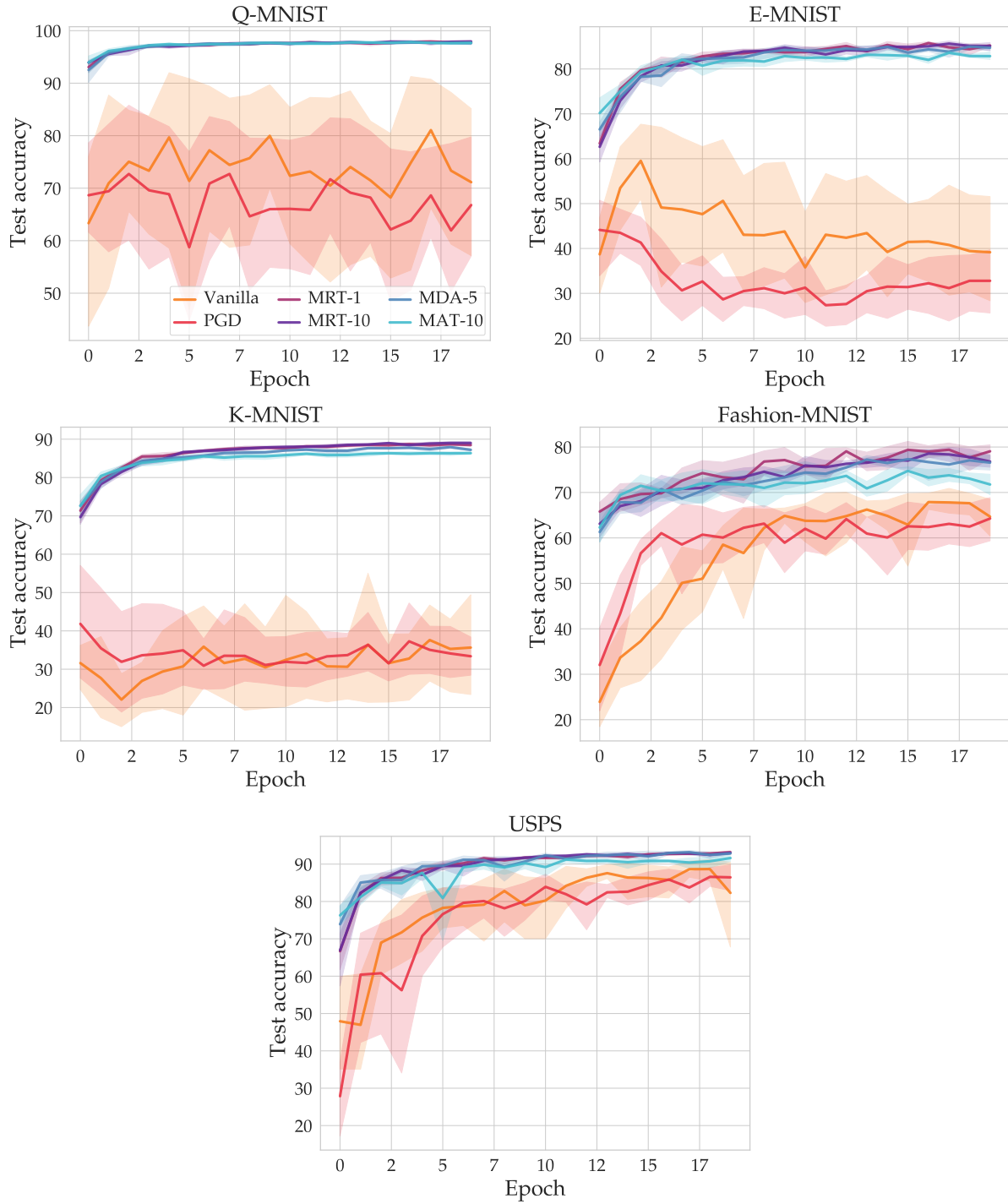


Figure 37: **Reusing a learned model on MNIST variants with mixed label colors.** For a range of MNIST-like datasets, we consider a task in which the training data has blue backgrounds and the test data has red backgrounds. The test accuracies corresponding to baseline and model-based algorithms are shown for each dataset in the above plots.

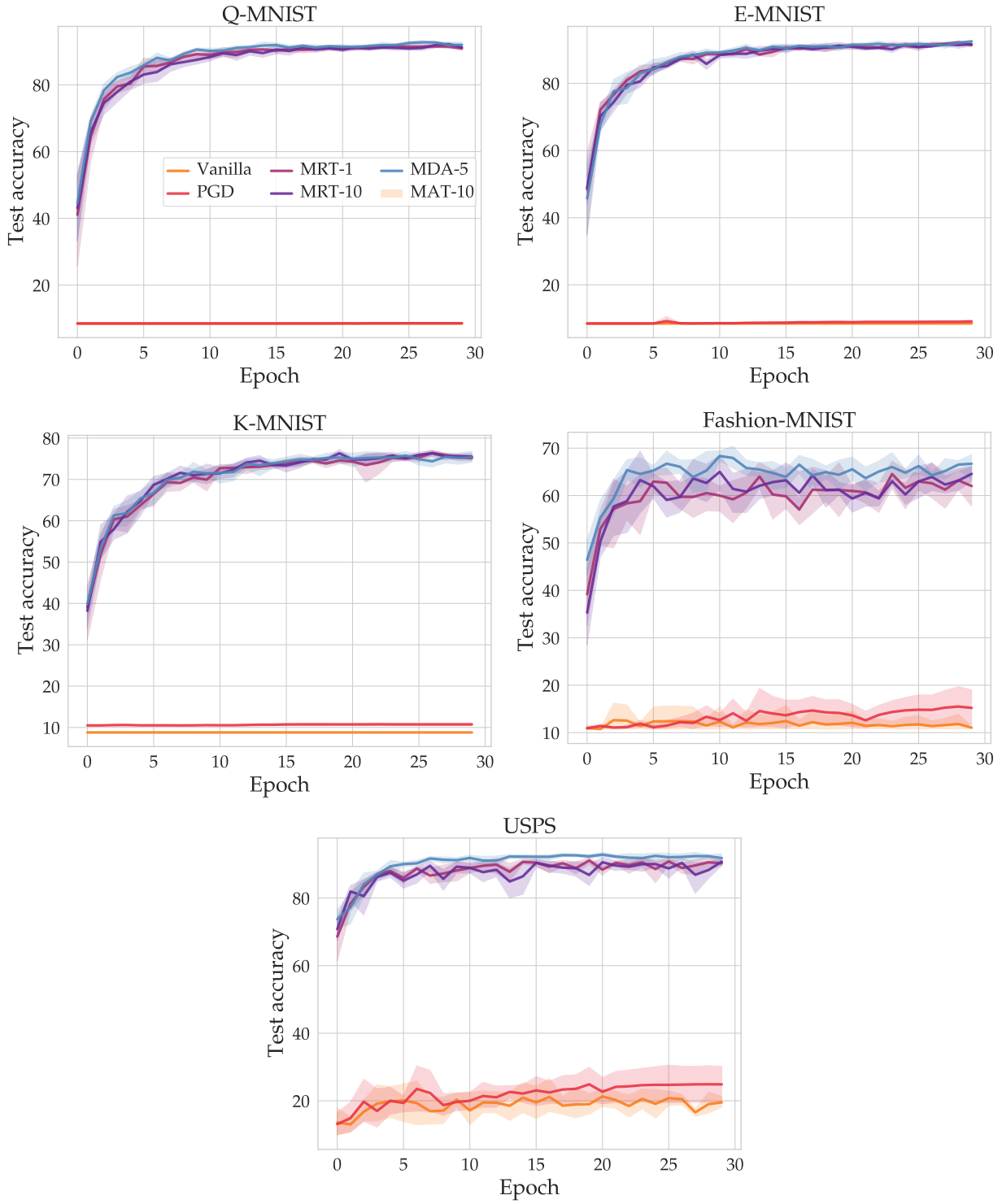
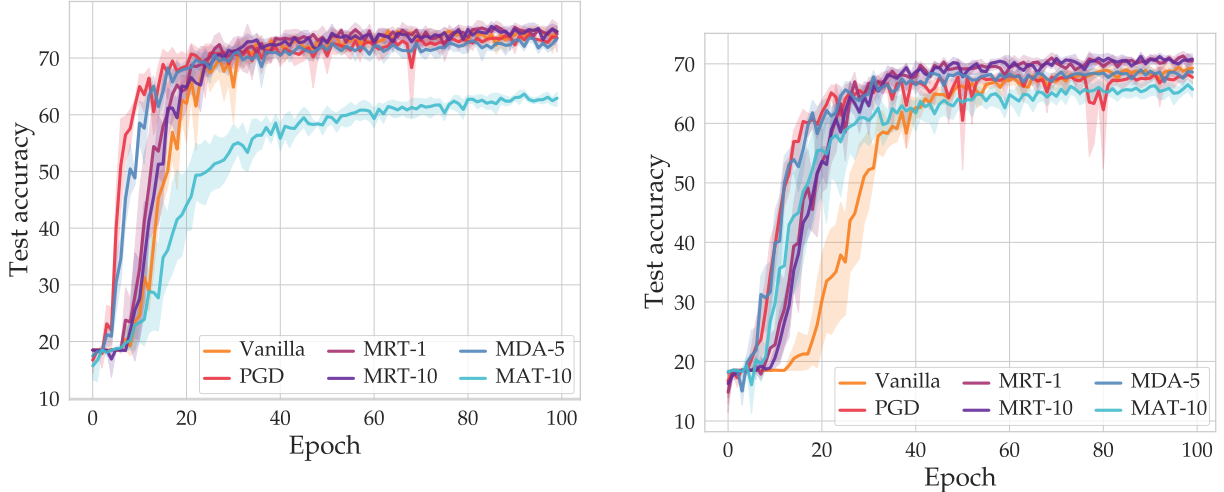


Figure 38: **Reusing a learned model of background colors on MNIST variants.** For a range of MNIST-like dataset, we train using a model trained on MNIST to perform model-based training.



(a) **RGB to grayscale.** As we showed in Appendix A, the task of providing robustness to the shift from RGB to grayscale is not as challenging as some of the other nuisances that we consider in this paper. All methods achieve approximately the same test accuracy.

(b) **Grayscale to RGB.** When we train on grayscale images from SVHN and test on RGB images, the model-based methods marginally improve over the baselines.

Figure 39: **Robustness to color on SVHN with a model learned on MNIST-m.** We consider the task of learning a model on MNIST-m and then using it to provide robustness to shifts between RGB and grayscale on SVHN.

B.2 MNIST-m and SVHN

In many cases, one can learn a model that accurately maps samples from one domain to another, but that does not result in larger performance improvements after model-based training. This largely stems from the fact that some nuisances are already well represented in the training data distribution. To illustrate this point, we consider two related experiments. In one experiment, we learned a model that mapped from grayscale to RGB images on MNIST-m; in the other, we learned a model that mapped in the opposite direction from RGB to grayscale images. Images generated by both models are shown in Figure 8. Note that these models learn very accurate mappings from RGB to grayscale and vice versa. In the first column, an RGB sample from SVHN is mapped to a grayscale image that closely resembles the input; similarly, the grayscale image in the right column is mapped to a convincing colorized version of the same number.

We performed model-based training using these models on samples from SVHN and compared the performance to the baselines. The results are shown in Figure 39. Note that in both tasks, we improve only marginally over the baselines. This is largely because the task is not inherently challenging enough. SVHN already contains images with a diversity of RGB images, some of which are close to grayscale.

Dataset \mathcal{D}'		
	SVHN	SVHN
Original samples from \mathcal{D}'		
Model-based samples		

Table 8: **Applying a model learned on MNIST-m to SVHN.** We show samples from SVHN in the top row; in the bottom row, we show the outputs produced by passing the top row images through models learned on MNIST-m of decolorization and colorization respectively.

B.3 GTSRB and CURE-TSR

In this subsection we perform model-based training by first learning a model on GTSRB and then using this model to perform model-based training on CURE-TSR. In Section 6.2.2, we showed that by learning a model of brightness on GTSRB, we can achieve large improvements in test accuracy against the same source of natural variation on CURE-TSR by using this model. In the left column of Table 9, we show a sample produced by this model.

We also considered the challenge of brightness or exposure on the same datasets. The model of natural variation was trained to map samples with low brightness to high brightness on GTSRB. The classifiers were then trained on samples from CURE-TSR challenge-level 0 data and tested them on CURE-TSR challenge-level 3 exposure data. Images from both of these CURE-TSR domains are shown in Figures 40a and 40b respectively.

Figure 40c shows that the MRT and MDA classifiers outperform the PGD classifiers by around 3% on average. Further, these classifiers outperform the vanilla classifier by almost 10%. Also notable is the fact that MAT outperforms all other algorithms by as much as 10%. Interestingly, the variance of the baselines is rather high when compared to the model-based classifiers.

Dataset \mathcal{D}'		
	CURE-TSR (Darkening)	CURE-TSR (Exposure)
Samples from \mathcal{D}'		
Model-based samples		

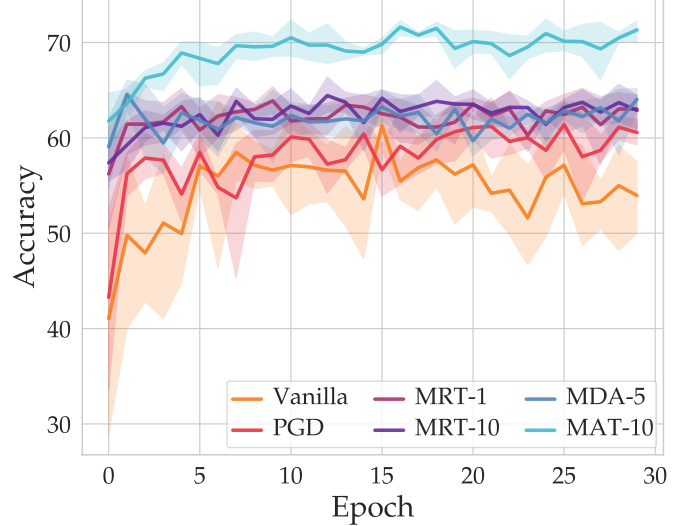
Table 9: **Applying a model learned on GTSRB to CURE-TSR.** We show samples from CURE-TSR in the top row; in the bottom row, we show the outputs produced by passing the top row images through models learned on GTSRB of darkening and exposure respectively.



(a) **Training data.** We trained all classifiers on challenge-level 0 images from CURE-TSR.



(b) **Test data.** We tested all classifiers on exposure challenge-level 3 images from CURE-TSR.



(c) **Results.** We see modest improvements over the baselines by the MRT and MDA classifiers. Notably, the MAT classifier outperforms all other methods by as much as 10%.

Figure 40: **Robustness to exposure on CURE-TSR using a model learned on GTSRB.** We trained a model on GTSRB to map from low-brightness to high-brightness samples. Then, we used the model to perform model-based training on challenge-level 0 samples from CURE-TSR and tested on challenge-level 3 exposure images from CURE-TSR.

C Appendix C: Out-of-distribution experiments

In Section 6.3, we considered out-of-distribution experiments using data from the CURE-TSR dataset. In particular, in Section 6.3.1, we showed that by learning a model of natural variation for the snow nuisance, we were able to outperform baseline classifiers which had access to the same data. In Table 6 in Section 6.3, we recorded similar experiments to the one presented in Section 6.3.1 for a variety of forms of natural variation. In this appendix, we provide additional analysis of these results. Throughout, we will show images from the CURE-TSD dataset to illustrate the different kinds of natural variation in the CURE-TSR dataset we provide robustness to. Note that the CURE-TSR dataset is derived from the CURE-TSD dataset by simply cropping out the street signs. We feel that it is more illustrative to show the full uncropped images when demonstrating the form of natural variation, which is why we display the images from CURE-TSD rather than from CURE-TSR. For completeness, in Appendix D, we show samples from the CURE-TSR dataset.

C.1 Decolorization

In a similar manner to the results obtained for the snow challenge on CURE-TSR, the decolorization challenge presents a significant challenge from a robustness perspective. In Figure 41a, we show data corresponding to each challenge level of decolorization. Note that challenge-level 0 is not decolorized at all, whereas challenge-level 5 is grayscale and thus completely decolorized.

In Figure 41b, we show the accuracies of baseline and model-based classifiers trained on data from the decolorization subset of CURE-TSR. We see that while baseline methods achieve around 90% test accuracy on challenge-level 2 when trained on challenge-levels 0 and 1, this figure drops by as much as 20% for the PGD classifier and 10% for the vanilla classifier. On the other hand, the test accuracies of the MRT and MDA classifiers do not drop significantly across any of the challenges. This demonstrates that simply by training on the least challenging data, we can provide robustness against even the most challenging data.

C.2 Haze

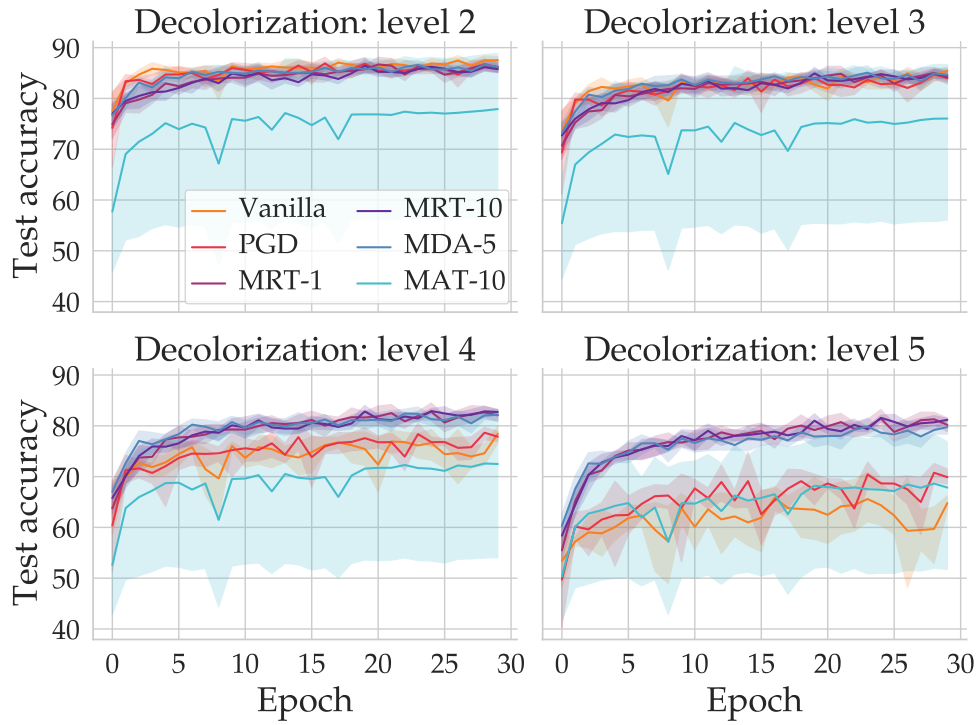
We repeated the experiment of the previous section with the data in CURE-TSR corresponding to the haze nuisance. In Figure 42a, we show images corresponding to the difference challenge levels. In Figure 42b, we see that as the challenge level increases, the gap between the MRT and MDA classifiers increases to nearly 10%.

C.3 Shadow

In Figure 43a, we show images corresponding to the challenge levels 0-5 for the shadow subsets of CURE-TSR. Notice that for challenge-level 0 data, there are no shadow stripes, whereas the dark stripes are very pronounced in challenge-level 5 data. In Figure 43b, we show that as the challenge level increases, the gap between the MRT and MDA classifiers and the baseline classifiers increases to nearly 10%.



(a) **Challenge levels.** Higher challenge levels correspond to more decolorization. That is, challenge-level 0 corresponds to an RGB image, whereas challenge-level 5 corresponds to a fully grayscale image.

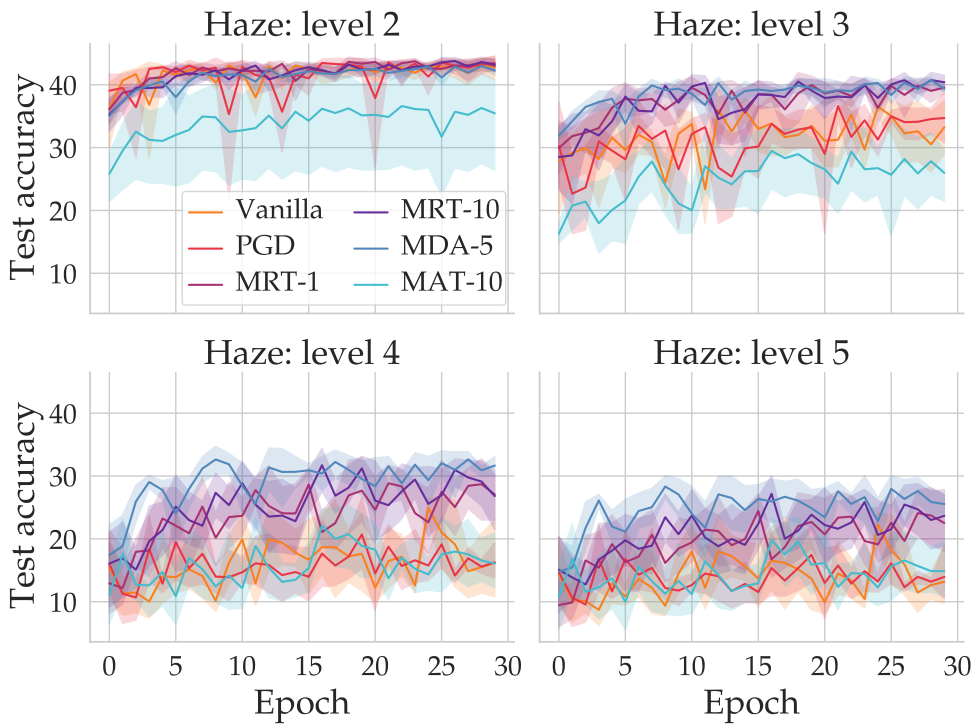


(b) **Results.** We show that as the decolorization challenge-level increases, the gap between the model-based and baseline classifiers increases. This demonstrates that the model-based classifiers provide additional robustness against out-of-distribution data corresponding to decolorization.

Figure 41: **Out-of-distribution robustness to decolorization on CURE-TSR.** We give an overview of the out-of-distribution decolorization experiment described in Table 6. In (a), we show data corresponding to different levels of decolorization. In (b), we show the test accuracies of trained baseline and model-based classifiers.

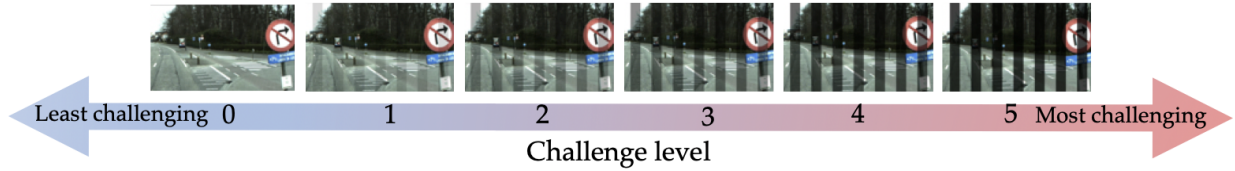


(a) **Challenge levels.** In this figure, we show different challenge levels corresponding to the CURE-TSR haze subsets. Challenge-level 0 does not contain any haze, whereas challenge-level 5 contains high levels of haze.

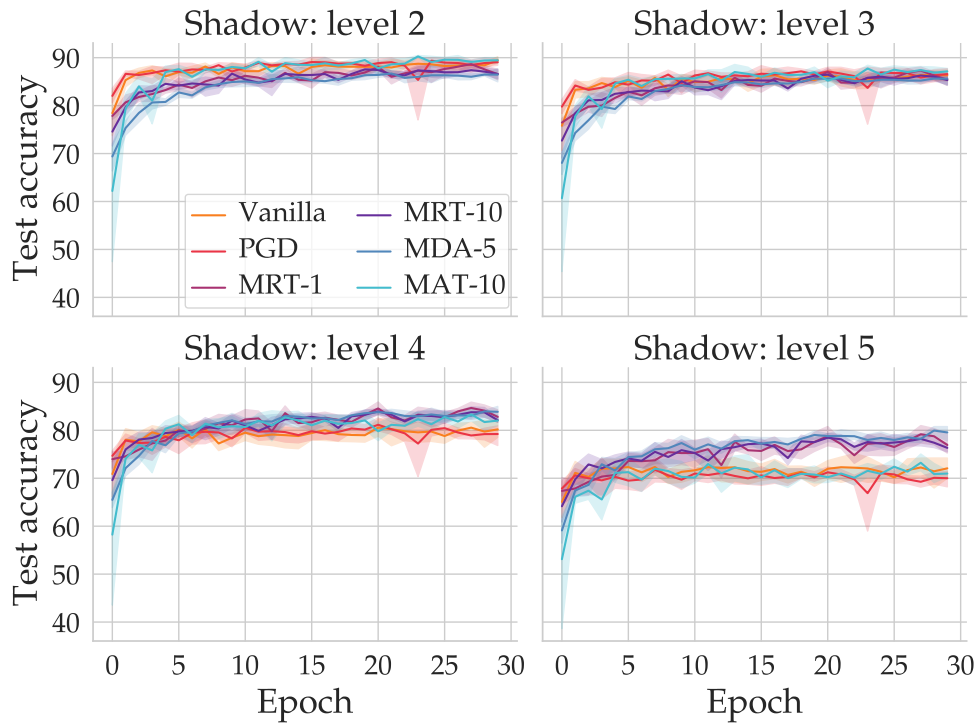


(b) **Results.** For challenge-level 2 test data, the MRT, MDA, and baseline classifiers all achieve nearly the same levels of accuracy. As we move to challenge-level 5 data, the gap between the MRT and MDA classifiers increases with respect to the baselines, reaching nearly 10%.

Figure 42: **Out-of-distribution robustness to haze on CURE-TSR.** For challenge levels 2-5, we show that as the test data becomes more challenging for haze data from CURE-TSR, the gap between baseline and model-based classifiers increases.



(a) **Challenge levels.** We show example images corresponding to different challenge-levels for shadow in the CURE-TSR dataset.

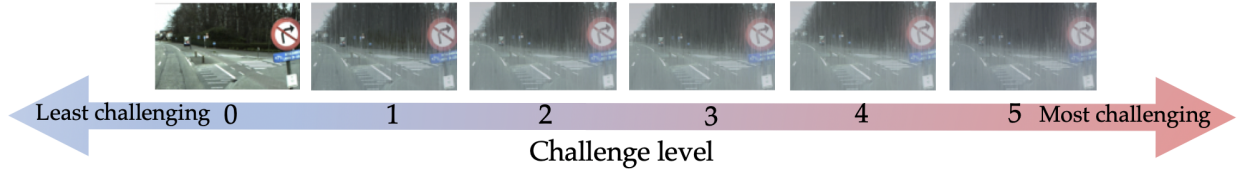


(b) **Results.** On challenge-level 2 data, the classifiers trained on shadow data all show approximately the same performance. However, on challenge-level 5 data, the gap between the baselines and model-based classifiers increases to almost 10%.

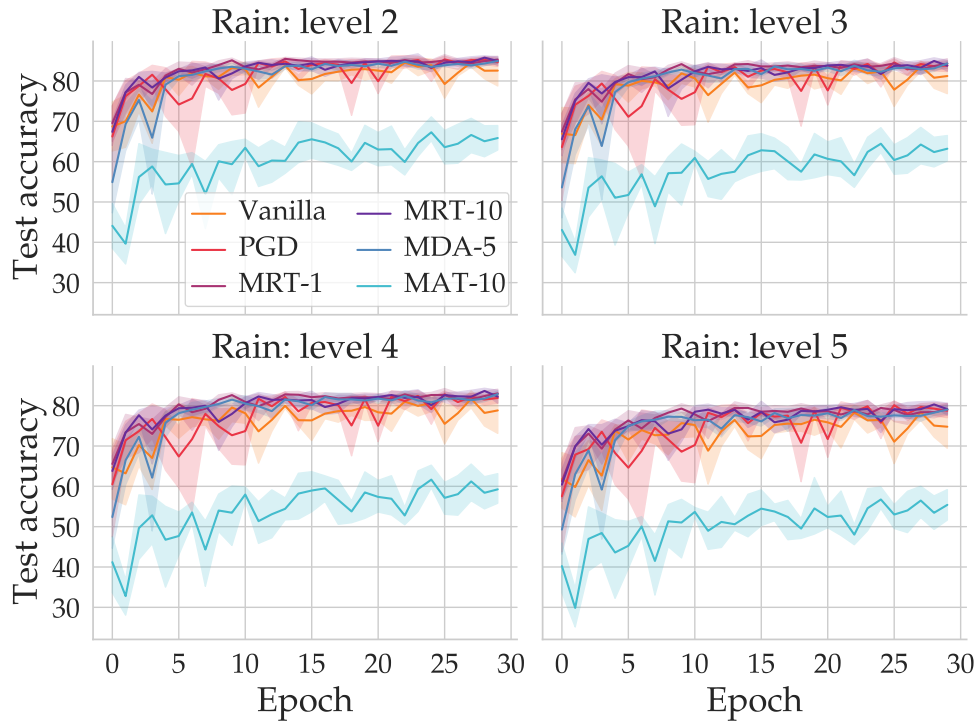
Figure 43: **Out-of-distribution robustness to shadow on CURE-TSR.** We train all classifiers on challenge-level 0 and 1 data and test on challenge-levels 2-5 corresponding to shadow. As the challenge levels increase, so does the gap between the baseline and model-based classifiers.

C.4 Rain

In Figure 44a, we show the challenge levels corresponding to the rain subsets of CURE-TSR. The out-of-distribution test accuracies for challenge-levels 2-5 are shown in Figure 44b. As opposed to the results for snow, decolorization, shadow, and haze, the results for the rain subset for CURE-TSR are less pronounced. All classifiers other than MAT achieve approximately the same accuracies across the different challenge levels.



(a) **Challenge levels.** We show examples from the subsets of CURE-TSR corresponding to different challenge levels for the rain nuisance.



(b) **Results.** Across all of the challenges, the MDA, MRT, and baseline classifiers all achieve similar levels of accuracy.

Figure 44: **Out-of-distribution robustness to rain on CURE-TSR.** We show out-of-distribution data and results for the rain subset of CURE-TSR.

Dataset	Description
MNIST [55]	The MNIST dataset contains grayscale images of handwritten numbers between 0 and 9.
SVHN [56]	The Street View House Numbers dataset contains images of numbers 0-9 cropped from a database of Google Street View images of houses.
GTSRB [57]	The German Traffic Signs Recognition Benchmark dataset contains images of common street signs.
CURE-TSR [34]	The Challenging Unreal and Real Traffic Signs Recognition dataset contains images of street signs with labeled factors of natural variation.
MNIST-m [65]	The MNIST-m dataset contains random background images overlaid with the MNIST digits.
Fashion-MNIST [66]	The Fashion-MNIST dataset contains grayscale images of ten different articles of clothing.
E-MNIST [67]	The E-MNIST dataset consists of grayscale images of uppercase and lowercase letters from the Latin alphabet.
K-MNIST [68]	The Kuzushiji-MNIST dataset contains grayscale images of Kuzushiji (cursive Japanese) characters.
Q-MNIST [69]	The Q-MNIST dataset contains images derived from the NIST [106] dataset in an attempt to rediscover the preprocessing steps used to curate MNIST.
USPS [70]	The USPS dataset contains grayscale images of handwritten numbers between 0 and 9.

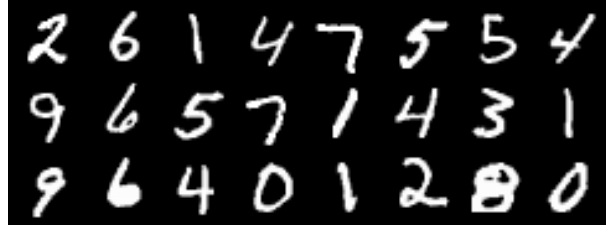
Table 10: **Dataset descriptions.** We provide a brief description of the datasets used in this paper.

D Appendix D: Details concerning datasets and domains

As mentioned in Section 6, we used ten different datasets in this work to fully evaluate the efficacy of the model-based algorithms we introduced in Section 5. For several of these datasets, we curated subsets corresponding to different factors of natural variation, which we refer to as *domains*. In this appendix, we briefly introduce each of the datasets that we used and we explain more fully how we curated the domains used in Section 6.

D.1 Datasets used in this paper

In Table 10, we provide a brief description of each of the datasets used in this paper, and in Figure 45 we show samples from each of these datasets. Many of these datasets are common benchmarks in machine learning, such as MNIST and SVHN. On the other hand, the CURE-TSR dataset was curated relatively recently to provide the machine learning community with data corresponding to realistic scenarios with labeled factors of natural variation. We will look toward extending this work toward datasets corresponding to tasks other than classification (e.g. detection) in future work.



(a) MNIST dataset.



(b) SVHN dataset.



(c) GTSRB dataset.



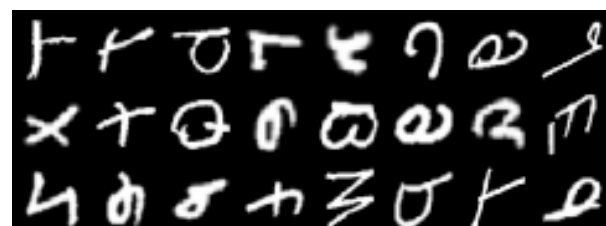
(d) CURE-TSR dataset.



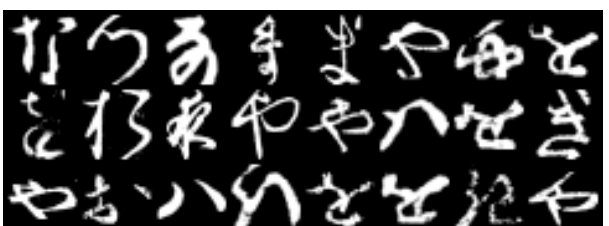
(e) MNIST-m dataset.



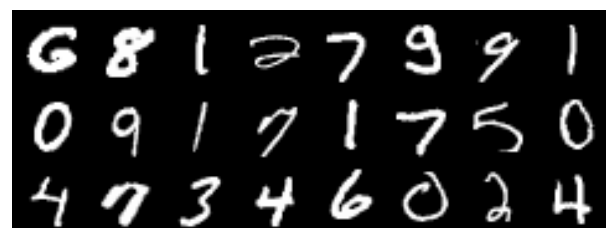
(f) Fashion-MNIST dataset.



(g) E-MNIST dataset.



(h) K-MNIST dataset.



(i) Q-MNIST dataset.



(j) USPS dataset.

Figure 45: **Datasets.** Figures (a)-(j) show samples from the datasets used in this paper.



(a) Batch from MNIST.

(b) Colorized batch from MNIST.

Figure 46: **Creating the colorized MNIST dataset.** The figure on the left shows a batch of images from the original MNIST dataset. Colored versions of these MNIST digits are shown on the right.

D.2 Curating dataset domains

Generally speaking, we obtain domains in one of two ways. When possible, we threshold datasets based on factors of natural variation that are easily computable based on pixel values. For example, a simple metric for determining the brightness in an image is the mean pixel value of that image. By thresholding images from a given dataset \mathcal{D} on such a metric, we can curate domains corresponding to different amounts of natural variation. Alternatively, when such metrics are difficult to compute or do not exist, we apply transformations to randomly selected datapoints to artificially create subsets with different kinds of natural variation.

In each of the following subsections, we provide additional details corresponding to how domains were curated on particular datasets.

D.2.1 MNIST dataset colorization

In Section 6.1.1, we used a colorized versions of the standard MNIST dataset. Each image in the MNIST dataset is a 28×28 array of pixels; the handwritten digit in each image is white and the background is black. So to colorize these images, we first stacked three copies of each image to form a three-tensor in $[0, 1]^{28 \times 28 \times 3}$. Then, by masking each image for pixels that were completely black, we replaced these pixels with the desired RGB values. Pseudocode for changing the background colors using this masking technique is provided in Algorithm 4 in Section A. One batch of the original MNIST dataset and the corresponding colorized digits are shown in Figure 46.

D.2.2 SVHN and GTSRB thresholding

In Sections 6.1.2 and 6.1.3, as well as in Appendix A, we used data from SVHN and GTSRB to train neural networks to be robust against contrast and brightness nuisance variation. We define the brightness $\mathcal{B}(x)$ of an RGB image x to be the mean pixel value of x , and we define the contrast $\mathcal{C}(x)$ to be the difference between the largest and smallest pixel values. Table 11 show the thresholds we chose for contrast and brightness on SVHN and GTSRB. Note that these thresholds were chosen somewhat subjectively to reflect our perception of low, medium and high values of brightness and contrast. We intend to experiment with different thresholds in future work.

Figure 47 shows a summary of the subsets of SVHN that we compiled corresponding to brightness. In particular, Figure 47a shows a histogram of the brightnesses of images in SVHN. We used this histogram to set thresholds for low, medium, and high brightness, which are given in

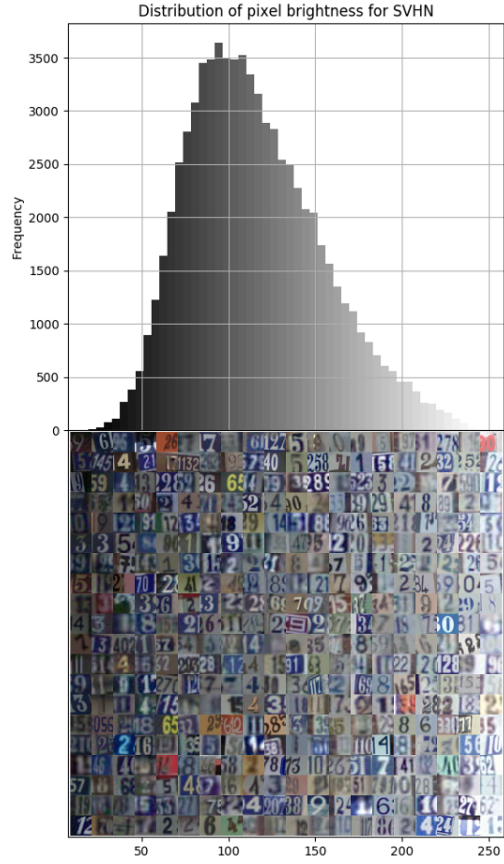
	SVHN			GTSRB		
	Low	Medium	High	Low	Medium	High
Brightness	$\mathcal{B} < 60$	$100 < \mathcal{B} < 150$	$\mathcal{B} > 160$	$\mathcal{B} < 40$	$85 < \mathcal{B} < 125$	$\mathcal{B} > 170$
Contrast	$\mathcal{C} < 70$	$80 < \mathcal{C} < 90$	$\mathcal{C} > 190$	$\mathcal{C} < 70$	$150 < \mathcal{C} < 200$	$\mathcal{C} > 240$

Table 11: **Brightness and contrast thresholds.** This table shows the thresholds we chose to represent low, medium, and high values of contrast and brightness for SVHN and GTSRB.

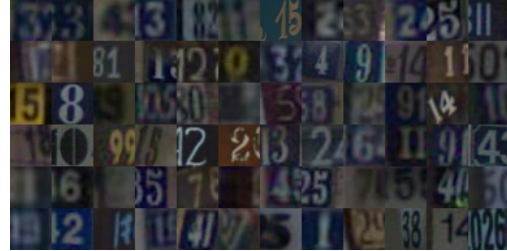
Table 11. The images below the histogram correspond to the bins of the histogram; that is, images further to the left in Figure 47a have lower brightness, whereas images further to the right have high brightness. In Figures 47b, 47c, and 47d, we show samples from the subsets of low, medium and high contrast subsets of SVHN that we compiled.

Figure 48 tells the same story as 47 for the contrast nuisances in SVHN. Again, Figure 48a shows a histogram and accompanying images corresponding to different values of contrast. Figures 48b, 48c, and 48d show samples from the subsets of low, medium, and high contrast images we compiled.

We repeat this analysis of the brightness and contrast thresholding operations for GTSRB in Figures 49 and 50. Again, the difference between high- and low-brightness samples is remarkable, as is the difference in the samples corresponding to high- and low-contrast. However, an interesting difference between the distributions of brightness and contrast on GTSRB vis-a-vis SVHN is that the distributions for GTSRB are skewed, whereas the distributions for SVHN are close to being symmetric.



(a) SVHN brightness histogram. The histogram shows the distribution of pixel brightness for SVHN. The images below the histogram correspond to the bins of the histogram, meaning samples to the left have low brightness whereas samples further to the right have higher brightness.



(b) Low brightness samples. Samples drawn from SVHN with $\mathcal{B}(x) < 60$.

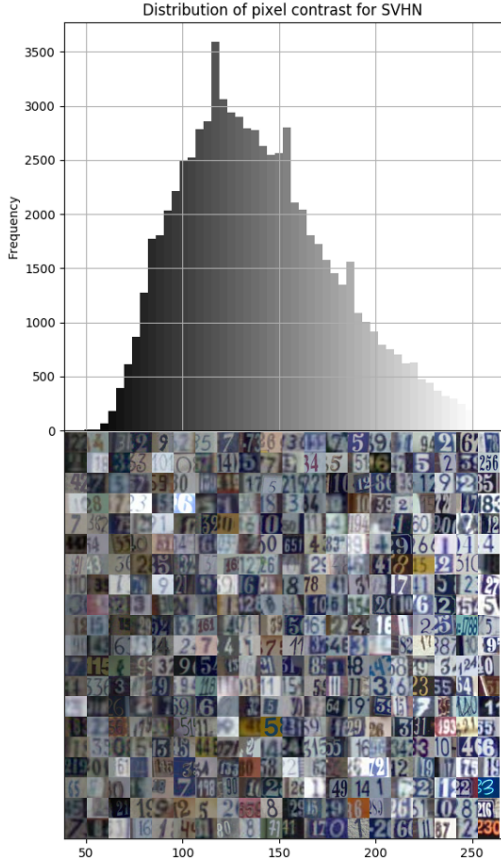


(c) Medium brightness samples. Samples drawn from SVHN with $100 < \mathcal{B}(x) < 150$.



(d) High brightness samples. Samples drawn from SVHN with $\mathcal{B}(x) > 160$.

Figure 47: **SVHN brightness thresholding overview.**



(a) **SVHN contrast histogram.** The histogram shows the distribution of pixel contrast for SVHN. The images below the histogram correspond to the bins of the histogram, meaning samples to the left have low contrast whereas samples further to the right have higher contrast.



(b) **Low contrast samples.** Samples drawn from SVHN with $\mathcal{C}(x) < 70$.

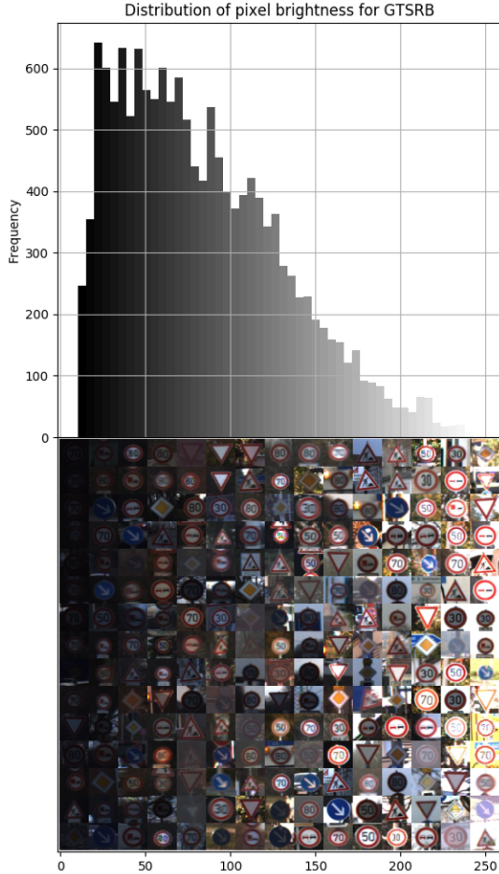


(c) **Medium contrast samples.** Samples drawn from SVHN with $80 < \mathcal{C}(x) < 90$.

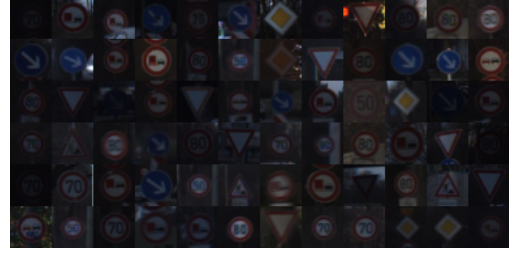


(d) **High contrast samples.** Samples drawn from SVHN with $\mathcal{C}(x) > 190$.

Figure 48: **SVHN contrast thresholding overview.**



(a) **GTSRB brightness histogram.** The histogram shows the distribution of pixel brightness for GTSRB. The images below the histogram correspond to the bins of the histogram, meaning samples to the left have low brightness whereas samples further to the right have higher brightness.



(b) **Low brightness samples.** Samples drawn from GTSRB with $\mathcal{B}(x) < 40$.

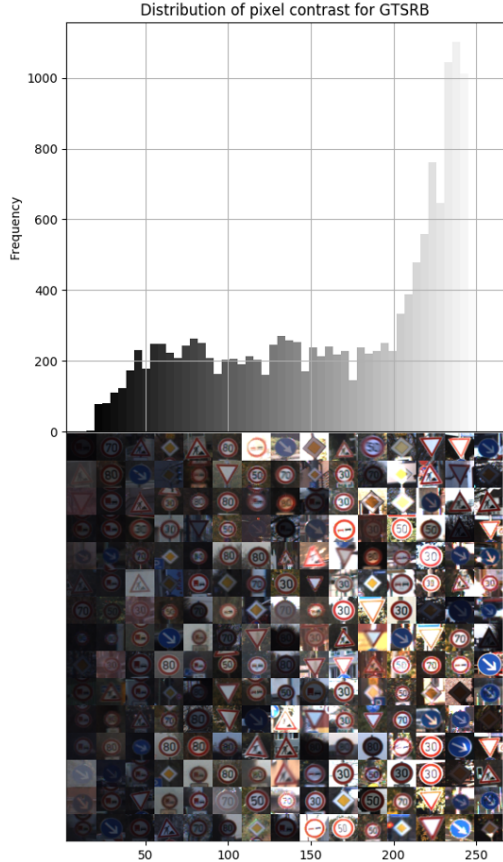


(c) **Medium brightness samples.** Samples drawn from GTSRB with $85 < \mathcal{B}(x) < 125$.

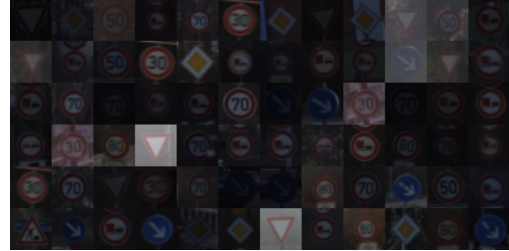


(d) **High brightness samples.** Samples drawn from GTSRB with $\mathcal{B}(x) > 170$.

Figure 49: GTSRB brightness thresholding overview.



(a) SVHN contrast histogram. The histogram shows the distribution of pixel contrast for SVHN. The images below the histogram correspond to the bins of the histogram, meaning samples to the left have low contrast whereas samples further to the right have higher contrast.



(b) Low contrast samples. Samples drawn from GT-SRB with $\mathcal{C}(x) < 70$.



(c) Medium contrast samples. Samples drawn from SVHN with $150 < \mathcal{C}(x) < 200$.

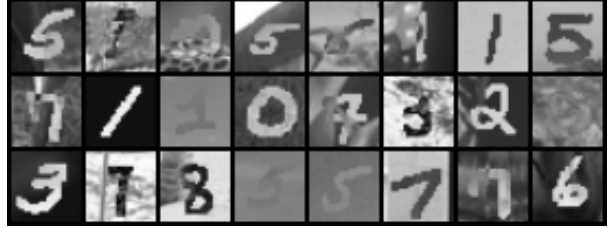


(d) High contrast samples. Samples drawn from SVHN with $\mathcal{C}(x) > 240$.

Figure 50: **SVHN contrast thresholding overview.**



(a) Batch from MNIST-m.



(b) Decolorized batch from MNIST-m.

Figure 51: Decolorized samples from MNIST-m.

D.2.3 Artificial transformations

In Sections 6.1 and 6.2, we also investigated the impact of nuisances such as random erasing, decolorization, and changes in hue. To create domains corresponding to these nuisances, we applied transformations from the `torchvision.transforms` library⁵. For example, in Figure 51, we show images from MNIST-m and the corresponding decolorized images using the `Grayscale` transform from the `torch.transforms` library. In future work, we plan to explore more of these data transformations.

D.2.4 CURE-TSR: labeled challenges

The CURE-TSR dataset was recently curated to provide challenging data with realistic forms of natural variation such as snow, rain, and haze. Usefully, this dataset contains labels corresponding to different factors of natural variation. By leveraging this structure, we were able to carry out the experiments by creating domains that corresponded to the labeled nuisances. In Figure 12 of Section 6.3 as well as Figures 41, 42, 43, and 44, we show samples corresponding to the labelled nuisances in this dataset.

⁵<https://pytorch.org/docs/stable/torchvision/transforms.html>

E Appendix E: Training details and architectures

This appendix details the implementation details of the neural networks trained in this work. All experiments described in Section 6 and 7 were run on four NVIDIA RTX 5000 GPUs.

E.1 MUNIT framework

For completeness, we give a brief overview of the MUNIT framework [4] and described the architecture we used for MUNIT in this paper.

To begin, let $x_A \in A$ and $x_B \in B$ be images from two unpaired image domains A and B ; in the notation of the previous section, we assume that these images are drawn from two marginal distributions \mathbb{P}_A and \mathbb{P}_B . Further, the MUNIT model assumes that each image from either domain can be decomposed into two components: a style code s that contains information about factors of natural or nuisance variation, and a content code c that contains information about higher level features such as the label of the image. Further, it is assumed that the content codes for images in either domain are drawn from a common set \mathcal{C} , but that the style codes are drawn from domain specific sets \mathcal{S}_A and \mathcal{S}_B . In this way, a pair of corresponding images (x_A, x_B) are of the form $x_A = \text{Dec}_A(c, s_A)$ and $x_B = \text{Dec}_B(c, s_B)$, where $c \in \mathcal{C}$, $s_A \in \mathcal{S}_A$, $s_B \in \mathcal{S}_B$, and where Dec_A and Dec_B are unknown decoding networks corresponding to domains A and B respectively. The authors of [4] call this setting a partially shared latent space assumption.

The MUNIT model consists of an encoder-decoder pair $(\text{Enc}_A, \text{Dec}_A)$ and $(\text{Enc}_B, \text{Dec}_B)$ for each image domain A and B . These encoder-decoder pairs are trained to learn a mapping that reconstructs its input. That is, $x_A \approx \text{Dec}_A(\text{Enc}_A(x_A))$ and $x_B \approx \text{Dec}_B(\text{Enc}_B(x_B))$. More specifically, $\text{Enc}_A : \mathcal{A} \rightarrow \mathcal{C} \times \mathcal{S}_A$ is trained to encode x_A into a content code $c \in \mathcal{C}$ and a style code $s_A \in \mathcal{S}_A$. Similarly, $\text{Enc}_B : \mathcal{B} \rightarrow \mathcal{C} \times \mathcal{S}_B$ is trained to encode x_B into $c \in \mathcal{C}$ and $s_B \in \mathcal{S}_B$. Then the decoding networks $\text{Dec}_A : \mathcal{C} \times \mathcal{S}_A \rightarrow A$ and $\text{Dec}_B : \mathcal{C} \times \mathcal{S}_B \rightarrow B$ are trained to reconstruct the encoded pairs (c, s_A) and (c, s_B) into the respective images x_A and x_B .

Inter-domain image translation is performed by swapping the decoders. In this way, to map an image x_A from A to B , x_A is first encoded into $\text{Enc}_A(x_A) = (c, s_A)$. Then, a new style vector s_B is sampled from \mathcal{S}_B from a prior distribution π_B on the set \mathcal{S}_B and the translated image $x_{A \rightarrow B}$ is equal to $\text{Dec}_B(c, s_B)$. The translation of x_B from B to A can be described via a similar procedure with Enc_B , Dec_A , and a prior π_A supported on \mathcal{S}_A . In this paper, we follow the convention used in [4] as use a Gaussian distribution for both π_A and π_B with zero mean and an identity covariance matrix.

Training an MUNIT model involves considering four loss terms. First, the encoder-decoder pairs $(\text{Enc}_A, \text{Dec}_A)$ and $(\text{Enc}_B, \text{Dec}_B)$ are trained to reconstruct their inputs my minimizing the following loss:

$$\ell_{\text{recon}} = \mathbb{E}_{x_A \sim \mathbb{P}_A} \|\text{Dec}_A(\text{Enc}_A(x_A)) - x_A\|_1 + \mathbb{E}_{x_B \sim \mathbb{P}_B} \|\text{Dec}_B(\text{Enc}_B(x_B)) - x_B\|_1$$

Further, when translating an image from one domain to another, the authors of [4] argue that we should be able to reconstruct the style and content codes. By rewriting the encoding networks as $\text{Enc}_A(x_A) = (\text{Enc}_A^c(x_A), \text{Enc}_A^s(x_A))$ and $\text{Enc}_B(x_B) = (\text{Enc}_B^c(x_B), \text{Enc}_B^s(x_B))$, the constraint on the content codes can be expressed in the following way:

$$\ell_{\text{recon}}^c = \mathbb{E}_{\substack{c_A \sim \mathbb{P}(c_A) \\ s_B \sim \pi_B}} \|\text{Enc}_B^c(\text{Dec}_B(c_A, s_B)) - c_A\|_1 + \mathbb{E}_{\substack{c_B \sim \mathbb{P}(c_B) \\ s_A \sim \pi_A}} \|\text{Enc}_A^c(\text{Dec}_A(c_B, s_A)) - c_B\|_1$$

Name	Value
Number of iterations	10000
Batch size	1
Weight decay	0.0001
Weight initialization	Kaiming
Learning rate	0.0001
Learning rate policy	Step
γ (learning rate decay amount)	0.5
λ_x	10
λ_c	1
λ_s	1

Table 12: MUNIT hyperparameters.

where $\mathbb{P}(c_A)$ is the distribution given by $c_A = \text{Enc}_A^c(x_A)$ where $x_A \sim \mathbb{P}_A$ and $\mathbb{P}(c_B)$ is the distribution given by $c_B = \text{Enc}_B^c(x_B)$ where $x_B \sim \mathbb{P}_B$. Similar, the constraint on the style codes can be written as

$$\ell_{\text{recon}}^s = \mathbb{E}_{\substack{c_A \sim \mathbb{P}(c_A) \\ s_B \sim \pi_B}} \|\text{Enc}_B^s(\text{Dec}_B(c_A, s_B)) - s_B\|_1 + \mathbb{E}_{\substack{c_B \sim \mathbb{P}(c_B) \\ s_A \sim \pi_A}} \|\text{Enc}_A^s(\text{Dec}_A(c_B, s_A)) - s_A\|_1.$$

Finally, two GANs corresponding to the two domains A and B are used to form an adversarial loss term. The GANs use the decoders Dec_A and Dec_B as the respective generators for domains A and B . By denoting the discriminators for these domains by D_A and D_B , we can write the GANs as (Dec_A, D_A) and (Dec_B, D_B) . In this way, the final loss term takes the following form:

$$\begin{aligned} \ell_{\text{GAN}} = & \mathbb{E}_{\substack{c_A \sim \mathbb{P}(c_A) \\ s_B \sim \pi_B}} [\log (1 - D_B(\text{Dec}_B(c_A, s_B)))] + \mathbb{E}_{x_B \sim \mathbb{P}_B} [\log D_B(x_B)] \\ & + \mathbb{E}_{\substack{c_B \sim \mathbb{P}(c_B) \\ s_A \sim \pi_A}} [\log (1 - D_A(\text{Dec}_A(c_B, s_A)))] + \mathbb{E}_{x_A \sim \mathbb{P}_A} [\log D_A(x_A)] \end{aligned}$$

Using the four loss terms we have described, the MUNIT framework uses first-order methods to solve the following nonconvex optimization problem:

$$\min_{\substack{\text{Enc}_A, \text{Enc}_B \\ \text{Dec}_A, \text{Dec}_B}} \max_{\substack{D_1, D_2}} \ell_{\text{GAN}} + \lambda_x \ell_{\text{recon}} + \lambda_c \ell_{\text{recon}}^c + \lambda_s \ell_{\text{recon}}^s$$

E.2 Hyperparameters and implementation of MUNIT

In this subsection, we discuss hyperparameters and implementation details for MUNIT. In particular, in Table 12 we record the hyperparameters we used for training MUNIT models of natural variation. The hyperparameters we selected are generally in line with those suggested in [4]. The most relevant difference is that for each of the models we learn in this paper, we use a two-dimensional latent space. This allows us to easily visualize the space of generated images. Analysis of the latent space of these learned models is available in Appendix A.

We use the same architectures for the encoder, decoder, and discriminative networks as are described in Appendix B.2 of [4].